

Summer 8-2018

Fluorescently Labeled siRNAs and their Theranostic Applications in Cancer Gene Therapy

Stephen David Kozuch
stephen.kozuch@student.shu.edu

Follow this and additional works at: <https://scholarship.shu.edu/dissertations>

 Part of the [Biochemistry Commons](#), [Cancer Biology Commons](#), [Chemistry Commons](#), and the [Nucleic Acids, Nucleotides, and Nucleosides Commons](#)

Recommended Citation

Kozuch, Stephen David, "Fluorescently Labeled siRNAs and their Theranostic Applications in Cancer Gene Therapy" (2018). *Seton Hall University Dissertations and Theses (ETDs)*. 2571.
<https://scholarship.shu.edu/dissertations/2571>

FLUORESCENTLY LABELED siRNAs AND THEIR THERANOSTIC APPLICATIONS IN CANCER GENE THERAPY

*A thesis submitted to the Department of Chemistry and Biochemistry at Seton Hall University in
partial fulfillment of the requirements for the degree of Doctor of Philosophy*

By

Stephen David Kozuch

August 2018

Department of Chemistry and Biochemistry
Seton Hall University
South Orange, New Jersey, USA

©Copyright by Stephen D. Kozuch

DISSERTATION COMMITTEE APPROVALS

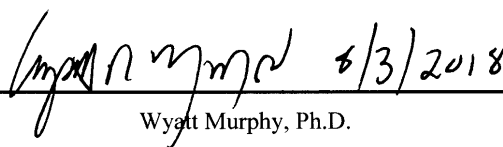
We certify that we have read this thesis and that in our opinion it is sufficient in scientific scope and quality as a dissertation for the degree of Doctor in Philosophy

APPROVED BY:



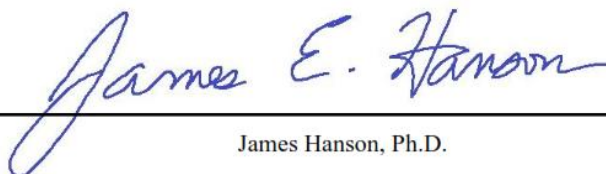
David Sabatino, Ph.D.

Advisor, Seton Hall University



Wyatt Murphy, Ph.D.

Reader, Member of Dissertation Committee, Seton Hall University



James Hanson, Ph.D.

Reader, Member of Dissertation Committee, Seton Hall University



Stephen Kelty, Ph.D.

Chair, Department of Chemistry and Biochemistry, Seton Hall University

Dedicated to my entire family, namely my mother, Sharon, and my brothers, Matthew and Christian for their unconditional love and support. This thesis work would not have been possible without their sacrifices. I also dedicate this thesis to my father, Stephen. Although he is not able to see me complete my Ph.D., I know he is looking down proud at all that I have been able to accomplish.

ABSTRACT

Gene therapy has emerged as a promising precision nano-medicine strategy in the treatment of numerous diseases including cancer. At the forefront of its utility are the applications of short-interfering RNA (siRNA), that silence oncogenic mRNA expression leading to cancer cell death through the RNA interference (RNAi) pathway. Despite the therapeutic potential, siRNAs are limited by poor pharmacological properties, which has hindered their translation into the clinic. Recent studies, however, have highlighted the applications of modified siRNAs, including the use of fluorescent probes and siRNA nanostructures in cancer detection and treatment. The siRNAs reported in this thesis are designed to target and silence the overexpression of the Glucose Regulated Proteins (GRPs) in cancer. The GRPs are a class of chaperone proteins involved in protein folding events within the endoplasmic reticulum. Under physiological or pathological stress, some GRPs translocate to the cell surface where they function as signaling receptors for oncogenic activity. Therefore, cancer cell surface GRPs have been classified as clinically proven biomarkers.

Chapter 2 outlines the design, synthesis and characterization of linear as well as novel V- and Y-shape RNA templates with the use of a ribouridine branchpoint synthon. The RNA templates self-assembled into spheres, triangles, squares, pentagons and hexagons of discrete sizes and shapes, confirmed by native PAGE while TEM imaging validated the sizes and shapes of the siRNA nanostructures. Moreover, thermal denaturation and CD spectroscopy were used to ascertain the prerequisite siRNA hybrids for their RNAi applications. Of interest from this initial study, the self-assembled siRNA hybrids (5 nM) that targeted GRP-75, 78 and 95 elicited a synergistic effect, which resulted in potent gene knockdown as well as cancer cell death.

The simultaneous integration of therapy and diagnostics (“theranostics”) has been utilized to diagnose and treat cancers at their earliest stages, when they are most likely curable or at least treatable. Building on the work described in Chapter 2, the covalently attachment of fluorescein isothiocyanate (FITC) allowed for monitoring cell uptake and biological activity of a wide range of siRNA motifs. Incorporation of FITC had negligible influence on the A-type helix of the siRNAs, while maintaining good hybrid thermal stability. The FL-siRNAs showed some degree of fluorescence quenching relative to the unlabeled siRNAs. However, the higher-order V- and Y-shape siRNA structures enabled the incorporation of multiple fluorescent reporters, which increased siRNA fluorescence but failed to overcome the quenching effects. Upon transfection within the PC-3 prostate cancer cells, the FL-siRNA hybrids (50 nM) exhibited less mRNA knockdown (~10-30%) when compared to their non-labeled counterparts (~40-80%). Conjugation of the FITC probe to the sense strand of the siRNAs re-established mRNA knockdown (~50-90%) efficiency which also translated to more potent cancer cell death over a 72 hr period (~20-95%). Time dependent flow cytometry and fluorescence microscopy revealed the sustained presence (up to 72 hr) of FITC within the PC-3 cells, thereby validating siRNA uptake for RNAi activity. Of significance, the multi-FITC labeled Y-branch siRNA targeting multiple GRPs demonstrated the most potent FITC-signaling and GRP mRNA knockdown, which potentiated cancer cell death. Taken together, this thesis will serve to highlight the synthesis, characterization and biological evaluation of a new class of theranostic siRNA molecular beacons for gene therapy applications in cancer.

KEYWORDS: siRNA nanostructures, Theranostics, Cancer gene therapy, Glucose Regulated Proteins (GRPs), FITC, Fluorescence, Prostate cancer

ACKNOWLEDGEMENTS

Life is full of surprises, the sooner we all realize this the better. Often, we think we know how our lives will end up with little thought on what it takes to get there. Obtaining my Ph.D. was not my first choice nor what I initially wanted, however, the more involved I became with research the more I felt like it was where I belonged. The journey towards my Ph.D. began in 2009, when I took my first classes here at Seton Hall University. From the first organometallic reactions all the way to my last *in-vitro* studies, I have been completely captivated. Over the last 5 years I have learned much in the field of biochemistry, and about myself.

I would like to express my sincere gratitude to my advisor Dr. David Sabatino for not only accepting me into his research group but for his continuous patience, motivation and support through the many ups and downs of my Ph.D. studies. Your guidance helped at every step of the way from the initial inception of the project through finishing this thesis. I could not have imagined having a better advisor and mentor for my Ph.D. study.

Besides my advisor, I would like to thank the rest of my thesis committee: Dr. Wyatt Murphy (exam chair), Dr. James Hanson, Dr. Sergiu Gorun and Dr. Monika Raj. I'd like to especially thank Dr. Wyatt Murphy and Dr. James Hanson for reading and reviewing my dissertation. Thank you not only for all your insightful comments, suggestions and encouragements; but also thank you for all the challenging questions, which allowed me to broaden my research perspectives. Special thanks to Dr. Jenny Zilberberg and colleagues at department of Biomedical Research at Hackensack University Medical Center for their collaborative efforts.

I would also like to thank the entire department of Chemistry and Biochemistry here at Seton Hall University for allowing me to continue my graduate studies. To all the professors I have had over the last 5 years or so, thank you for always challenging me to do better. Also, a big thank you to Ms. Maureen Grutt for everything she has done to help me over the last five years.

I thank my fellow group members for all the fun I have had over the last 5 years. From the stimulating discussions that kept me motivated to even the days where we just talked about everything other than research. Mayur, Mariana, Niki, Chris, Rachel, Sunil, Keith, Claudia, Adah and Andrieh you all are like family to me, I appreciate everything we have been through together. Also, I thank the friends I've made throughout my studies: Erik, Hader and Jeff, even though you may not know it you all helped me get to this point.

Last but certainly not least, I would like to thank my family: my mom, Sharon, my brothers, Matt and Chris and my grandparents, Barbara and Paul Asmus. All your support throughout the last 5 years and my life in general has been amazing; words cannot describe how lucky I am to have all of you in my life.

I apologize to anyone I have unintentionally forgotten, or anything people have helped me with that I have not properly acknowledged. To all of you, I sincerely thank you.

TABLE OF CONTENTS

DEDICATION	iv
ABSTRACT	v
ACKNOWLEDGEMENTS	vii
TABLE OF CONTENTS	viii
LIST OF FIGURES	xii
LIST OF TABLES	xiv
LIST OF SCHEMES	xiv
ABBREVIATIONS AND SYMBOLS	xv
APPENDIX	A1
CHAPTER 1: GENERAL INTRODUCTION INTO THE SELF-ASSEMBLY AND BIOLOGICAL FUNCTION OF SiRNAs IN CANCER DETECTION AND THERAPY	
1.1 SiRNA STRUCTURE AND FUNCTION IN THE RNAi PATHWAY	1
1.2 SiRNA APPLICATIONS IN CANCER GENE THERAPY	5
1.3 METHODS AND APPLICATIONS OF SiRNA SELF-ASSEMBLY AND NON-COVALENT CONJUGATION FOR THERAPEUTICS	8
1.4 COVALENT BIOCONJUGATION STRATEGIES WITH SiRNA	11
1.5 APPLICATION OF FLUORESCENT SiRNAs IN LIVE CELL IMAGING AND GENE THERAPY	13
1.6 THESIS OBJECTIVES	18
1.7 REFERENCES	21
CHAPTER 2: DEVELOPMENT OF HIGHER-ORDER SiRNA HYBRIDS FOR RNAi MEDIATED CANCER GENE THERAPY	
2.1 ABSTRACT	26
2.2 INTRODUCTION	27
2.3 CHAPTER OBJECTIVES	29
2.4 RESULTS AND DISCUSSION	30

2.4.1	SYNTHESIS OF BRANCHPOINT PHOSPHORAMIDITE	30
2.4.2	V-AND Y-SHAPED RNA SYNTHESIS	35
2.4.3	ANALYSIS, PURIFICATION AND CHARACTERIZATION OF siRNA HYBRIDS	37
2.4.4	GRP-TARGETING siRNA HYBRIDS IN HUMAN CANCER CELL LINES	44
2.5	CONCLUSIONS	46
2.6	EXPERIMENTAL	46
2.6.1	GENERAL METHODS	46
2.6.2	SYNTHESIS	47
2.6.3	SOLID PHASE RNA SYNTHESIS	50
2.6.4	CLEAVAGE AND DEPROTECTION OF RNA	51
2.6.5	POLYACRYLAMIDE GEL ELECTROPHORESIS (PAGE)	51
2.6.6	ION PAIRING REVERSE PHASE HPLC (IP RP HPLC)	52
2.6.7	ELECTROSPRAY IONIZATION MASS SPECTROMETRY (ESI MS)	53
2.6.8	CD SPECTROSCOPY	53
2.6.9	THERMAL DENATURATION (T_m) STUDIES	53
2.6.10	CELL CULTURE	54
2.6.11	siRNA TRANSFECTIONS IN AN3CA CELLS	54
2.6.12	RNA ISOLATION AND QUANTITATIVE RT-PCR	55
2.6.13	WESTERN BLOTS	56
2.6.14	CELL CYTOTOXICITY	56
2.7	REFERENCES	57

CHAPTER 3: FLUORESCENTLY LABELED siRNAs AND THEIR THERANOSTIC APPLICATIONS IN CANCER GENE THERAPY

3.1	ABSTRACT	59
3.2	INTRODUCTION	60
3.2.1	siRNAs AS THERANOSTIC AGENTS	60
3.2.2	THE GLUCOSE REGULATED PROTEINS AS THERAPEUTIC TARGETS	65
3.3	PROJECT OBJECTIVES	69
3.4	RESULTS AND DISCUSSION	71
3.4.1	FITC SOLID PHASE RNA BIOCONJUGATION	71

3.4.2	ANALYSIS AND PURIFICATION OF FITC-RNA TEMPLATES	72
3.4.3	FITC-siRNA HYBRIDIZATION AND NATIVE PAGE	74
3.4.4	CIRCULAR DICHROISM (CD) SPECTROSCOPY OF siRNA HYBRIDS	76
3.4.5	THERMAL DENATURATION (T _m) ANALYSIS OF siRNA HYBRIDS UV-SPECTROSCOPY	78
3.4.6	UV ABSORPTION AND FLUORESCENCE EMISSION SPECTRA	80
3.4.7	TRANSFECTION AND RT-PCR IN PC3 CELLS	85
3.4.8	INTERNALIZATION EFFICIENCY VIA FLOW CYTOMETRY AND FLUORESCENT MICROSCOPY	86
3.4.9	WESTERN BLOT	91
3.4.10	CELL VIABILITY	92
3.5	CONCLUSIONS	93
3.6	EXPERIMENTAL METHODS	93
3.6.1	MATERIALS AND METHODS	93
3.6.2	FITC BIOCONJUGATION OF LINEAR, V- AND Y-SHAPE siRNAs	94
3.6.3	RP IP HPLC	95
3.6.4	MASS SPECTROMETRY	96
3.6.5	DENATURING POLYACRYLAMIDE GEL ELECTROPHORESIS	96
3.6.6	siRNA HYBRIDIZATION	96
3.6.7	NON-DENATURING, NATIVE POLYACRYLAMIDE GEL ELECTROPHORESIS (PAGE)	96
3.6.8	CIRCULAR DICHROISM (CD) SPECTROSCOPY	97
3.6.9	THERMAL DENATURATION (T _m)	97
3.6.10	FLUORESCENCE EMISSION AND QUANTUM YIELD (ϕ) DETERMINATION	98
3.6.11	CELL CULTURE	98
3.6.12	siRNA TRANSFECTIONS IN PC-3 CELLS AND CELLULAR UPTAKE VIA FLOW CYTOMETRY AND FLUORESCENCE MICROSCOPY	98
3.6.13	GENE KNOCKDOWN VIA QUANTITATIVE REAL-TIME POLYMERASE CHAIN REACTION (qRT-PCR)	99
3.6.14	WESTERN BLOT	100
3.6.15	CELL VIABILITY	100
3.7	REFERENCES	101

CHAPTER 4: CONCLUSIONS AND CONTRIBUTIONS TO KNOWLEDGE

4.1	CONCLUSIONS AND CONTRIBUTIONS TO KNOWLEDGE MADE IN THIS THESIS	104
4.1.1	DEVELOPMENT OF HIGHER-ORDER siRNA HYBRIDS FOR RNAi MEDIATED CANCER GENE THERAPY	104
4.1.2	FLUORESCENTLY LABELED siRNAs AND THEIR THERANOSTIC APPLICATIONS IN CANCER GENE THERAPY	105
4.2	FUTURE WORK	107
4.3	PUBLICATIONS, INVENTION DISCLOSURES AND CONFERENCE PRESENTATIONS	108
4.3.1	ACCEPTED MANUSCRIPTS FOR PUBLICATION	108
4.3.2	MANUSCRIPTS IN PREPARATION/REVIEW	108
4.3.3	POSTER PRESENTATIONS	108

LIST OF FIGURES

Figure 1.1	Structural comparison of thymidine and ribouridine	2
Figure 1.2	Differences between miRNA and siRNA	3
Figure 1.3	SiRNA mediated gene silencing via RNAi mechanism	5
Figure 1.4	Oligonucleotide delivery strategies	11
Figure 1.5	Oligonucleotide conjugation Strategies	13
Figure 1.6	Structures of Fluorescent Dyes	16
Figure 1.7	FRET probe detection of siRNA duplex stability	17
Figure 1.8	Design and self-assembly of siRNA nanostructures	19
Figure 1.9	Linear, V- and Y-shaped FL-siRNAs	20
Figure 2.1	Design and self-assembly of siRNA nanostructures	30
Figure 2.2	COSY NMR	33
Figure 2.3	³¹ P NMR	34
Figure 2.4	Native, non-denaturing 16% PAGE	40
Figure 2.5	Circular dichroism spectroscopy of V- and Y-shaped siRNAs	41
Figure 2.6	Thermal denaturation of V- and Y-shaped siRNAs	43
Figure 2.7	RNAi screening	45
Figure 3.1	Multifunctional applications of theranostic agents	65
Figure 3.2	Design of FL-siRNA bioconjugates	70
Figure 3.3	Denaturing PAGE of FITC-labeled siRNAs	74
Figure 3.4	Native PAGE of FITC-labeled siRNAs	75
Figure 3.5	Native PAGE of multi-FITC-labeled siRNAs	76
Figure 3.6	Circular dichroism spectroscopy	77

Figure 3.7	Thermal denaturation studies of FITC-siRNAs	79
Figure 3.8	UV absorption spectra of FITC-siRNAs and multi-FITC siRNAs	81
Figure 3.9	FL-siRNA Hybrids containing 1, 2 and 3 FITC probes	82
Figure 3.10	Fluorescence emission of FITC-labeled siRNAs and multi-FITC labeled siRNAs	84
Figure 3.11	qRT-PCR analysis of GRP75, 78 and 94 gene knockdown	86
Figure 3.12	Flow cytometry of 50nM FL-siRNA transfection at 3 and 20 h	87
Figure 3.13	Fluorescent microscope images of FL-siRNA transfected PC-3 cells at 4 and 24 hours post transfection	88
Figure 3.14	Protein and mRNA knockdown levels of GRP75, 78 and 94	91
Figure 3.15	Cell viability determined using Propidium Iodide (PI)	92

LIST OF TABLES

Table 1.1	Cancer-associated genes targeted by siRNAs	6
Table 1.2	Therapeutic siRNAs in clinical development	8
Table 2.1	Characterization data for GRPs targeting linear, V- and Y-shape siRNA sense and antisense sequences	38
Table 3.1	Overexpression of GRPs in different cancer types	68
Table 3.2	Characterization data for FL-GRPs targeting linear, V- and Y-shape siRNA sense and antisense sequences	73

LIST OF SCHEMES

Scheme 2.1	Synthesis of ribouridine branchpoint phosphoramidite	35
Scheme 2.2	Solid-phase synthesis of V- and Y-shaped RNA templates	37
Scheme 3.1	Solid phase bioconjugation of linear, V- and Y- shape FITC-RNA bioconjugates	71

ABBREVIATIONS AND SYMBOLS

%H	Percent Hyperchromicity
(P/S)	Penicillin/streptomycin
©	Copyright
®	Registered
°C	Degrees Celsius
μL	Microliter
μM	Micromolar
μmol	Micromole
μmol/g	Micro mole per gram
1° mAb	Primary monoclonal antibody
¹³ CNMR	Carbon nuclear magnetic resonance
¹ HNMR	Proton nuclear magnetic resonance
³¹ PNMR	Phosphorus nuclear magnetic resonance
A	Adenosine
Å	Angstrom
A.U.	Absorbance units
A ₂₆₀ or Abs	UV absorbance measure at 260 nm
Ac	Acetyl
Ade	Adenine
AgCl	Silver Chloride
AgNO ₃	Silver Nitrate
Argo2	Argonaute 2 complex
AMA	Ammonium hydroxide/methylamine
Ar _(g)	Argon Gas
asRNA	Antisense Ribonucleic Acid
ATC	Anaplastic thyroid cancer
Bax	Bcl-2-like protein 4

BCL-2	B-cell lymphoma 2
BCR-Abl	breakpoint cluster region protein-Abelson murine leukemia viral oncogene
BiP	Immunoglobulin heavy chain binding protein
Bp	Base-pair
BRAF	Murine sarcoma viral oncogene homolog B
BSA	Bovine serum albumin
C	Cytidine
Ca ²⁺	Calcium
CAR-T	Chimeric antigen receptor T cells
CD	Circular dichroism
CDC25	Cell division cycle phosphatase
cDNA	Complimentary DNA
Cdots	Carbon dots
CH	Methine group
CHOP	DNA-damage inducible transcript 3
Cl-P(OCEt)N(<i>i</i> -Pr) ₂	N,N-diisopropylamino cyanoethyl phosphonamidic-chloride
c-MYB	Myeloblastosis proto-oncogene protein
CNET	cyanoethyl
CO ₂	Carbon dioxide
COSY	Homonuclear correlation spectroscopy
CPG	Controlled pore glass
CPPs	Cell penetrating peptides
CPS	Counts per second
CRISPR-Cas9	Clustered Regularly Interspaced Short Palindromic Repeats
CTPs	Cancer Targeting peptides
CuAAC	Cu(I)-catalyzed azide-alkyne cycloaddition
CuSO ₄	Copper (II) Sulfate
Cy3	Cyanine 3 dye

Cy5	Cyanine 5 dye
Cy7	Cyanine 7 dye
DCA	Dichloroacetic acid
DCC	Dicyclohexylcarbodiimide
DCM	Dichloromethane
DCU	Dicyclohexylurea
DIEA	Diisopropylethylamine
DLS	Dynamic light scattering
DMEM	Dulbecco's Modified Eagle medium
DMF	Dimethylformamide
DMSO	Dimethylsulfoxide
DMT	Dimethoxy trityl
DNA	Deoxyribonucleic Acid
dsRNA	Double-Stranded Ribonucleic Acid
DTT	Dithiothreitol
e.g	For example
EDTA	Ethylenediaminetetraacetic acid
eGFP	Enhanced green fluorescent protein
EGFR	Epidermal growth factor receptor
EPPT1	Synthetic peptide (YCAREPPTRTFAYWG)
ER	Endoplasmic Reticulum
ESI-MS	Electrospray ionization mass spectrometry
Et ₃ N	Triethylamine
EtOAc	Ethyl Acetate
EtOH	Ethanol
ETT	5-ethylthiotetrazole
FAK	Focal adhesion kinase
FAM	Carboxyfluorescein

FBS	Fetal Bovine Serum
FITC	Fluorescein Isothiocyanate
FL-siRNA	Fluorescently-labeled short interfering Ribonucleic acid
FRET	Fluorescence resonance energy transfer
G	Guanosine
GAPDH	Glyceraldehyde 3-phosphate dehydrogenase
GFP	Green fluorescent protein
GRP170	Glucose Regulated Protein of 170 kilodaltons
GRP75	Glucose Regulated Protein of 75 kilodaltons
GRP78	Glucose Regulated Protein of 78 kilodaltons
GRP94	Glucose Regulated Protein of 94 kilodaltons
H ₂ O	Water
H ₂ SO ₄	Sulfuric Acid
HCl	Hydrochloric acid
HEX	Hexachlorofluorescein
HIF	Hypoxia-inducible factors
HP1 γ	Heterochromatin protein
HPV E6	Human papillomavirus gene 6
hr	Hour
HRP	Horseradish peroxidase
KSP	Kinesin spindle protein
LC/MS	Liquid chromatography/ mass spectrometry
LDH	Lactate dehydrogenase
LDS	Lithium dodecyl sulfate
LMP-1	Latent membrane protein-1
LNPs	Lipid nanoparticles
Lv	Levulinyl
M	Molar

m/z	Mass per charge ratio
MDR	Multidrug resistance
Me	2'-methyl
MeCN	Acetonitrile
MEM	Minimum Essential Medium
MeOH	Methanol
mg	Milligram
MgSO ₄	Magnesium Sulfate
Min	minute
miRNA	Micro Ribonucleic Acid
mL	Milliliter
mM	Millimolar
mmol	Millimole
MMT	Mono-methoxytrityl
MMT-Cl	Monomethoxytrityl chloride
MPAP	Myristoylated polyarginine peptides
MRI	Magnetic resonance imaging
mRNA	Messenger Ribonucleic Acid
MS	Mass spectrometry
N ₂	Nitrogen gas
Na ₂ SO ₄	Sodium Sulfate
N-Ac	N-Acetyl
NaCl	Sodium chloride
NaCl _(aq)	Saturated Sodium Chloride in water
NaHCO _{3(aq)}	Saturated Sodium bicarbonate in water
NaOAc	Sodium Acetate
<i>n</i> -BuOH	<i>N</i> -Butanol
<i>N</i> -Bz	<i>N</i> -Benzoyl

ncRNA	Noncoding Ribonucleic Acid
NH ₂ NH ₂ ·H ₂ O	Hydrazine hydrate
NH ₄ OH	Ammonium hydroxide
<i>N</i> -iBu	<i>N</i> -isobutyl
NIH	National institute of Health
NIR	Near-infrared
nm	Nanometer
nM	Nanomolar
nmol	Nanomole
nsRNA	Nonspecific ribonucleic acid
O.D.	Optical density
ϕ	Quantum Yield
PAGE	Polyacrylamide gel electrophoresis
PAGE	polyacrylamide gel electrophoresis
PAMAMs	Poly(amidoamine)
PDAC	Pancreatic ductal adenocarcinoma
PEG	Polyethylene glycol
PEI	Polyethylenimine
PI	Propidium iodide
Pim-1	Serine/threonine kinase
PKC- α	Protein kinase C alpha
PKN3	Protein kinase N3
PLK-1	Polo-like kinase 1
pM	Picomolar
pmol	Picomole
polyPCPDTBT	Poly[2,6-(4,4-bis-(2-ethylhexyl)-4 <i>H</i> -cyclopenta [2,1- <i>b</i> ;3,4- <i>b'</i>]dithiophene)- <i>alt</i> -4,7(2,1,3-benzothiadiazole)]
PVDF	Polyvinylidene fluoride
qRT-PCR	Qualitative real-time polymerase chain reaction

RISC	RNA-Induced Silencing Complex
RNA	Ribonucleic Acid
RNAi	Ribonucleic Acid Interference
RNaseH	Ribonuclease H
ROX	Rhodamine X
RP IP HPLC	Reverse-phase Ion Paring High Performane liquid chromatography
Rpm	Revolutions per minute
RPMI	Roswell Park Memorial Institute medium
RRM2	Ribonucleotide reductase M2 subunit
RSV	Respiratory syncytial virus
RTP801/REDD1	Regulated in Development and DNA damage responses
RT-PCR	Real-time polymerace chain reaction
rU	Ribouridine
S	Second
SAR	Structure-activity relationship
SDS-PAGE	Sodium dodecyl sulfate polyacrylamide gel electrophoresis
siPLK1	siRNA targeting PLK1
siRNA	Short/Small Interfering Ribonucleic Acid
SPION	Superparamagnetic iron oxide nanoparticles
ssRNA	Single-stranded ribonucleic acid
STAT-3	Signal transducer and activator of transcription 3
SYK	Spleen tyrosine kinase
T	Thymidine
TAE	Tris/Acetic Acid/EDTA
TBDMS	<i>tert</i> -butyldimethylsilyl
TBE	Tris/Borate/EDTA buffer
TBST	Tris-buffered saline/Tween
TEA:3HF	Triethylamine:trihydrofluoride

TEAA	Triethylammnonium acetate
TEM	Transmission electron microscopy
TET	tetrachlorofluorescein
TGF- β	Transforming growth factor beta
THF	Tetrahydrofuran
TLC	Thin-layer chromatography
T_m	Thermal Denaturation
TRIS	Tris(hydroxymethyl)aminomethane
tRNA	Transfer Ribonucleic Acid
TTR	Transthyretin
TM	Trademark
U	Uridine
uMUC1	Tumor antigen under glycosylated MUC1
UPR	Unfolded Protein response
UTR	Untranslated region
UV-Vis	Ultraviolet–visible spectrophotometry
VEGF	Vascular endothelial growth factor
VEGF-R1	Vascular endothelial growth factor receptor 1
V-raf	Serine/threonine-protein kinase-transforming protein raf
<i>vs</i>	Versus
ϵ	molar absorptivity
Θ	MOLAR ELIPTICIY
λ_{em}	Wavelength of emission
λ_{ex}	Wavelength of Excitation
π	pi

CHAPTER 1: GENERAL INTRODUCTION INTO THE SELF-ASSEMBLY AND BIOLOGICAL FUNCTION OF SiRNAs IN CANCER DETECTION AND THERAPY

1.1 SiRNA STRUCTURE AND FUNCTION IN THE RNAi PATHWAY

Ribonucleic acid (RNA) is a biomacromolecule that is essential in various biological roles such as coding, regulation, and expression of genes. Similar to DNA, RNA consists of a long polynucleotide chain composed of nucleotide building blocks linked via phosphodiester bonds. Unlike DNA, RNA is more often found in nature as a single-stranded biological polymer with a high tendency to fold onto itself (self-fold), forming a wide range of RNA secondary structures, including hairpins, loops, junctions and double-stranded hybrid motifs that are self-assembled via intramolecular hydrogen bonding. DNA and RNA are also distinguished by variances within their structures (**Figure 1.1**), which includes: 1) RNA and DNA contain adenine, cytosine and guanine bases, but thymine is found in DNA and uracil in RNA. 2) RNA contains a 2' hydroxyl on the sugar backbone while DNA does not. These hydroxyl groups make RNA less stable than DNA because it is more prone to hydrolysis, which leads to isomerization and cleavage of the 3'-5'-phosphodiester bonds. Due to this innate difference in stability, DNA was selected for the function of the storage and transmission of genetic information in cells. Studies on the origin of life have shown that DNA and RNA might have evolved from nucleic acid building blocks, which may have self-assembled into structures that represents RNA as the starting point of the "RNA World" hypothesis.¹⁻³ In this model, RNA was found to be the original scaffold for storing and expressing genetic information into the evolution of life on earth.² Most 'RNA World' hypotheses include three basic assumptions: (1) genetic continuity was assured by the replication of RNA; (2) Watson-Crick base pairing is the key to replication; and (3) genetically encoded proteins were not involved as catalysts.²

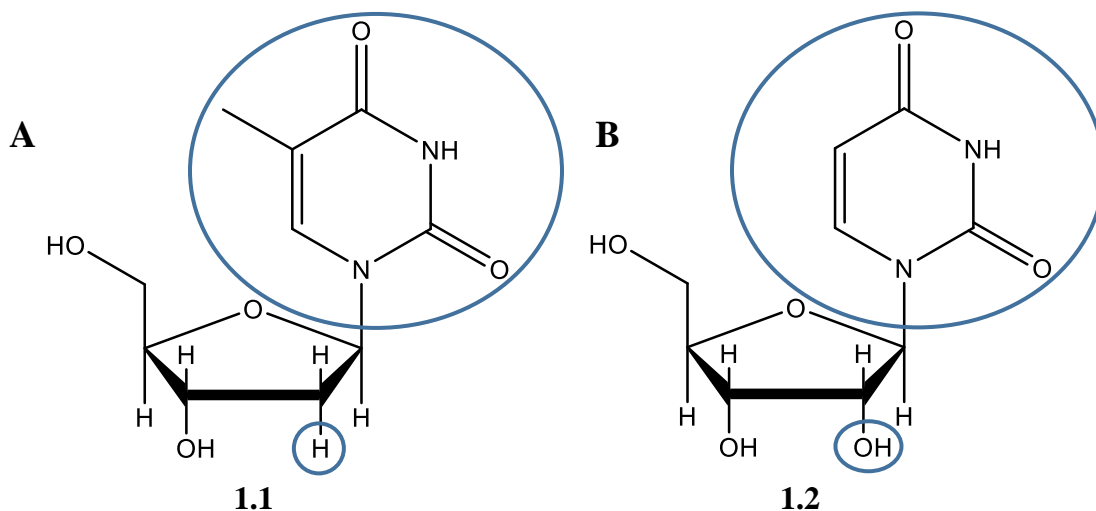


Figure 1.1 Structural comparison of thymidine, (**A**), and ribouridine, (**B**), differences circled in blue. Drawn in ChemDraw.

RNAs have played a pivotal role in the central dogma of molecular biology.^{4,5} In general, cellular organisms use messenger RNA (mRNA) to transfer genetic information that is transcribed from DNA and translated into functional proteins. Importantly, the primary transcript of mRNA, called pre-mRNA, undergoes a series of post-transcriptional modifications, including capping of the 5' end with a 7-methylguanine nucleotide diphosphate, the incorporation of a polyadenylate tail at the 3' end and numerous splicing reactions, which remove the non-coding sequences, introns, and splice together the coding regions, exons. RNAs that are used for purposes other than protein synthesis are called as noncoding RNAs (ncRNAs); numerous ncRNAs are responsible for the regulation of gene expression.^{6,7} In prokaryotic cells, small antisense RNAs (asRNAs) regulate gene expression by binding and inhibiting the expression of the target mRNA. In eukaryotic cells, many small ncRNAs exert inhibitory properties as well; among those, microRNAs (miRNAs)⁸ and small interfering RNA (siRNAs)^{9,10} are the most studied.

siRNAs are a class of double-stranded RNA (dsRNA) molecules, 20-25 base pairs in length, that operate within the RNA interference (RNAi) pathway, similar to miRNAs.¹¹ In this pathway, the siRNAs exhibit their inhibitory activity by silencing mRNA expression.¹² siRNAs can be naturally obtained by enzymatic processing of long dsRNAs by the Dicer enzyme.¹³ These siRNA fragments have a well-defined structure, consisting of phosphorylated 5'ends and hydroxylated 3'ends containing two overhanging nucleotides (**Figure 1.2**).^{14,15}

miRNA versus siRNA

	Occurrence	Configuration	Length	Complementarity to target mRNA	Biogenesis	Action	Function
miRNA	In plants and animals	Single stranded	19–25 nt	Not exact - a single miRNA may target hundreds of mRNAs	Expressed by genes whose purpose is to make miRNAs, but regulate genes (mRNAs) other than the ones that expressed them	Inhibit translation of mRNA	Regulators (inhibitors) of genes
siRNA	In plants and lower animals In mammals??	Double stranded	21–22 nt	100% perfect match, and therefore siRNAs knock down specific genes, with rare exceptions	Regulate the same genes that express them	Cleave mRNA	Gene-silencing in plants and animals that do not have antibody-or cell-mediated immunity

Figure 1.2 Differences between miRNA and siRNA. Reprinted with permission from Springer Nature: Mack, G.S. *Nature Biotechnol.* **2007**, 25 (6), 631–638.¹⁶

In the RNAi pathway, siRNAs are transfected into the cytoplasm of the cell with the use of a transfection reagent. A transfection reagent is a cationic polymer that can effectively condense and facilitate siRNA cell permeability.^{17,18} The siRNAs are released, via endosomal escape, and recruited into the RNA-Induced Silencing Complex (RISC). (**Figure 1.3**) The Argonaute (Ago2), protein which features a RNase III type domain, selects the antisense strand (guide strand),^{19,20}

and degrades the sense strand (non-guide strand) of the siRNA hybrid.²¹ The antisense strand serves as a template for mRNA recognition and binds to the complementary mRNA sequence. Cleavage sites for sense strand are located near the central region of the siRNA duplex. The 5' end, and not the 3' end, of the guide siRNA strand sets the position of mRNA cleavage.^{22,23} Degradation of mRNA prevents protein translation which may compromise cell-based function and cell viability. The latter can be applied in gene therapy strategies to effectively silence unwanted gene products and alter cell-based function.¹² The RNAi mechanism for silencing gene expression has received substantial attention since the pioneering work of Fire and Mello produced a full understanding of the RNAi pathway in *Caenorhabditis elegans* in 1998,²⁴ from which they were later awarded the Nobel Prize in 2006. Upon discovery, others quickly reported that synthetic siRNAs, introduced into cells by transfection, could induce RNAi in mammalian cells.⁹ Since in principle any gene²⁵ can be knocked down by synthetic siRNA through the RNAi pathway, it has become evident that this treatment strategy has immense potential in suppression of diseased gene targets. Thus, the RNAi strategy has been developed into a precise, efficient, stable and more potent technology for gene suppression when compared to pre-existing (*i.e.* antisense or antigene) strategies.²⁶

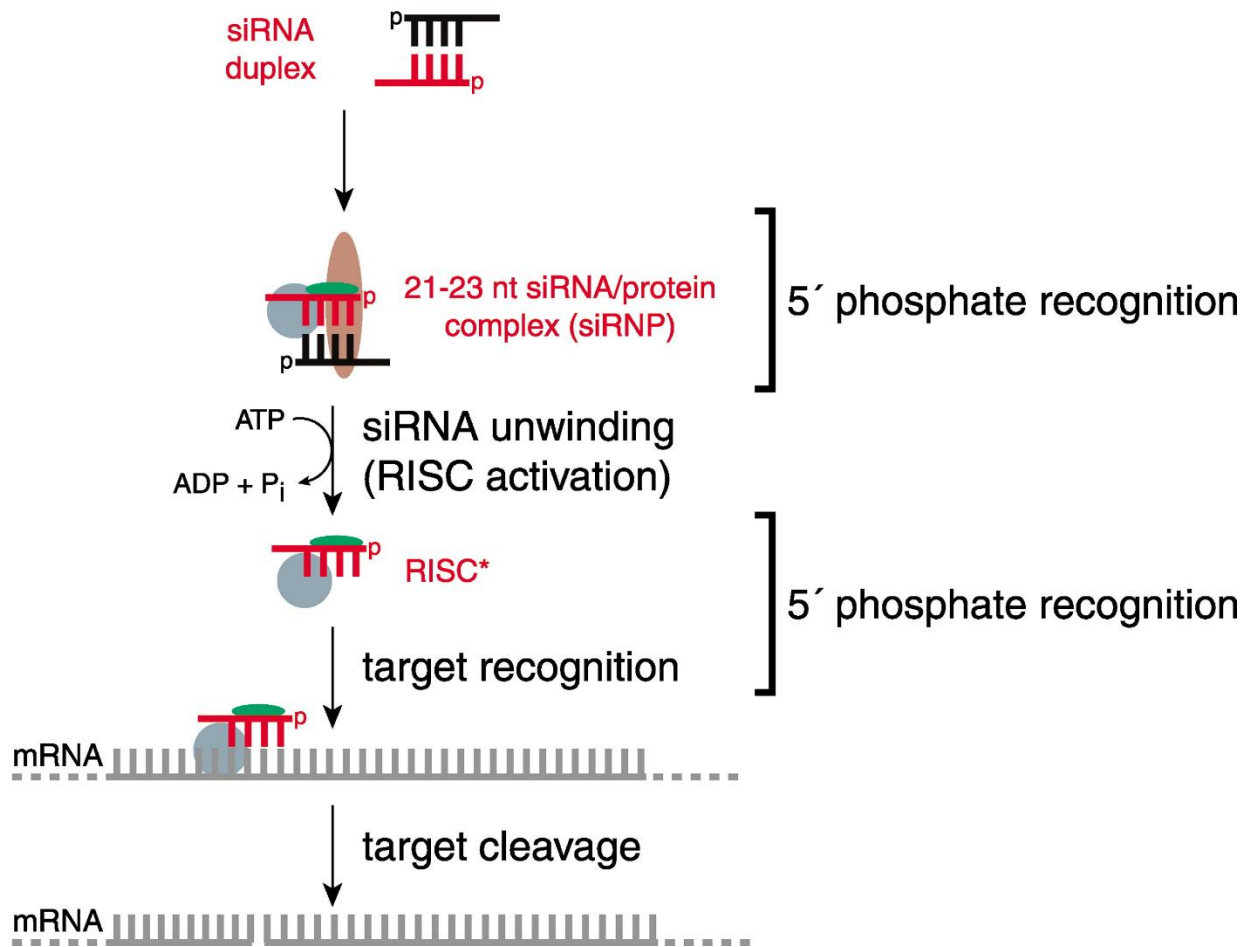


Figure 1.3 Schematic representation of siRNA mediated gene silencing via RNAi mechanism. Adapted with permission from Elsevier: Schwarz, D.S.; Hutvagner, G.; Haley, B.; Zamore, P.D. *Molecular Cell*. **2002**, *10* (3), 537-548.¹¹⁹

1.2 siRNA APPLICATIONS IN CANCER GENE THERAPY

The ability for siRNAs to silence target genes with high efficiency and specificity has stimulated efforts to develop these molecules into therapeutic agents. Oncogenes, mutated tumor suppressor genes and others involved in tumor progression are viable oncogene targets for silencing by the RNAi-based therapy approach. This important precision medicine strategy contains the capabilities of effectively targeting and inhibiting the expression of oncogenes with

high affinity and specificity when compared to non-specific chemo- or radio-therapies or invasive surgical procedures. RNAi-based therapy is especially compelling with difficult or undruggable oncoprotein targets that may be effectively suppressed by silencing their oncogene expression upstream.²⁷ The major advantage of RNAi in cancer therapy is the ability to target multiple genes in the various cellular pathways involved in tumor progression.²⁸ This RNAi screening strategy has been applied for the validation of important oncogene targets (**Table 1.1**).

Pathway	Target gene	Pathway	Target gene
Apoptosis	Bax ²⁹ Bcl-2 ^{30, 31}	Signaling	H-Ras, ³⁰ K-Ras ³⁷ PLK-1 ³⁸ TGF- β ³⁰ STAT3 ³⁹ EGFR ^{40,41} PKC- α ³⁰
Angiogenesis	Focal adhesion kinase (FAK) ²³²		
Adhesion	Matrix metalloproteinase ³³		
Cell-cell communication	VEGF ^{30,34}		
Lipid metabolism	Fatty acid synthase ³⁵		
Transport	MDR ³⁶	Viral, oncogenes, nuclear	LMP-1 ⁴² HPV E6 ⁴³ BCR-Ab1 ^{44,45} Telomerase ⁴⁶

Table 1.1 Cancer-associated genes targeted by siRNAs. Adapted from: Devi, G.R. *Cancer Gene Therapy*. 2006, 13 (9), 819-26.⁴⁷

Although siRNAs are promising candidates for cancer gene therapy, there are several challenges that must be overcome to help translate the application of siRNAs from pre-clinical to clinical utility. For example, un-modified (native) siRNAs are readily degraded within the cellular environment by nucleases they exhibit poor uptake and low resident time at desired cellular target sites which results in limited potency as well as a relatively high propensity of off-target side-effects.⁴⁸ The pursuit of clinically viable antisense drugs has led to the development of various strategies that can overcome these problems. Various carriers of siRNA have been developed to increase siRNA stability and loading efficacy within RNAi which, in turn leads to long-term knockdown of targeted genes.^{27,49} Carriers typically involve a positively charged vector (e.g., cationic cell-penetrating peptides, cationic polymers and lipids), lipid and polymer-based systems for encapsulating and releasing the siRNA at the target sites.^{27,50} Despite the challenges, the effectiveness of siRNA therapies has been extensively demonstrated in preclinical studies, and some have already entered clinical trials for the treatment of cancer and several other diseases.^{51,52} **(Table 1.2)** Therapeutic siRNAs can be designed to target various biological targets (markers) in cancer, including those related to: (1) cell-cycle: polo-like kinase 1 (PLK1),⁵³ kinesin spindle protein (KSP),⁵⁴ and ribonucleotide reductase M2 subunit (RRM2);⁵⁵ (2) signaling: KRAS(G12D);⁵⁶ (3) proliferation: protein kinase N3 (PKN3)^{57,58} and tenascin C;⁵⁹ and (4) angiogenesis: vascular endothelial growth factor (VEGF).^{30,34}

Therapeutic siRNAs	Target	Pharmaceutical Company
ALN-RSV01	RSV nucleocapsid	Alnylam Pharmaceuticals
ALN-TTR02	transthyretin (TTR)	Alnylam Pharmaceuticals
PF-04523655 (formerly known as RTP-801i)	HIF-1-responsive gene, RTP801	Quark Pharmaceuticals
QPI-1002	p53	Quark Pharmaceuticals
Excellair	spleen tyrosine kinase (SYK)	Zabecor Pharmaceuticals
ALN-VSP	VEGF gene, kinesin spindle (KSP) protein gene	Alnylam Pharmaceuticals
CALAA-01	M2 subunit of ribonucleotide reductase (RRM2) gene	Calando Pharmaceuticals
Atu-027	protein kinase N3 gene	Silence Therapeutics
PF-655 (formerly REDD14NP and RTP801i)	RTP801 gene	Quark Pharm
QPI-1007	caspase-2 gene	Quark Pharm
AGN211745	VEGF-R1 gene	Sirna Therapeutics
ApoB SNALP	apolipoprotein B gene	Tekmira Pharmaceuticals
RXI-109	connective tissue growth factor (CTGF) gene	RXi Pharmaceuticals
SYL040012	β_2 -adrenergic receptor gene	Sirna Therapeutics
Bevasiranib	VEGF gene	OPKO Health
AGN21174	VEGF-R1 gene	Allergan
SPC2996	Bcl-2 gene	Santaris Pharma

Table 1.2 Therapeutic siRNAs in clinical development. Adapted from: Chakraborty, C.; Sharma, A. R.; Sharma, G.; Doss, C.G.P.; Lee, S. *Molecular Therapy. Nucleic Acids*. **2017**, 8, 132–143.⁶⁰

1.3 METHODS AND APPLICATIONS OF SIRNA SELF-ASSEMBLY AND NON-COVALENT CONJUGATION FOR THERAPEUTICS

Most biologically active RNAs, including mRNA, transfer RNA (tRNA), ribosomal RNA (rRNA) and other ncRNAs contain self-complementary sequences which templates RNA folding⁶¹ and self-pairing to form double-stranded RNA (dsRNA) helices as well as other

secondary structures. The unique ability for RNA to self-assemble as well as interact with other biological molecules makes RNA a promising tool for a variety of applications in nanomedicine and synthetic biology.⁶²⁻⁶⁶ There are two main RNA self-assembly strategies; template and non-template self-assembly. Template assembly involves the interaction of RNA molecules under the influence of specific external sequences, forces, or spatial constraints which helps pre-organize intermolecular RNA folding interactions. In contrast, non-template assembly involves the formation of larger structures by individual components without the influence of external forces and is a contributing factor in RNA self-folding. Single-stranded RNA (ssRNA) assembly is one of at least four distinct types of RNA self-assembly strategies.⁶⁷ ssRNA assembly relies on complementary RNA that self-assemble through kinetic and thermodynamically driven Watson-Crick base pairing or hydrogen-bonding interactions. The ability of RNA to produce kinetically controlled self-assemblies using the endogenous transcription machinery has gained widespread attraction in the formation of bio-synthetic RNA nanostructures *in-vitro* or *in-vivo*.⁶⁸⁻⁷¹

The application of functional, self-assembled RNAs is contingent on efficient and biocompatible cell delivery methods. There are two broad strategies for RNA delivery into cells, tissues and live organisms. RNA can be condensed into an ionic complex to form a nanocarrier or RNA can be directly chemically modified, most commonly with a targeting ligand, while preserving the molecular nature of the conjugate that is amenable to RNA intracellular delivery (**Figure 1.4**). A fundamental difference between the two approaches lies in the size of the delivery moiety, nanoscale versus macro scale, which has profound effects on the biological distribution and actions of the transfected RNA. A commonly used delivery approach in pre-clinical and clinical applications is related to the formation of ionic complexes in between the negatively charged RNAs with the cationic lipids, thus forming lipid nanoparticles (LNPs).⁷²⁻⁷⁴ LNPs are

especially useful for therapeutic siRNAs⁷⁵ delivery and have been successfully applied in clinical trials.⁷⁶ While LNPs are effective as cell culture siRNA transfection agents, their use *in vivo* is limited. Another common approach involves the direct complexation of RNA with cationic molecules that have some degree of endosomal escape capability that is inherent in their chemistry. This would include formation of nanoscale polyplexes involving cell penetrating peptides (CPPs),^{77,78} cationic dendrimers such as PAMAMs^{79,80} or linear or cross-linked poly ethyleneimine (PEI).⁸¹ CPPs have been extensively studied in siRNA delivery applications due to their inherent abilities to form stable ionic complexes that can efficiently penetrate the cell membrane and release the siRNAs intracellularly for RNAi activity.⁸²⁻⁸³ Moreover, CPPs are biocompatible and exhibit minimal toxicity or immunostimulatory effects. Cancer targeting peptides (CTPs) are also utilized in siRNA delivery. These peptides are designed to target specific receptors located at the cell surface, which allows for targeted delivery of siRNA. CTPs have been conjugated with siRNAs⁸⁴⁻⁸⁶ while CPPs are formulated into stable ionic complexes for RNAi application.^{87,88} These are usually in the 100–200 nm range with a surface charge density that depends on the chemistry of the CPP and the ratio of cationic peptide to siRNA.

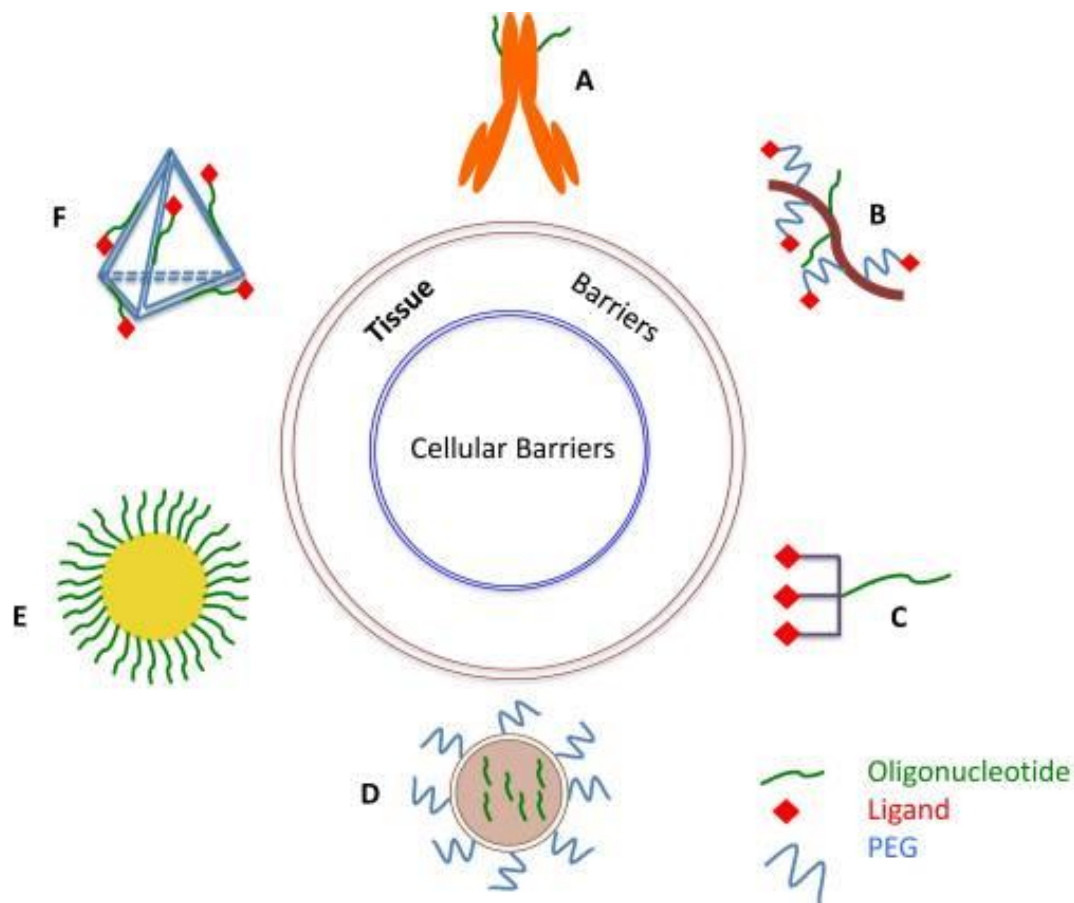


Figure 1.4: Oligonucleotide delivery strategies. (A) Antibody-oligonucleotide conjugate. (B) Polymer-oligonucleotide conjugate with PEGylation and targeting ligand. (C) Molecular scale ligand-oligonucleotide conjugate with triantennary carbohydrate ligand. (D) Lipid nanoparticle with PEGylation. (E) Gold nanoparticle with dense oligonucleotide coat. (F) DNA nanostructure with oligonucleotide and targeting ligand incorporated. Reprinted with permission from Oxford University Press: Juliano, R.L. *Nucleic Acids Research*. **2016**, 44 (14), 6518–48.⁸⁹

1.4 COVALENT BIOCONJUGATION STRATEGIES WITH siRNA

Covalent modifications of siRNAs have also been developed to help improve cell permeability and RNAi activity. siRNA modifications have been introduced at the 5' and 3' termini as well sequence modifiers which introduces chemically modified RNA during solid phase synthesis. Solid phase synthesis of RNA bioconjugates provides the ability to effectively

synthesize the desired bioconjugate on solid support. Solid phase conjugation allows the use of excess reagents to push the reaction towards completion. Upon completion, excess reagents are simply washed away leaving behind the desired bioconjugate to be subsequently cleaved from the solid support and purified. In certain cases, however, solution phase conjugation is the method of choice particularly when the conjugate moiety is unstable under typical ammonia cleavage conditions.⁹⁰⁻⁹² Several types of reversible and irreversible linkages have been exploited in siRNA conjugation chemistry. Bio-orthogonal conjugation approaches have received special attention in this area. These post-synthetic conjugation methods can be efficiently utilized in both solid supported and solution phase synthesis.

A common modification in siRNA conjugation chemistry consists of a reactive primary amine which forms an irreversible amide bond when reacted with an activated carboxyl group,⁹³ or a thiourea linkage upon reaction with an isothiocyanate.⁹⁴ Another valuable conjugation strategy involves the use of sulfur containing linkages such as disulfides.⁹⁵ Disulfides are interesting linkages due to their reversible nature under redox conditions. The cytosol within the cellular environment is typically a reducing environment, which allows the disulfide-linked siRNAs to be liberated for RNAi activity. Synthesis of disulfide linkages can be obtained by reaction of free thiol group with an adjacent reactive thiol. The use of “click-chemistry”, also known as Huisgen 1,3-dipolar cycloaddition, has also been developed for functionalizing oligonucleotides.⁹⁶ The click reaction usually works with high efficiency and involves a Cu(I)-catalyzed azide-alkyne cycloaddition (CuAAC), forming a stable triazole linkage in aqueous solvents at room temperature. This reaction, however, requires the removal of the copper catalyst from the reaction mixture which may be cytotoxic in biological assays. Alternatively, copper-free click reactions have recently been developed by using strained cyclooctyne derivatives, which reacts with an azide

moiety very efficiently, without any catalyst and the reaction can be performed in aqueous medium.^{97,98} A wide range of chemically reversible and irreversible covalent linkages have been developed to functionalize siRNAs with new reporter groups and bio-active probes that have served to improve the biological activity of siRNAs in live cells and *in vivo* applications (**Figure 1.5**).

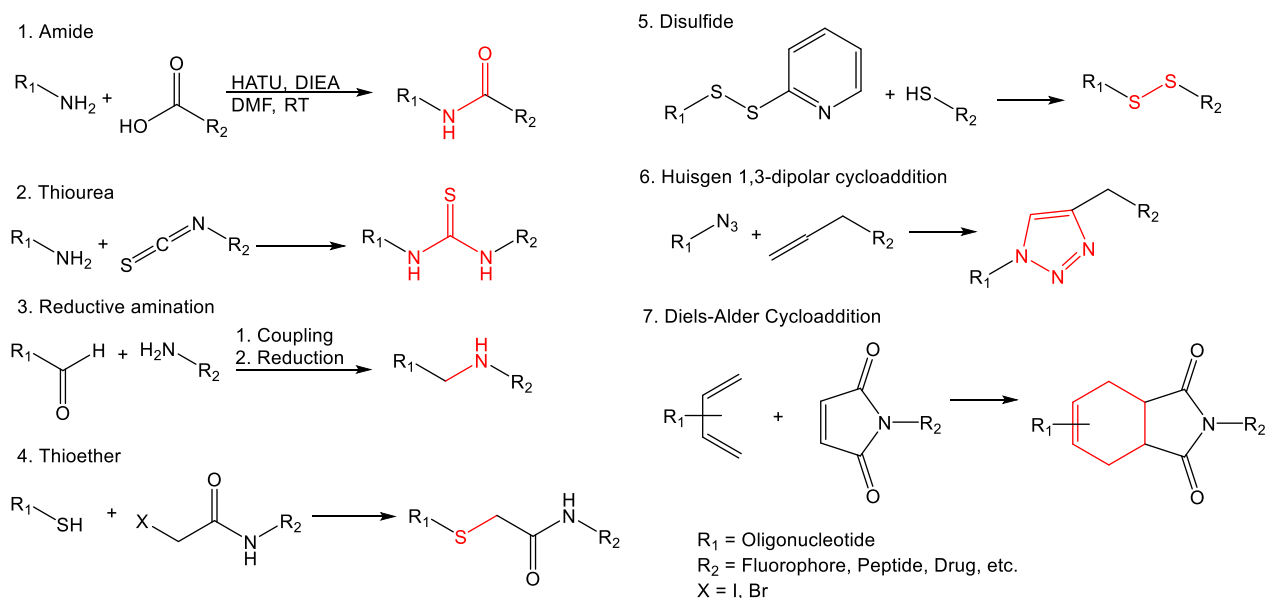


Figure 1.5 Examples of solution and solid-phase oligonucleotide bioconjugation strategies. Drawn in ChemDraw. For more examples see: Singh, Y.; Murat, P.; Defrancq, E. *Chem. Soc. Rev.* **2010**, 39, 2054-2070.⁹¹

1.5 APPLICATION OF FLUORESCENT siRNAs IN LIVE CELL IMAGING AND GENE THERAPY

siRNA bioconjugates have been extensively applied as theranostic (therapeutic and diagnostic) agents in oncology in order to specifically detect and treat the malignant tumor at the localized site in a preventative precision medicine strategy. Moreover, the introduction of fluorescent probes represents an important development in siRNA conjugation and are widely used in real time PCR, flow cytometry, intracellular localization and detection of molecular

interactions.^{99,100} Labeling of the siRNAs with a fluorescent reporter is typically achieved at either the 3' or 5' terminus but labeling can also be achieved on nucleobases (mainly at the C-5 position of pyrimidines) as well as on the sugar backbone.¹⁰¹ To date, a large number of fluorescence probes have been designed for labeling the biomolecules and investigating their structure, biophysical and biological properties.¹⁰² A common fluorescent probe(s) used for imaging within the cellular environment are the cyanine family of dyes.

Cyanine dyes (Cy3, **1.7**, and Cy5, **1.8**) are composed of two indole rings and three or five methine (CH) groups (**Figure 1.6**). Its advantages include sharp absorption bands, high extinction coefficients, great photo-stability and low pH sensitivity.¹⁰³ These cyanine dyes also have unique properties when conjugated within the same siRNA; they can function as fluorescence resonance energy transfer (FRET) probes. A siRNA-based molecular beacon was developed for the detection and knockdown of telomerase expression in human breast cancer cells.¹⁰⁴ The molecular beacon, containing the FRET pair (Cy3/ Cy5), was activated upon binding to the telomerase messenger RNA in cells. Aside from reported gene-silencing (~80%), the activation of the molecular beacon in cancer cells facilitated visualization of live cell images that were collected by with fluorescence microscopy. Although the Cy3 and Cy5 dyes have been used siRNA applications, their incorporation have been mostly limited to the sense strand. It has been assumed that modifications at the 5' terminus of the antisense strand negatively influences RISC incorporation of the siRNA bioconjugates.¹⁰⁵ This is partly due to the requirement of a 5' phosphate for siRNA incorporation into RISC. To test whether the introduction of a fluorescent probe on the antisense strand would have an adverse effect on siRNA silencing, siRNA that was either unlabeled, labeled with Cy3 alone (on the antisense stand), or doubly labeled with Cy3 on the antisense strand and FAM on the sense strand was administered to immortalized human pancreatic endocrine cell lines targeting the

3' untranslated region (UTR) of c-myc.^{106,107} Labeled and unlabeled siRNA performed similarly in this study clearly demonstrating that the labeled and unlabeled siRNAs were equally capable of reducing protein expression, whereas the samples transfected with labeled and unlabeled scrambled control siRNAs showed no silencing of the targeted c-myc gene.

Carboxyfluorescein (FAM) is another commonly used fluorescein derivative; its advantages include efficient synthetic incorporation, stability in water and excellent fluorescence emission quantum yields with limited photobleaching. FAM can bind to biological macromolecules by two carboxyl groups and be widely used for labeling proteins and nucleic acids in biomedical research.^{108,109} With siRNA therapeutics on the rise, companies like Glen Research and ChemGenes, among others, now offer numerous fluorescent probes within commercially available RNA phosphoramidites for their incorporation within RNA sequences by automated solid phase synthesis. **(Figure 1.6)** Examples include: fluorescein variants FAM (**1.3**), HEX (**1.4**), TET (**1.5**), ROX (**1.6**); cyanine dyes: Cy3 (**1.7**), Cy5 (**1.8**), and Cy7(**1.9**), Alexafluor (**1.10**; fluorescein replacement) and AquaPhlor® (**1.11**; Glen Research). These products are designed to cover a wide range of fluorescence excitation and emission profiles making them extremely desirable to researchers.

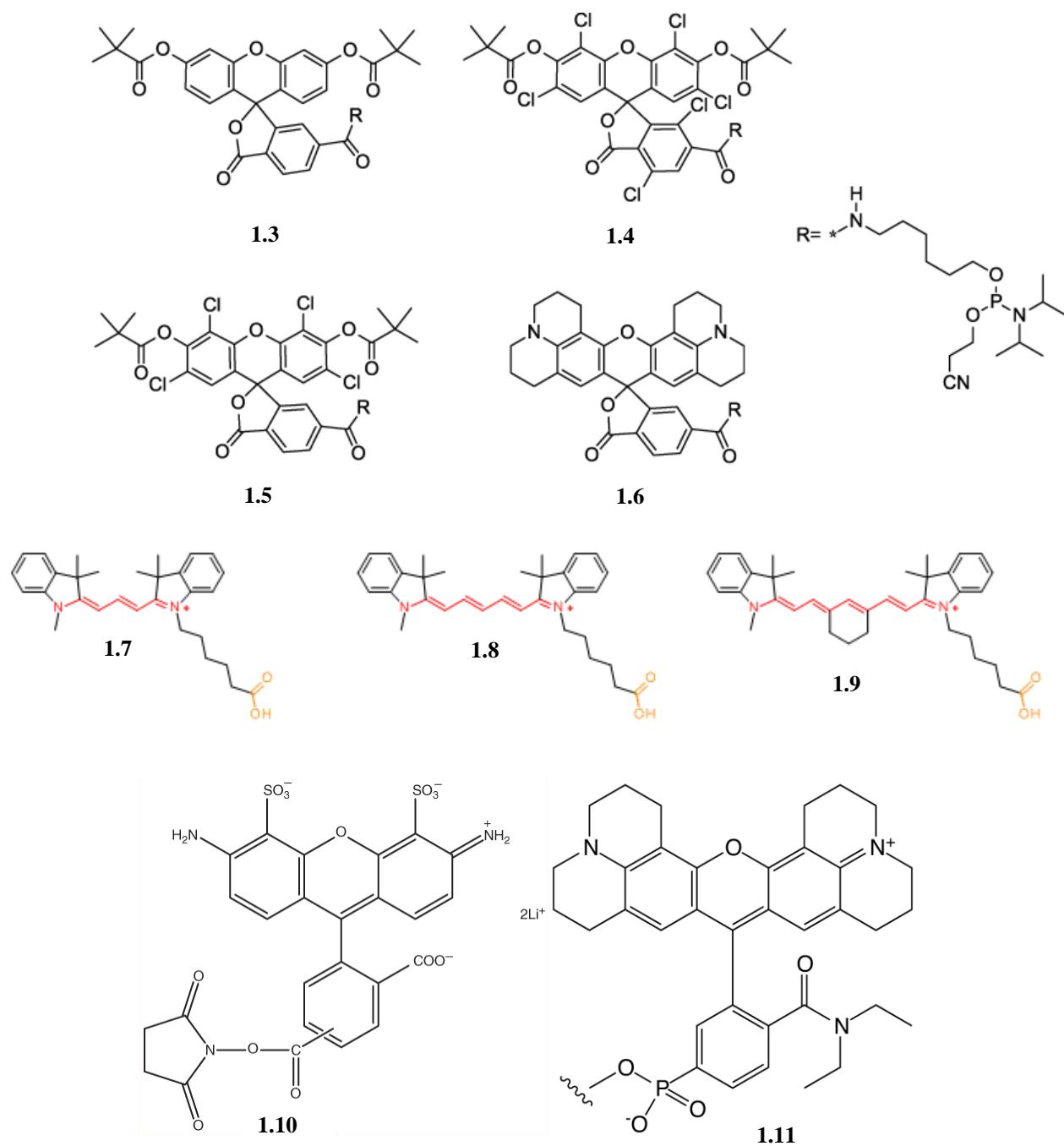


Figure 1.6 Structures of Fluorescent Dyes utilized in Oligonucleotide Modifications

As previously mentioned, FRET probes have significant utility in not only tracking siRNA transfection efficiency, but also siRNA stability within the cellular matrix. When two fluorophores

(donor and acceptor) are in close proximity, excitation of the donor results in transmission of the energy to the acceptor, which emits light at longer wavelengths. If the light filter does not transmit the donor background emission, only acceptor fluorescence is seen when the donor is excited. FRET-based labeling and imaging allows for non-destructive and non-invasive assessment of the state of siRNAs in cultured cells. RNAi efficiency of siRNA duplexes is superior to ssRNA by several orders of magnitude¹¹⁰ clearly illustrating the importance of tracking the stability and location of the siRNA duplex in the cell. Labeling only one strand of the siRNA duplex does allow monitoring of siRNA transfection efficiency but provides limited information on siRNA based activity in live cells. Therefore, the use of FRET probes enabled siRNA mechanistic studies and imaging of its activity in live cells as well as *in vivo*.¹¹¹⁻¹¹³

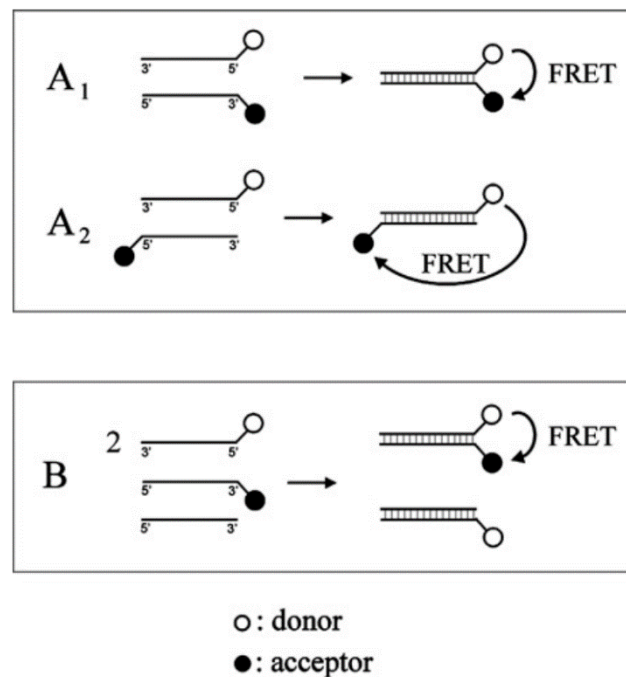


Figure 1.7 Representation of FRET probe detection of siRNA duplex stability. Reprinted with permission from Springer Nature: Gruber, M.; Wetzl, B.; Oswald, B.; Enderlein, J.; Wolfbeis, O.S. *J Fluoresc.* **2005**, *15* (3), 207-214.¹¹⁴

1.6 THESIS OBJECTIVES

This thesis highlights significant advances in the field of siRNA functionalization for theranostic applications in the precision detection and treatment of cancer. The identification of the Glucose Regulated Protein of 78 kilodaltons (GRP78) as a biological marker in tumors that is typically over-expressed and cell surface localized on a variety of cancer cell types^{115,116} forms the basis of our cancer-targeted gene therapy strategy. In our novel approach, linear, V- and Y-shape siRNAs have been designed to target GRP78, GRP94 and GRP75, three main glucose regulated chaperones within the unfolded protein response system (UPR).¹¹⁶ The UPR is a cellular stress response related to the endoplasmic reticulum (ER) stress.¹¹⁷ The UPR is activated in response to an accumulation of unfolded or misfolded proteins in the lumen of the endoplasmic reticulum. The UPR has three aims: 1) to restore normal function of the cell by halting protein translation, 2) degrading misfolded proteins, and 3) activating the signaling pathways that lead to increasing the production of molecular chaperones involved in protein folding. If these objectives are not achieved within a certain time span or the disruption is prolonged, the UPR triggers cell-based apoptosis. In this cancer intervention strategy, we aim to target and silence the three main GRPs within the UPR in an effort to potentiate a synergistic gene silencing effect which may lead to more effective cancer cell death.

Chapter 2 of this thesis will focus on the initial development of our RNAi nanotechnology approach in which we designed V- and Y-shape RNA templates which held the propensity to self-assemble into discrete, higher-ordered siRNA nanostructures targeting the oncogenic glucose regulated chaperones in a panel of cancer cell lines (**Figure 1.8**). These siRNAs self-assembled into genetically encoded spheres, triangles, squares, pentagons and hexagons of discrete sizes and shapes according to TEM imaging and DLS measurements. In a 24-sample siRNA screen

conducted within the AN3CA endometrial cancer cells known to overexpress tumorigenic GRP78, the self-assembled siRNAs targeting multiple sites of GRP78 mRNA demonstrated more potent and long-lasting anticancer activity relative to their linear controls. The self-assembled siRNA hybrids targeting of GRP-75, 78 and 95 resulted in significant (50- 95%) knockdown of the glucose regulated chaperones, which led to synergistic effects in tumor cell cycle arrest (50-80%) and death (50-60%) within endometrial (AN3CA), cervical (HeLa) and breast (MDA-MB-231) cancer cell lines. Taken together, these results validate that the self-assembled, GRP-targeting siRNA nanostructures exhibit potent silencing of GRP expression resulting in significant cell death effects in tumor cells that exhibit a strong dependence on GRP activity and the UPR.¹¹⁸

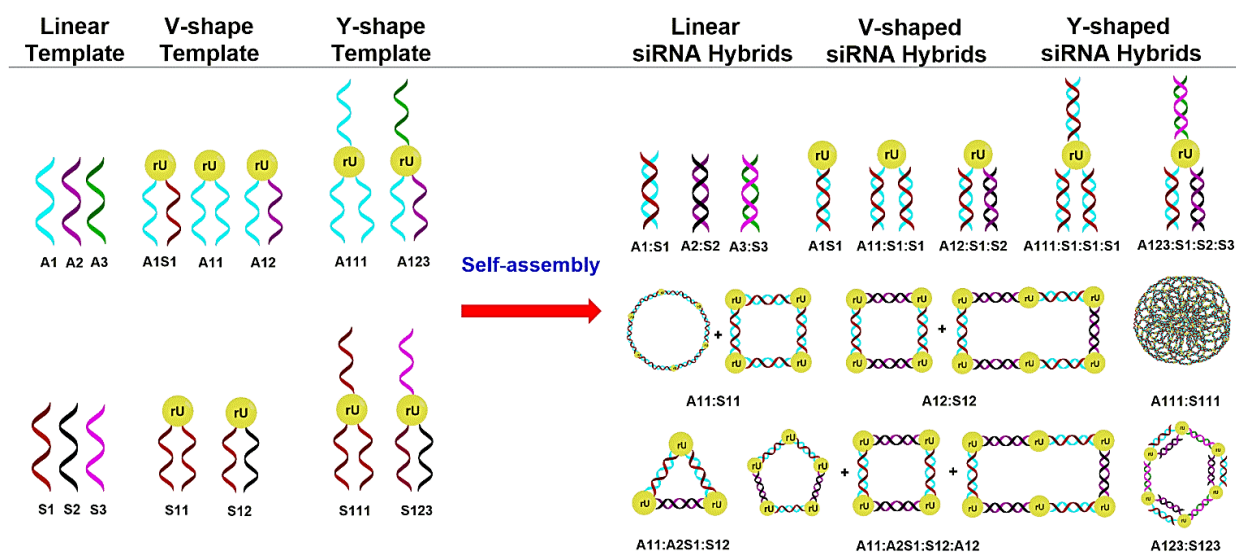


Figure 1.8 Design and self-assembly of siRNA nanostructures. The RNA templates, namely, linear, V- and Y-shaped RNA were designed and synthesized according to our previously described methodology.¹¹ The V- and Y-shaped templates incorporate a branchpoint ribouridine (rU) which facilitates the hybridization of complementary sense (S) and antisense (A) RNA. These templates preorganizes the self-assembly of siRNA hybrid nanostructures having discrete sizes and shapes, including those belonging to circles, triangles, squares, rectangles, pentagons, hexagons and porous-type structures. These siRNA nanostructures are genetically encoded to target a single (1), double (1, 2) and triple (1, 2, 3) sites of oncogenic GRP-75, 78 and 94 mRNA. Reprinted with permission: Patel MR, Kozuch SD, Cultrara CN, Yadav R, Huang S, Samuni U, Koren J 3rd, Chiosis G, Sabatino D. *Nano Lett.* **2016**, 16(10), 6099–6108. Copyright 2016 American Chemical Society.

Chapter 3 will focus on expanding the potential clinical utility of these V and Y-shaped higher ordered siRNA motifs while shedding insight into their mechanism of internalization and RNAi activity in live cancer cells with the incorporation of a fluorescent probe, FITC, covalently bound to the siRNA constructs (**Figure 1.9**). Interestingly, the fluorescent label is conjugated to the antisense strand, for linear and V-shaped hybrids, and the sense linear strands for Y-shaped hybrids. The fluorescently labeled siRNA were characterized by UV-Vis and fluorescence spectroscopy, which confirmed their photo-physical properties while PAGE, T_m and CD spectroscopy validated the hybrid stabilities and siRNA A-type helical structures for their RNAi applications in cancer cells. The fluorescently labeled antisense strand will potentially allow for extended fluorescence-based imaging of siRNA activity in live cells.

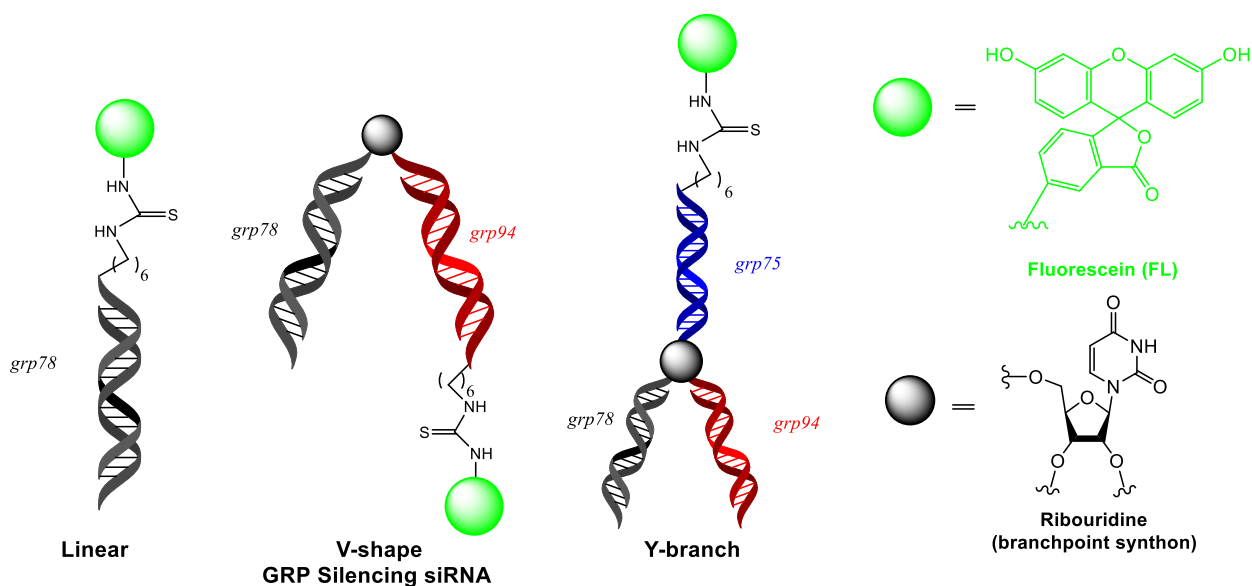


Figure 1.9 Rational design of linear, V- and Y-shaped siRNAs containing a covalently linked FITC probe. Drawn with ChemDraw.

1.7 REFERENCES

- 1) Gilbert, W. *Nature* **1986**, 319, 618.
- 2) Robertson, M.P.; Joyce, G.F. *Cold Spring Harbor Perspectives in Biology*. **2012**, 4 (5), a003608
- 3) Cech, T.R. *Cold Spring Harbor Perspectives in Biology*. **2012**, 4 (7), a006742.
- 4) Cech, T.R.; Zaugg, A.J.; Grabowski, P.J. *Cell*. **1981**, 27, 487-496.
- 5) Guerrier-Takada, C.; Gardiner, K.; Marsh, T.; Pace, N.; Altman, S. *Cell*. **1983**, 35, 849-857.
- 6) Grosshans, H., Filipowicz, W. *Nature*. **2008**, 451, 414-416.
- 7) Mattick, J. S. *PLoS Genet*. **2009**, 5, e1000459.
- 8) Esteller, M. *Nature Rev. Genet*. **2011**, 12, 861-874.
- 9) Elbashir, S. M.; Harborth J.; Lendeckel, W.; Yalcin, A.; Weber, K.; Tuschl, T. *Nature*. **2001**, 411, 494– 498.
- 10) Hannon, G. J.; Rossi, J. J. *Nature*. **2004**, 431, 371-378.
- 11) Khvorova, A.; Reynolds, A.; Jayasena, S.D. *Cell*. **2003**, 115, 209–216.
- 12) Agrawal, N.; Dasaradhi, P.V.; Mohmmmed, A.; Malhotra, P.; Bhatnagar, R.K.; Mukherjee, S.K. *Microbiol. Mol. Biol. Rev.* **2003**, 67 (4), 657–685.
- 13) Bernstein, E.; Caudy, A.A.; Hammond, S.M.; Hannon, G.J. *Nature*. **2001**, 409 (6818), 363–366.
- 14) Zamore, P.D.; Tuschl, T.; Sharp, P.A.; Bartel, D.P. *Cell*. **2000**, 101 (1): 25–33.
- 15) Vermeulen, A.; Behlen L.; Reynolds, A.; Wolfson, A.; Marshall, W.; Karpilow, J.; Khvorova, A. *RNA*. **2005**, 11 (5), 674–682.
- 16) Mack, G.S. *Nature Biotechnol.* **2007**, 25 (6), 631–638.
- 17) Dalby, B.; Cates, S.; Harris, A.; Ohki, E.C.; Tilkins, M.L.; Price, P.J.; Ciccarone, V.C. *Methods*. **2004**, 33 (4), 94-103.
- 18) Jensen, K.; Anderson, J.A.; Glass, E.J. *Veterinary Immunology and Immunopathology*. **2014**, 158 (3-4), 224-232.
- 19) Siomi, H.; Siomi M.C. *Nature*. **2009**, 457 (7228), 396–404.
- 20) Preall, J.B.; He, Z.; Gorra, J.M.; Sontheimer, E.J. *Current Biology*. **2006**, 16 (5), 530–535.
- 21) Gregory, R.I.; Chendrimada, T.P.; Cooch, N.; Shiekhattar, R. *Cell*. **2005**, 123 (4), 631–640.
- 22) Elbashir, S.M.; Lendeckel, W.; Tuschl, T. *Genes Dev*. **2001**, 15 (2), 188–200.
- 23) Elbashir, S.M.; Martinez, J.; Patkaniowska, A.; Lendeckel, W.; Tuschl, T. *EMBO J*. **2001**, 20 (23), 6877–6888.
- 24) Fire, A.; Xu, S.; Montgomery, M.K.; Kostas, S.A.; Driver, S.E.; Mello, C.C. *Nature*. **1998**, 391, 806–811.
- 25) Rossi, J.J.; Kim, D.H. *Nature*. **2007**, 8, 173-184.
- 26) Saurabh, S.; Vidyarthi, A.S.; Prasad D. *Planta*. **2014**, 239 (3), 543–564.
- 27) Wu, S.Y.; Lopez-Berestein, G.; Calin, G.A.; Sood, A.K. *Sci. Transl. Med.* **2014** 6 (240), ps7.
- 28) Burnett, J.C.; Rossi, J.J. *Chem. Biol*. **2012**, 19 (1), 60-71.
- 29) Grzmil, M., Thelen, P., Hemmerlein, B., Schweyer, S., Voigt, S., Mury, D.; Burfeind, P. *Am. J. Pathol.* **2003**, 163 (2), 543–552.
- 30) Yin, J.Q.; Gao, J.; Shao, R.; Tian, W.N.; Wang, J.; Wan, Y. *J. Exp. Ther. Oncol*. **2003**, 3 (4), 194–204.

- 31) Futami, T.; Miyagishi, M.; Seki, M.; Taira, K. *Nucleic Acids Res. Suppl.* **2002**, *2*, 251–252.
- 32) Duxbury, M.S.; Ito, H.; Benoit, E.; Zinner, M.J.; Ashley, S.W.; Whang, E.E. *Biochem. Biophys. Res. Commun.* **2003**, *311*, 786–92.
- 33) Sanceau, J.; Truchet, S.; Bauvois, B. *J. Biol. Chem.* **2003**, *278*, 36537–46.
- 34) Zhang, L.; Yang, N.; Mohamed-Hadley, A.; Rubin, S.C.; Coukos, G. *Biochem. Biophys. Res. Commun.* **2003**, *303*, 1169–78.
- 35) De Schrijver, E.; Brusselmans, K.; Heyns, W.; Verhoeven, G.; Swinnen, J.V. *Cancer Res.* **2003**, *63*, 3799–04.
- 36) Nieth, C.; Priebisch, A.; Stege, A.; Lage, H. *FEBS Lett.* **2003**, *545*, 144–150.
- 37) Lois, C.; Refaeli, Y.; Qin, X.F.; Van Parijs, L. *Curr Opin Immunol.* **2001**, *13* (4), 496–504.
- 38) Spankuch-Schmitt, B.; Bereiter-Hahn, J.; Kaufmann, M.; Strebhardt, K. *J Natl Cancer Inst.* **2002**; *94* (24), 1863–77.
- 39) Konnikova, L.; Kotecki, M.; Kruger, M.M.; Cochran, B.H. *BMC Cancer.* **2003**, *3*, 23.
- 40) Nagy, P.; Arndt-Jovin, D.J.; Jovin, T.M. *Exp Cell Res.* **2003**, *285* (1), 39–49.
- 41) Zhang, M.; Zhang, X.; Bai, C.X.; Chen, J.; Wei, M.Q. *Acta Pharmacol Sin.* **2004**, *25*, 61–67.
- 42) Li, X.P.; Li, G.; Peng, Y.; Kung, H.F.; Lin, M.C. *Biochem Biophys Res Commun.* **2004**, *315* (1), 212–218.
- 43) Butz, K.; Ristriani, T.; Hengstermann, A.; Denk, C.; Scheffner, M.; Hoppe-Seyler, F. *Oncogene.* **2003**, *22* (38), 5938–45.
- 44) Wohlbold, L.; van der Kuip, H.; Miething, C.; Vornlocher, H.P.; Knabbe, C.; Duyster J.; Aulitzky, W.E. *Blood.* **2003**, *102*, 2236–39.
- 45) Wilda, M.; Fuchs, U.; Wossmann, W.; Borkhardt, A. *Oncogene.* **2002**, *21* (37), 5716–24.
- 46) Kosciolk, B.A.; Kalantidis, K.; Tabler, M.; Rowley, P.T. *Mol Cancer Ther.* **2003**, *2* (3), 209–16.
- 47) Devi, G.R. *Cancer Gene Therapy.* **2006**, *13* (9), 819-26.
- 48) Bora, R.S.; Gupta, D.; Mukkur, T.K.; Saini, K.S. *Mol Med Rep.* **2012**, *6* (1), 9–15.
- 49) Lam, J.K.; Chow, M.Y.; Zhang, Y.; Leung, S.W. *Mol Ther Nucleic Acids.* **2015**, *4*, e252.
- 50) Wang, J.; Lu, Z.; Wientjes, M.G.; Au, J.L. *AAPS J.* **2010**, *12* (4), 492-503.
- 51) Bakhtiyari, S.; Haghani, K.; Basati, G.; Karimfar, M.H. *Ther Delivery.* **2013**, *4* (1), 45-57.
- 52) Kanasty, R.; Dorkin, J.R.; Vegas, A.; Anderson, D. *Nat Mater.* **2013**, *12* (11), 967-77.
- 53) Reagan-Shaw, S.; Ahmad, N. *FASEB J.* **2005**, *19* (6), 611-13.
- 54) Cervantes, A.; Alsina, M.; Taberero, J.; Infante, J.R.; LoRusso, P.; Shapiro, G.; Paz-Ares L.G.; Falzone, R.; Hill, J.; Cehelsky, J.; White, A.; Toudjarska, I.; Bumcrot, D.; Meyers, R.; Hinkle, G.; Svrzikapa, N.; Sah, D.W.; Vaishnav, A.; Gollob, J.; Burris, H.A. *J Clin Oncol.* **2011**, *29*, 3025.
- 55) Zuckerman, J.E.; Gritli, I.; Tolcher, A.; Heidel, J.D.; Lim, D.; Morgan, R.; Chmielowski, B.; Ribas, A.; Davis, M.E.; Yen, Y. *Proc Natl Acad Sci USA.* **2014**, *111*, 11449-11454
- 56) Golan, T.; Khvalevsky, E.Z.; Hubert, A.; Gabai, R.M.; Hen, N.; Segal, A.; Domb, A.; Harari, G.; David, E.B.; Raskin, S.; Goldes, Y.; Goldin, E.; Eliakim, R.; Lahav, M.; Kopleman, Y.; Dancour, A.; Shemi, A.; Galun, E. *Oncotarget.* **2015**, *6* (27), 24560–70.
- 57) B. Schultheis. *J Clin Oncol.* **2016**, *34*

- 58) Schultheis, B.; Strumberg, D.; Santel, A.; Vank, C.; Gebhardt, F.; Keil, O.; Lange, C.; Giese, K.; Kaufmann, J.; Khan, M.; Dreves, J. *J Clin Oncol.* **2014**, *32* (36), 4141-48.
- 59) Rolle, K.; Nowak, S.; Wyszko, E.; Nowak, M.; Zukiel, R.; Piestrzeniewicz, R.; Gawronska, I.; Barciszewska, M.Z.; Barciszewski, J. *Cancer Biol Ther.* **2010**, *9* (5), 396-406
- 60) Chakraborty, C.; Sharma, A. R.; Sharma, G.; Doss, C.G.P.; Lee, S. *Molecular Therapy. Nucleic Acids.* **2017**, *8*, 132-143.
- 61) Tinoco, I.; Bustamante C. *J. Mol. Biol.* **1999**, *293* (2), 271-281.
- 62) Afonin, K.A.; Lindsay, B.; Shapiro, B.A. *DNA RNA Nanotechnol.* **2013**, *1*, 1- 15.
- 63) Grabow, W.; Jaeger, L. *FI000Prime Rep.* **2013**, *5*, 46.
- 64) Guo, P. *Nat. Nanotechnol.* **2010**, *5*, 833- 842.
- 65) Ishikawa, J.; Furuta, H.; Ikawa, Y. *WIREs RNA.* **2013**, *4* (6), 651-664.
- 66) Chakraborty, S.; Mehtab, S.; Krishnan, Y. *Acc. Chem. Res.* **2014**, *47* (6), 1710-19.
- 67) Grabow, W.W.; Jaeger, L. *Acc. Chem. Res.* **2014**, *47* (6), 1871-1880.
- 68) Afonin, K.A.; Kasprzak, W.K.; Bindewald, E.; Kireeva, M.; Viard, M.; Kashlev, M.; Shapiro, B.A. *Acc. Chem. Res.* **2014**, *47* (6), 1731-41.
- 69) Afonin, K.A.; Bindewald, E.; Yaghoubian, A.J.; Voss, N.; Jacovetty, E.; Shapiro, B.A.; Jaeger, L. *Nat. Nanotechnol.* **2010**, *5*, 676- 682.
- 70) Delebecque, C.J.; Lindner, A.B.; Silver, P.A.; Aldaye, F.A. *Science.* **2011**, *333*, 470- 474.
- 71) Afonin, K.A.; Kireeva, M.; Grabow, WW.; Kashlev, M.; Jaeger, L.; Shapiro, B.A. *Nano Lett.* **2012**, *12* (10), 5192-95.
- 72) Huang L.; Liu Y. *Annu. Rev. Biomed. Eng.* **2011**, *13*, 507-530.
- 73) Yin H.; Kanasty R.L.; Eltoukhy A.A.; Vegas A.J.; Dorkin J.R.; Anderson D.G. *Nat. Rev. Genet.* **2014**, *15*, 541-555.
- 74) Li, J.; Wang, Y.; Zhu, Y.; Oupickym D. *J Control Release.* **2013**, *172*, 589-600.
- 75) Leung A.K.; Tam Y.Y.; Cullis P.R. *Adv. Genet.* **2014**, *88*, 71-110.
- 76) Ozcan, G.; Ozpolat, B.; Coleman, R.L.; Sood, A.K.; Lopez-Berestein, G. *Adv Drug Deliv Rev.* **2015**, *8*, 108-19.
- 77) Lönn, P.; Dowdy, S.F. *Expert Opin Drug Deliv.* **2015**, *12* (10), 1627-36.
- 78) Kauffman, W.B.; Fuselier, T.; He, J.; Wimley, W.C. *Trends Biochem Sci.* **2015**, *40* (12), 749-64.
- 79) Zhao, J.; Feng S.S. *Nanomedicine (Lond).* **2015**, *10* (14), 2199-228.
- 80) Biswas, S.; Torchilin, V.P.; *Pharmaceuticals (Basel).* **2013**, *6* (2), 161-83.
- 81) Neuberg, P.; Kichler, A. *Adv Genet.* **2014**, *8*, 263-88.
- 82) Boisguérin, P.; Deshayes, S.; Gait, M.J.; O'Donovan, L.; Godfrey, C.; Betts, C.A.; Wood, M.J.; Lebleu, B. *Adv Drug Deliv Rev.* **2015**, *87*, 52-67.
- 83) Lehto, T.; Kurrikoff, K.; Langel, Ü. *Expert Opin Drug Deliv.* **2012**, *9* (7), 823-36.
- 84) Moschos, S.A.; Jones, S.W.; Perry, M.M.; Williams, A.E.; Erjefalt, J.S.; Turner, J.J.; Barnes, P.J.; Sproat, B.S.; Gait, M.J.; Lindsay, M.A. *Bioconjug Chem.* **2007**, *18*, 1450-59.
- 85) Alam, M.R.; Ming, X.; Fisher, M.; Lackey, J.G.; Rajeev, K.G.; Manoharan, M.; Juliano, R.L. *Bioconjug Chem.* **2011**, *22*, 1673-81.
- 86) Detzer, A.; Overhoff, M.; Wunsche, W.; Rompf, M.; Turner, J.J.; Ivanova, G.D.; Gait, M.J.; Sczakiel, G. *RNA.* **2009**, *15*, 627-36.
- 87) Beloor, J.; Zeller, S.; Choi, C.S.; Lee, S.K.; Kumar, P. *Ther Deliv.* **2015**, *6* (4), 491-507.

- 88) Ishihara, T.; Goto, M.; Kodera, K.; Kanazawa, H.; Murakami, Y.; Mizushima, Y.; Higaki, M. *Drug Delivery*. **2009**, *16* (3), 153-159.
- 89) Juliano, R. L. *Nucleic Acids Research*. **2016**, *44* (14), 6518–48.
- 90) Nair, J. K.; Willoughby, J.L.S.; Chan, A.; Charisse, K.; Alam, Md.R.; Wang, Q.; Hoekstra, M.; Kandasamy, P.; Kel'in A.V.; Milstein, S.; Taneja, N.; O'Shea, J.; Shaikh, S.; Zhang, L.; van der Sluis, R.J.; Jung, M.E.; Akinc, A.; Hutabarat, R.; Kuchimanchi, S.; Fitzgerald, K.; Zimmermann, T.; van Berkel, T.J.C.; Maier, M.A.; Rajeev, K.G.; Manoharan, M. *J. Am. Chem. Soc.* **2014**, *136*, 16958–61.
- 91) Singh, Y.; Murat, P.; Defrancq, E. *Chem. Soc. Rev.* **2010**, *39*, 2054-70.
- 92) Spinelli, N.; Defrancq, E.; Morvan, F. *Chem. Soc. Rev.* **2013**, *42*, 4557-73.
- 93) Aaronson, J.G.; Klein L.J.; Momose A.A.; O'Brien A.M.; Shaw A.W.; Tucker T.J.; Yuan Y.; Tellers D.M. *Bioconjug Chem.* **2011**, *22* (8), 1723-28.
- 94) Murakami, A.; Nakaura, M.; Nakatsuji, Y.; Nagahara, S.; Tran-Cong, Q.; Makino, K.; *Nucleic Acids Research*. **1991**, *19* (5), 4097-102.
- 95) Saito, G.; Swanson, J.A.; Lee, K.D. *Adv. Drug Deliv. Rev.* **2003**, *55*, 199-215.
- 96) Winkler, J. *Ther. Deliv.* **2013**, *4*, 791–809.
- 97) El-Sagheer, A.H.; Brown, T. *Chem. Soc. Rev.* **2010**, *39*, 1388-1405.
- 98) Agard, N.J.; Prescher, J.A.; Bertozzi, C.R. *J. Am. Chem. Soc.* **2004**, *126*, 15046–47.
- 99) Alabi, C.A.; Love, K.T.; Sahay, G.; Stutzman, T.; Young, W.T.; Langer, R.; Anderson, D.G. *ACS Nano* **2012** *6* (7), 6133-6141
- 100) Alabi, C.A.; Sahay, G.; Langer, R.; Anderson, D.G.; *Integr Biol (Camb)*. **2013**, *5* (1), doi:10.1039/c2ib20155k.
- 101) Asseline, U. *Curr. Org. Chem.* **2006**, *10*, 491–518.
- 102) Goncalves, M.S. *Chem. Rev.* **2009**, *109*, 190–212.
- 103) Moreira, B.G.; You, Y.; Owczarzy, R. *Biophysical Chemistry*. **2015**, *198*, 36–44.
- 104) Chang, E.; Zhu, M.Q.; Drezek, R. *Biotechnol J.* **2007**, *2*, 422–25.
- 105) Schwarz, D.S.; Hutvagner, G.; Haley, B.; Zamore, P.D. *Mol. Cell.* **2002**, *10*, 537-48.
- 106) Jarvis, R.A.; Ford, L.P. *TechNotes*. **2001**, *8* (5), 3-5.
- 107) Demeterco, C.; Itkin-Ansari, P.; Tyrberg, B.; Ford, L.P.; Jarvis, R.A.; Levine, F. *The Journal of Clinical Endocrinology & Metabolism*. **2002**, *87* (7), 3475–85.
- 108) Sohn, S.Y.; Bae, W.J.; Kim, J.J.; Yeom, K.H.; Kim, V.N.; Cho, Y. *Nat Struct Mol Biol.* **2007**, *14*, 847–53.
- 109) Wang, K.; Gao, Y.; Peng, X.; Yang, G.; Gao, F.; Li, S.; Yingguo, Z. *Mol. Biol. Rep.* **2010**, *37*, 2871–75.
- 110) Holen, T.; Amarzguioui, M.; Babaie, E.; Prydz, H. *Nucleic Acids Res.* **2003**, *31*, 2401–07.
- 111) Uhler, S.A.; Cai, D.; Man, Y.; Figge, C.; Walter, N.G. *J. Am. Chem. Soc.* **2003**, *125*, 14230–31.
- 112) Chiu, Y.L.; Dinesh, C.U.; Chu, C.Y.; Ali, A.; Brown, K.M.; Cao, H.; Rana, T.M. *D Chem. Biol.* **2005**, *12*, 643–48.
- 113) Raemdonck, K.; Remaut, K.; Lucas, B.; Sanders, N.N.; Demeester, J.; De Smedt, S.C. *Biochemistry*. **2006**, *45*, 10614–23.
- 114) Gruber, M.; Wetzl, B.; Oswald, B.; Enderlein, J.; Wolfbeis, O.S. *J Fluoresc.* **2005**, *15* (3), 207-214.
- 115) Lee, A.S. *Trends Biochem Sci.* **2001**, *26* (8), 504-10.

- 116) Lee, A.S. *Nat Rev Cancer*. **2014**, *14* (4), 263-76.
- 117) Schröder, M.; Kaufman, R.J. *Mutat Res*. **2005**, *569* (1-2), 29-63.
- 118) Patel, M.R.; Kozuch, S.D.; Cultrara, C.N.; Yadav, R.; Huang, S.; Samuni, U.; Koren, J.; Chiosis, G.; Sabatino, D. *Nano Letters* **2016** *16* (10), 6099-6108.
- 119) Schwarz, D.S.; Hutvágner, G.; Haley, B.; Zamore, P.D. *Molecular Cell*. **2002**, *10* (3), 537-548.

CHAPTER 2: DEVELOPMENT OF HIGHER-ORDER siRNA HYBRIDS FOR RNAI MEDIATED CANCER GENE THERAPY

2.1 Abstract

With the rapid expansion and advances that have been made in the field of RNA nanotechnology, the ability to design single siRNA nanostructures that can deliver multiple siRNAs presents an intriguing opportunity for screening of a wide range of oncogene targets while potentiating cancer gene therapy effects. This chapter will discuss the optimized synthesis strategy of a branchpoint amidite which can be incorporated within the solid phase synthesis of RNAs for the rapid production of novel V- and Y-shaped RNAs. A 5'-OLv 2'-OMMT ribouridine phosphoramidite was synthesized by a three-step solution phase synthesis approach in which the 5'-OLv and 2'-OMMT served as orthogonal protecting groups for the selective construction of asymmetric V- and Y-shape RNA on solid support. Automated solid phase RNA synthesis was used to produce the requisite linear, V- and Y-shape RNA. Following isolation and characterization by RP IP HPLC and ESI MS, the RNAs were hybridized with their complementary single stranded RNA to form the siRNA hybrids. The siRNAs were further characterized by a combination of native PAGE, UV-Vis and CD spectroscopy which confirmed hybrid structures and stabilities for their RNAi applications. The V- and Y-shape RNA effectively served as templates for the self-assembly of hybrid siRNAs targeting multiple oncogenes related to overexpression of the Glucose Regulated Proteins (GRPs). The GRPs function as chaperones mediating protein folding events in all cell types. In cancer, the GRPs are overexpressed and cell surface localized where they mediate tumorigenic behavior. In this study, the linear, V-, and Y-shape siRNAs adopted genetically encoded shapes targeting GRP-75, 78 and 94 in a panel of tumorigenic cell lines. More specifically, the self-assembled siRNA

hybrids (5 nM) resulted in significant (50-95%) knockdown of the selected GRPs, which led to synergistic effects in tumor cell cycle arrest (50-80%) and death (50-60%) within endometrial (AN3CA), cervical (HeLa) and breast (MDA-MB-231) cancer cell lines. Interestingly, a non-cancerous lung (MRC5) cell line displaying normal GRP levels was found to tolerate siRNA treatment and demonstrated less toxicity (5-20%) relative to the cancer cells that were found to be addicted to the glucose regulated chaperones. These remarkable self-assembled siRNA nanostructures may thus encompass a new class of potent siRNAs that may be useful in screening important oncogene targets while improving siRNA therapeutic efficacy and specificity in cancer.

2.2 Introduction

Cancer gene therapy has gained a renaissance over the last few years due to the many advances in the areas of RNAi, plasmid DNA, CRISPR-Cas9 and CAR T cell technologies.¹ In these applications, several cancer gene therapy strategies have been proven to be effective *in vitro*, and *in vivo*, paving the way for their successful applications in clinical trials.² Among the most promising gene therapy approaches, the short-interfering RNA (siRNA) have been successfully applied in pre-clinical and clinical cancer therapy.³ More specifically, modified siRNAs and their improved formulations have enhanced the knockdown effect of oncogenic mRNA resulting in potent tumor cell death responses.⁴ This RNA interference (RNAi) mechanism has shown exceptional catalytic efficacy and tolerance for a wide range of modified siRNAs including those incorporating modified nucleic acids, bioconjugation and self-assembly into higher order nanostructure formulations. The latter has effectively served to screen a variety of oncogene targets while potentiating gene silencing effects.⁵

The rise of RNA nanotechnology has led to the development of multi-functional RNAs for a variety of applications, including the development of nanomedicines.^{6,7} Recently, siRNA nanostructures have been applied for multiple knockdown effects of gene targets. For example, RNA nanocubes composed of six double-stranded dsRNA Dicer substrates have been formulated and designed to release multiple siRNAs in

breast cancer cells.⁸ The intracellular release of the siRNAs was found to trigger the RNAi response for knockdown of the reporter, enhanced green fluorescent protein, (eGFP) for up to twelve days. In a related study, the multifunctional RNA nanorings containing six siRNAs within the nanoparticle formulation were shown to silence eGFP expression at concentrations as low as 1 nM over a nine-day period which outperformed the linear variants.⁹ Moreover, the siRNA nanoparticles were functionalized with RNA aptamers which displayed selective binding to the epidermal growth factor receptor (EGFR) overexpressed human breast cancer cells. In another proof-of-concept study, the branched siRNA nanostructures targeting multiple mRNA sites of the luciferase firefly reporter gene were shown to self-assemble into three- and four-way junctions.¹⁰ These nanoparticle formulations released multiple siRNAs upon Dicer cleavage and effectively silenced luciferase activity in HeLa cells. Taken altogether, these representative examples demonstrate the ability for higher-ordered siRNA nanostructures to release multiple siRNAs that ultimately lead to synergistic gene knockdown effects by the RNAi mechanism.

We previously reported the synthesis, characterization and RNAi evaluation of branch and hyperbranched siRNAs.¹¹ These novel siRNA structures were synthesized by automated solid phase RNA synthesis and incorporated a 5'-OLv 2'-OMMT ribouridine branchpoint synthon. The branchpoint synthon was composed of orthogonal protecting groups which facilitated the selective extension of three distinct RNA sequences targeting the Glucose Regulated Proteins (GRPs). In this preliminary study, GRP78 was selected as a client chaperone protein target which is located in the endoplasmic reticulum and plays a pivotal role in regulating protein misfolding by signaling the unfolded protein response (UPR) mechanism.¹² While GRP78 is primarily found in the cytosol of healthy cells, in cancer, GRP78 is overexpressed and cell surface localized where it functions as a signaling receptor for tumorigenic activity.¹³ Moreover, GRP78 is associated with other stress-inducible members of the GRP family of chaperones, including GRP-75 and 94 which have also been found to play a pivotal role in the progression of certain types of cancers.¹⁹ GRP knockdown or inhibition has been shown to sensitize cancer cells to treatment, resulting in tumor cell cycle arrest and apoptosis in difficult to treat tumors.¹⁴⁻²⁰ Thus, GRP78

and the related GRPs have been validated as clinically relevant targets for cancer detection and therapy.¹⁹ In our previous study, the branch and hyperbranch siRNAs led to 50-60% silencing of GRP78 expression which translated to approximately 20% cell death of the HepG2 liver cancer cells.¹¹ Therefore, the branch and hyperbranch siRNAs have effectively expanded the repertoire of modified siRNAs that may be useful in the development of more potent RNAi therapeutics.

2.3 Chapter Objectives

Towards this goal, this thesis chapter builds upon the pioneering work of Anthony Maina, Ph.D. and Mayurbhai Patel, Ph.D. which describes the synthesis, characterization and biological evaluation of a new class of high-ordered RNA structures. My contributions to these studies as described in this thesis chapter involve the optimization of the solution phase synthesis procedure for the generation of the requisite 5'-OLv 2'-OMMT ribouridine branchpoint phosphoramidite for its incorporation within V- and Y-shaped RNA templates. The V- and Y-shape RNA templates will then be synthesized by automated solid phase RNA synthesis, with selected modifications to the synthetic protocol¹¹ in order to facilitate the efficient insertion, selective deprotection and RNA synthesis from the putative branchpoint synthon. Following synthesis, the RNA templates will be analyzed, purified and characterized by a combination of RP IP HPLC and ESI MS. Complementary, linear single stranded RNA will also be prepared by automated solid phase RNA synthesis for the self-assembly of GRP-targeting siRNA hybrids (Figure 2.1). This combinatorial self-assembly approach will enable the formulation of a library (30) of siRNA hybrids for exploring structure-activity relationships (SARs) within GRP overexpressing cancer cell lines.²⁰ Significantly, this study will demonstrate for the first time novel siRNA nanostructures that can effectively target and silence multiple oncogene targets within a selected panel of tumor cell lines. The latter provides a new contribution to modified siRNAs that can prove to be potent therapeutics in cancer gene therapy applications.

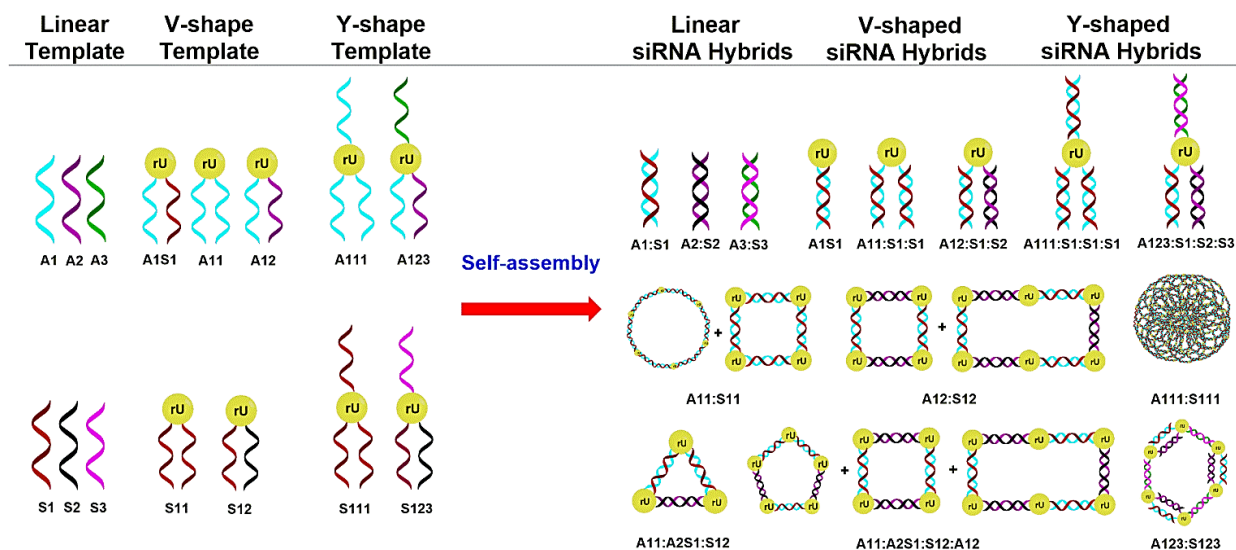


Figure 2.1. Design and self-assembly of siRNA nanostructures. The RNA templates, namely, linear, V- and Y-shaped RNA were designed and synthesized according to our previously described methodology.¹¹ The V- and Y-shaped templates incorporate a branchpoint ribouridine (rU) which facilitates the hybridization of complementary sense (S) and antisense (A) RNA. These templates preorganizes the self-assembly of siRNA hybrid nanostructures having discrete sizes and shapes, including those belonging to circles, triangles, squares, rectangles, pentagons, hexagons and porous-type structures. These siRNA nanostructures are genetically encoded to target a single (1), double (1, 2) and triple (1, 2, 3) sites of oncogenic GRP-75, 78 and 94 mRNA. Reprinted with permission: Patel MR, Kozuch SD, Cultrara CN, Yadav R, Huang S, Samuni U, Koren J 3rd, Chiosis G, Sabatino D. *Nano Lett.* **2016**, 16(10), 6099–6108.²⁰ Copyright 2016 American Chemical Society.

2.4 Results and Discussion

2.4.1 Synthesis of 5'-OLv 2'-OMMT ribouridine branchpoint phosphoramidite

The solution-phase synthesis of the requisite branchpoint amidite, 5'-O-levulinyl (Lv) 2'-O-monomethoxytrityl (MMT) ribouridine phosphoramidite was completed by an optimized solution phase synthesis method based on literature precedence.¹¹ The synthetic branchpoint amidite was obtained via a 3-step synthesis strategy featuring: (a) synthesis of levulinic anhydride followed by chemo-enzymatic levulation of the 5' ribouridine hydroxyl group, (b) anomerically favored tritylation of the 2' hydroxyl group and (c) phosphitylation of the

remaining 3' hydroxyl group (**Scheme 2.1**). Synthesis of levulinic anhydride was achieved by reacting levulinic acid with dicyclohexylcarbodiimide (DCC) in diethyl ether until; 1) formation of insoluble dicyclohexylurea (DCU), 2) and changes in product mobility by thin-layer chromatography (TLC) were observed. Following reaction completion, the mixture was filtered to remove the DCU precipitate and subsequently evaporated to a viscous oil. The following step entailed the regio-selective chemo-enzymatic 5'-levulination of ribouridine using lipase acrylic resin from *Candida antarctica*.²¹ The levulinic anhydride is dissolved in anhydrous dioxane and added to a reaction vessel containing a slurry of the ribouridine starting material and the resin bound lipase suspended in dioxane. This reaction produced selectively the desired 5'-levulinyl ribouridine in 60-90% conversion (monitored by TLC) within 3 hours. Reaction with fresh enzyme afforded the higher yields with subsequent uses of the same batch of enzyme showing diminished conversions. This is due to the recovery of the enzyme once the reaction is complete. Previously methanol/ethanol were used to recover the enzyme as the unreacted ribouridine base is highly soluble in both those solvents; however, further research into the cause of the diminished yields revealed that upon washing the lipase bound enzyme, the short chain alcohols (methanol/ethanol) are suspected to occupy the active site of the enzyme, outcompeting substrate binding and limiting enzyme efficiency.²² According to literature, the enzyme regains some activity by washing the resin with a bulky alcohol, such as t-butanol. Purification of the desired 5'-O-Lv ribouridine was achieved via silica gel column chromatography with a gradient of 1-5% methanol (MeOH) in dichloromethane (DCM). Validation of the 5'-O-Lv ribouridine product was confirmed by ¹H NMR and ESI-MS which validated the product, **2.2**. The pure 5'-O-Lv ribouridine was subsequently tritylated using monomethoxytrityl chloride (MMT-Cl), silver nitrate (AgNO₃) and pyridine in tetrahydrofuran (THF) as the solvent. The reaction was

performed in anhydrous conditions with nitrogen flushing the reaction flask for approximately 15 minutes prior to reaction. The reaction proceeded smoothly at room temperature and yielded both the 2' and 3' tritylated regioisomers. The desired 2'-regioisomer, **2.4**, was obtained in greater yields (50%) due to the enhanced nucleophilicity of the ribouridine 2'- vs. 3'-hydroxyl, which is in part related to the inductive effects of the neighboring anomeric nucleobase.²³ The reaction proceeded to approximately 80% conversion (TLC analysis) in about 3-4 hours, with a product ratio of 2:1 in favor of the 2' MMT regioisomer, **2.4**. This reaction was monitored by: 1) formation of insoluble silver chloride (AgCl) precipitate and 2) TLC indicating the conversion of the starting material, **2.2**, to the more non-polar products, **2.3** and **2.4**. Upon completion of the reaction, the product was filtered to remove AgCl_(s) and extracted in ethyl acetate (EtOAc) which was washed (NaHCO_{3(aq)} and NaCl_(aq)) and dried (MgSO₄). Reaction analysis by TLC proved difficult due to the presence of pyridine. In this case, pyridine was found to migrate with the product making it difficult to determine conversion efficiency and establishing good eluent conditions for column chromatography. In our optimized method, pyridine removal was successively accomplished by washing the organic phase with a 10% aqueous copper(II) sulfate (CuSO₄) solution²⁴ which effectively removed the latent pyridine from the solution. This allowed for more accurate TLC analysis. Purification of the desired 2'-O-MMT regioisomer was therefore achieved via silica gel column chromatography using a gradient of 0-25% acetone in DCM with the desired 2'-O-MMT product being isolated in 45-50% yields. The identity of the pure regioisomers was ascertained by ¹H NMR, in which a COSY correlation cross-peak was used to explicitly assign the 3'-hydroxyl group (**Figure 2.2**).

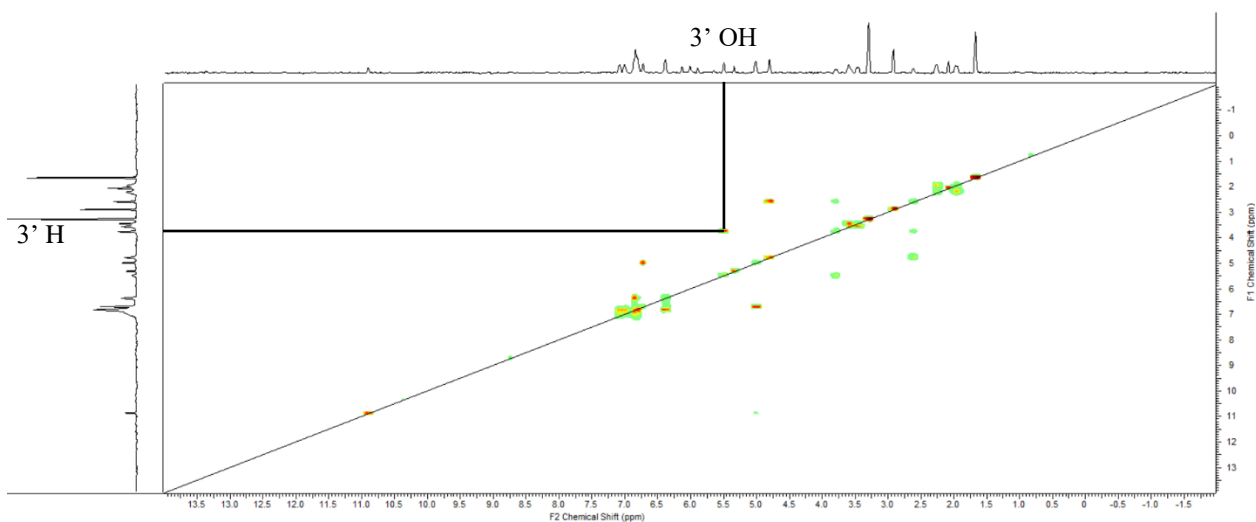


Figure 2.2 1H-1H COSY NMR correlating the 3' H with 3' OH, 2.4

In the final reaction step, the 5'-O-Lv, 2'-O-MMT ribouridine was phosphitylated using commercially available N,N-diisopropylamino cyanoethyl phosphonamidic-chloride, diisopropylethylamine (DIEA) in THF. The reaction was performed at room temperature under anhydrous conditions and the reaction progress was tracked by: 1) formation of the insoluble diisopropylethylamine-chloride salt, and 2) TLC. The reaction proceeded to approximately 80% conversion following 3-4 hr reaction, with the phosphoramidite diastereomers being observed as a single spot on TLC. Following solvent extraction, product washing and drying, the phosphoramidite diastereomers were dried to a viscous oil. The mixture was purified by silica gel column chromatography using a gradient of 20-45% acetone in hexanes with the 3'-phosphoramidite product being isolated in 60% yield. To verify the identity of the 5'-O-Lv, 2'-O-MMT, 3'-phosphoramidite product, ^{31}P NMR confirmed the phosphoramidite diastereomers as two peaks (148.46 and 152.16 ppm) (**Figure 2.3**). The phosphoramidite diastereomers are perfectly amenable to solid phase RNA synthesis, in which during the synthetic cycle, the

chirality at phosphorous is removed during the oxidation step. With the branchpoint phosphoramidite in hand, synthesis of V- and Y- shaped RNA was completed.

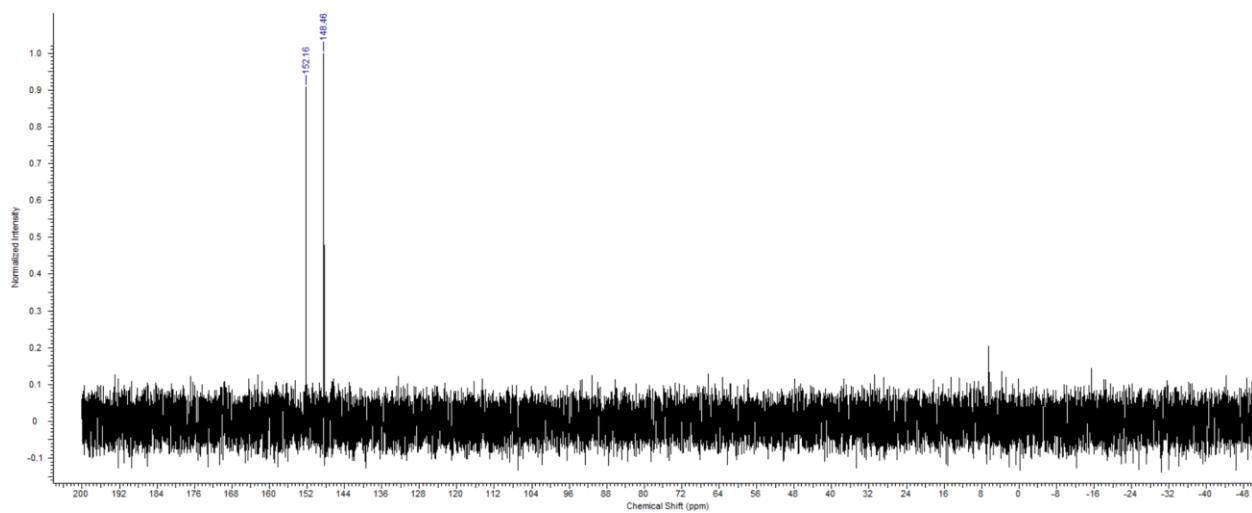
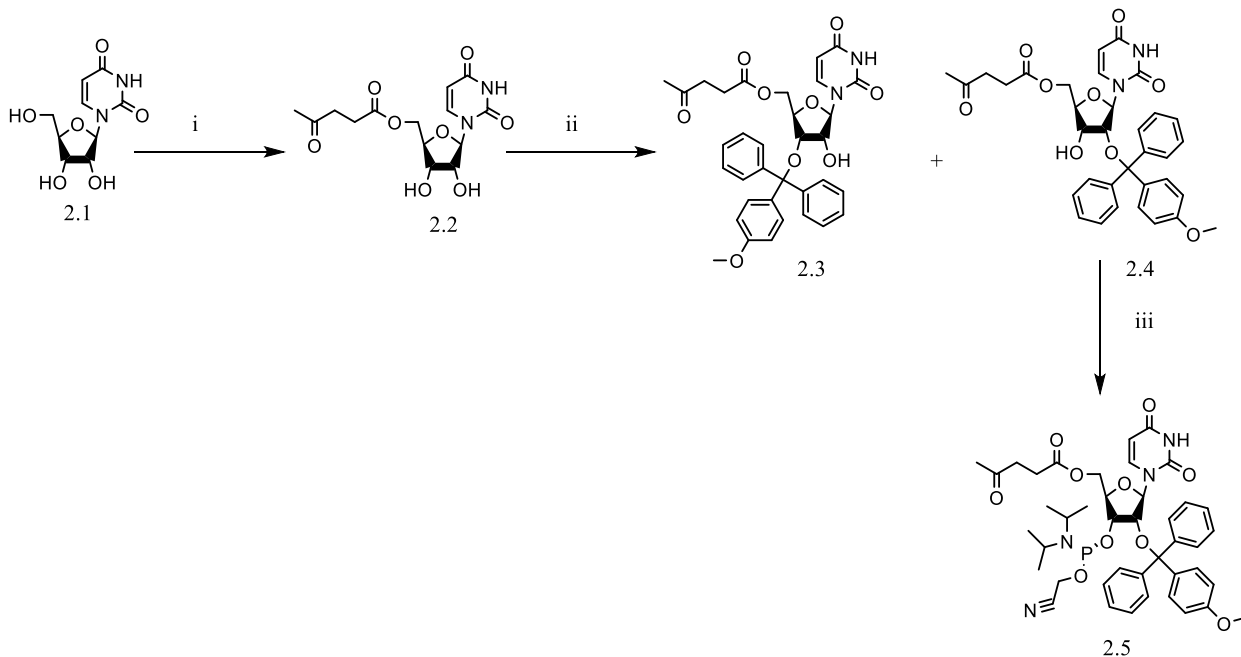


Figure 2.3 ^{31}P NMR spectrum of the branchpoint phosphoramidite diastereomers, **2.5**

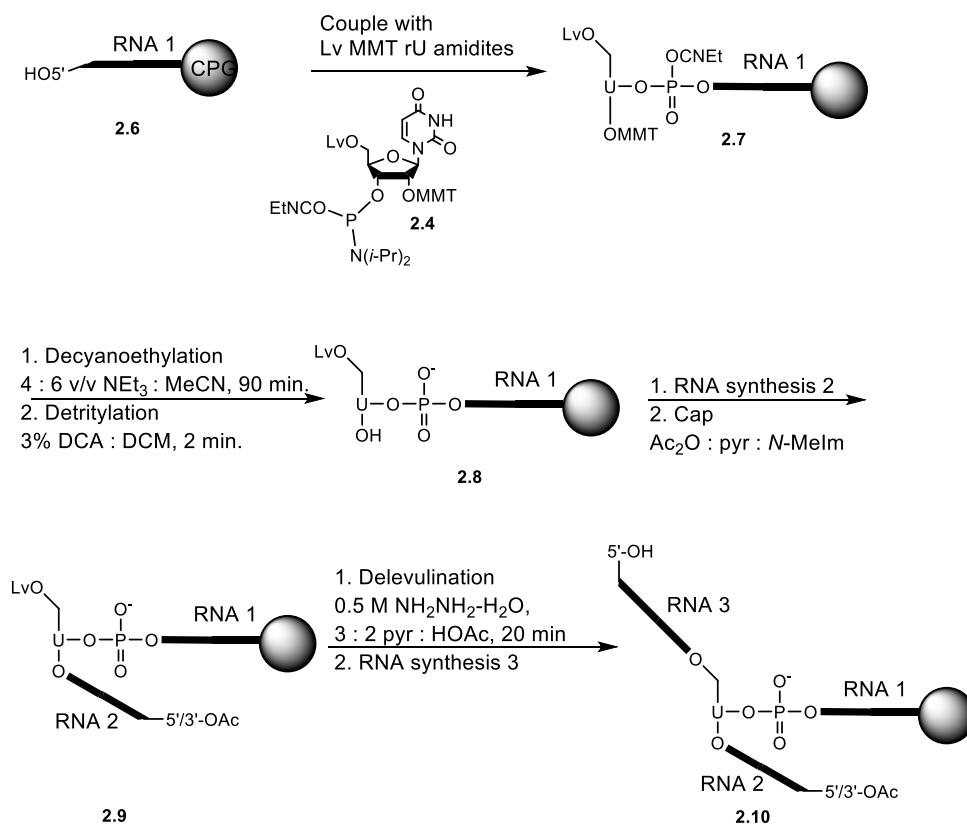


Scheme 2.1. Synthesis of 5'-OLv 2'-OMMT ribouridine branchpoint phosphoramidite. Reaction and Conditions: (i). Lv_2O , *Candida antarctica* Lipase resin, 1,4-dioxane, 22 °C, 3 hrs, 2.2: 90%. (ii). MMT-Cl, AgNO_3 , THF, pyridine. 22 °C, 3 hrs, 2.3: 25% and 2.4: 50%, (iii). Cl-P(OCE)N(iPr)_2 , Et-N(iPr)_2 , THF, 22 °C, 3 hrs, 2.5: 70%. Drawn with ChemDraw.

2.4.2 V- and Y-Shaped RNA Synthesis

The automated solid phase RNA synthesis procedure and its extension into V- and Y-shape RNA has been previously documented.^{11,20} Taking full advantage of this existing methodology, the synthesis of V-shape and Y-shape RNA templates along with their complementary RNA sequences were completed on solid-phase (**Scheme 2.2**). Briefly, the synthesis strategy involved automated RNA synthesis assembling commercially available 5'-ODMT 2'-OTBDMS RNA phosphoramidites on the controlled pore glass (CPG) solid support.²⁵ At the 5'-end of the linear RNA bound sequence, the 5'-OLv 2'-OMMT ribouridine branchpoint phosphoramidite was coupled using 5-ethylthiotetrazole (ETT) as activator and with an extended coupling time of 20 minutes (typical RNA amidites require 10 min coupling

times). Following branchpoint amidite coupling, a decyanoethylation step using 2:3 v/v triethylamine:acetonitrile ($\text{Et}_3\text{N}:\text{MeCN}$) for 90 min was conducted to remove the phosphate backbone cyanoethyl protecting groups thereby converting the reactive phosphite triester to the more stable phosphite diester bond.²⁶ Following decyanoethylation, the 2' MMT protecting group at the branchpoint position was removed using 3% DCA:DCM for 2 min to ensure complete detritylation at the more sterically encumbered 2'-position vs typical 5'-detritylation of the commercial RNA amidites. RNA synthesis from the liberated 2'-OH of the branchpoint synthon afforded the V-shape RNA template. Coupling times for the second RNA strand were increased from 10 to 22 min to ensure sufficient synthesis of the V-shaped RNA. A capping step, with acetic anhydride: N-methylimidazole in pyridine was repeated twice to ensure complete acetylation of the terminal 5'-hydroxyl group of the V-shape RNA in order to prevent side-reactions or unwanted elongation of the RNA sequence. The 5'-Lv group at the branchpoint position was then selectively removed using 0.5 M hydrazine hydrate ($\text{NH}_2\text{NH}_2\cdot\text{H}_2\text{O}$), buffered in 3:2 v/v pyridine:acetic acid for 20 min. Synthesis of the third RNA strand from the branchpoint 5'-position led to the generation of the Y-shape RNA template. In the selection of our RNA sequences, they were designed to target complementary sites of GRP-75, 78 and 94 mRNA expression in human cancer cells.^{27,28} Following solid phase synthesis, the linear, V-shape and Y-shape RNA templates were cleaved and deprotected from the solid support using 3:1 v/v $\text{NH}_4\text{OH}:\text{EtOH}$ at 60 °C for 16 hrs. The 2'-TBDMS protecting groups were then desilylated using 1:1.5 v/v $\text{DMSO}:\text{TEA}:\text{3HF}$ at 55 °C for 2 hr. The crude RNA pellets were then precipitated in 3M NaOAc (25 μL) and n-BuOH (1 mL), isolated upon centrifugation and dissolved in autoclaved, Millipore H_2O for analysis and purification.



Scheme 2.2: Solid-phase synthesis of V- and Y-shaped RNA templates. Drawn with ChemDraw

2.4.3 Analysis, Purification and Characterization of siRNA hybrids

The RNA templates were quantified by UV-Vis spectroscopy, measuring the absorbance at ~ 260 nm which provides molar extinction coefficients associated with the π - π^* and n - π^* electronic transitions of the nitrogenous nucleobases and is directly correlated to sample concentration by the Beer-Lambert law.²⁹ The RNA templates were subsequently analyzed and purified by RP IP HPLC³⁰ ($\geq 96\%$) and their identities were confirmed by electrospray ionization mass spectrometry (ESI MS),³¹ (Table 2.1).

NO.	Name	Sequence ^a	% Yield ^b	% Purity ^c	Mass ^d
1.	A1	5'-AUC AGA AUC UUC CAA CAC U-3'	91%	>99%	5949.6(5949.8)
2.	A2	5'-UCU AGU AUC AAU GCG CUC C-3'	90%	>99%	5958.6(5958.8)
3.	A3	5'-GUA ACA ACU GCA UGG GUA ACC UUC-3'	89%	>99%	7636.6(7636.8)
4.	S1	5'-AGU GUU GGA AGA UUC UGA U-3'	92%	>99%	6103.7(6103.7)
5.	S2	5'-GGA GCG CAU UGA UAC UAG A-3'	91%	>99%	6124.7(6124.2)
6.	S3	5'-GAA GGU UAC CCA UGC AGU UGU UAC-3'	90%	>99%	7653.6(7653.8)
7.	NS _A	5'-AGU UCA ACG AGU AUC AGC A-3'	92%	>99%	6068.7(6068.5)
8.	NS _S	5'-UGC UGA UAC UCG UUG AAC U-3'	91%	>99%	5998.8(5998.6)
9.	A11	2'3'-UCA CAA CCU UCU AAG ACU A-5' rU 3'5'-AUC AGA AUC UUC CAA CAC U-3'	82%	>98%	12266.4(12267.6)
10.	A12	2'3'-CCU CGC GUA ACU AUG AUC U-5' rU 3'5'-AUC AGA AUC UUC CAA CAC U-3'	80%	>99%	12275.4(12277.0)
11.	S11	2'3'-UAG UCU UAG AAG GUU GUG A-5' rU 3'5'-AGU GUU GGA AGA UUC UGA U-3'	83%	>99%	12574.5(12575.5)
12.	S12	2'3'-AGA UCA UAG UUA CGC GAG G-5' rU 3'5'-AGU GUU GGA AGA UUC UGA U-3'	79%	>99%	12595.6(12596.2)
13.	A2S1	2'3'-UAG UCU UAG AAG GUU GUG A-5' rU 3'5'-UCU AGU AUC AAU GCG CUC C-3'	81%	>99%	12429.7(12430.6)
14.	A1S1	2'3'-UAG UCU UAG AAG GUU GUG A-5' rU 3'5'-AUC AGA AUC UUC CAA CAC U-3'	80%	>99%	12421.2(12421.6)
15.	A111	2'3'-UCA CAA CCU UCU AAG ACU A-5' 5'-AUC AGA AUC UUC CAA CAC U-3'5'-U 3'5'-AUC AGA AUC UUC CAA CAC U-3'	71%	>96%	18278.0(18278.4)
16.	A123	2'3'-CCU CGC GUA ACU AUG AUC U-5' 5'-GUA ACA ACU GCA UGG GUA ACC UUC -3'5'-U 3'5'-AUC AGA AUC UUC CAA CAC U-3'	68%	>96%	19975.2(19975.8)
17.	S111	2'3'-UAG UCU UAG AAG GUU GUG A-5' 5'-AGU GUU GGA AGA UUC UGA U-3'5'-U 3'5'-AGU GUU GGA AGA UUC UGA U-3'	70%	>98%	18739.2(18740.6)
18.	S123	2'3'-AGA UCA UAG UUA CGC GAG G-5' 5'- GAA GGU UAC CCA UGC AGU UGU UAC -3'5'-U 3'5'-AGU GUU GGA AGA UUC UGA U-3'	64%	>99%	20531.2(20634.0)
19.	GRP94 _A	5'-GGU AAU CAG AUG CUU CUU C-3'	93%	>99%	5999.6(5999.8)
20.	GRP94 _S	5'-GAA GAA GCA UCU GAU UAC C-3'	92%	>99%	6068.7(6068.9)
21.	GRP75 _A	5'-UUG UAU UCU CCG AGU CAG U-3'	93%	>98%	5976.6(5976.8)
22.	GRP75 _S	5'-ACU GAC UCG GAG AAU ACA A-3'	91%	>99%	6091.8(6092.0)
23.	GRP7894	2'3'-CUU CUU CGU AGA CUA AUG G-5' rU 3'5'-AUC AGA AUC UUC CAA CAC U-3'	79%	>98%	12929.7(12929.9)
24.	GRP7875	2'3'-UGA CUG AGC CUC UUA UGU U'3' rU 3'5'-AUC AGA AUC UUC CAA CAC U-3'	76%	>98%	12906.7(12906.9)
25.	GRP9475	2'3'-UGA CUG AGC CUC UUA UGU U'3' rU 3'5'-GGU AAU CAG AUG CUU CUU C-3'	75%	>97%	12956.6(12956.8)
26.	GRP789475	2'3'-CUU CUU CGU AGA CUA AUG G-5' 5'-UUG UAU UCU CCG AGU CAG U-3'5'-U 3'5'-AUC AGA AUC UUC CAA CAC U-3'	62%	>97%	18395.9(18396.1)

Table 2.1. ^a Linear sequence number 1,2,3,7,19 and 21 represents antisense (A) siRNA sequence to its complimentary sense (S) sequences 4,5,6,8,20 and 22 respectively. V-shaped siRNA sequences 9-14 contains two siRNA sequences targeting GRP78 mRNA. Y-shaped siRNA sequences 15-18 contains three siRNA sequence targeting three different sites of GRP78 mRNA. Sequences 19-22 are linear siRNA sequences targeting GRP94 and GRP75. Sequences 23-25 are V-shape siRNA targeting two GRP mRNAs and sequence 26 is a Y-shape siRNA targeting three GRP mRNAs (GRP78, GRP94, GRP75). ^b Determined by UV-Vis Spectroscopy. ^c Obtained by RP-IP-HPLC using 0.1 mM TEAA in 0-20% MeCN, pH: 7.2 over 26 min. ^d Calculated mass (observed mass) by ESI-MS in negative mode (Novatia LLC, Newton, PA). Reprinted with permission: Patel MR, Kozuch SD, Cultrara CN, Yadav R, Huang S, Samuni U, Koren J 3rd, Chiosis G, Sabatino D. *Nano Lett.* **2016**, 16(10), 6099–6108. Copyright 2016 American Chemical Society.

Furthermore, a denaturing urea PAGE gel was used to confirm the relative electrophoretic mobilities of the RNA templates.³² In this study, the linear RNA sequences migrated the fastest on gel whereas the lengthier, bulkier V- and Y-shape RNA templates were found to be more retained on the gel. The RNA templates were hybridized with their complementary strands in annealing buffer (10 mM Tris, 50 mM NaCl, 1 mM EDTA, pH 7.5–8.0). Hybridization and self-assembly were promoted by heating the RNA templates and their complementary sequences at 90 °C (5-10 min) followed by slow cooling to room temperature (22 °C) for 1 hr, and overnight storage at 4 °C. siRNA hybridization efficiency was confirmed by a native, non-denaturing 16% PAGE. The lower molecular weight templates (linear, V- and Y-shape RNA) migrated fastest on the gel and were found to be equivalent to the observed migration of the 23-50 bp RNA ladder. The V- and Y-shaped RNA templates hybridized to their complementary RNA single strands and migrated slower on the gel, with electrophoretic mobilities comparable to the migration of the 30-50 bp RNA ladder and the 150-300 bp RNA ladder. The self-assembled V- and Y-shape siRNA hybrids migrated the slowest on the gel. The self-assembled V-shape siRNA hybrids migrated with similar electrophoretic mobility when

compared to the V-shape siRNA hybrids formed with their complementary linear RNA sequences. The siRNA hybrid combinations formed with multiple Y- and V-RNA templates were found to be ≥ 300 bp RNA ladder suggesting the formation of higher-ordered siRNA nanostructures (**Figure 2.4**).

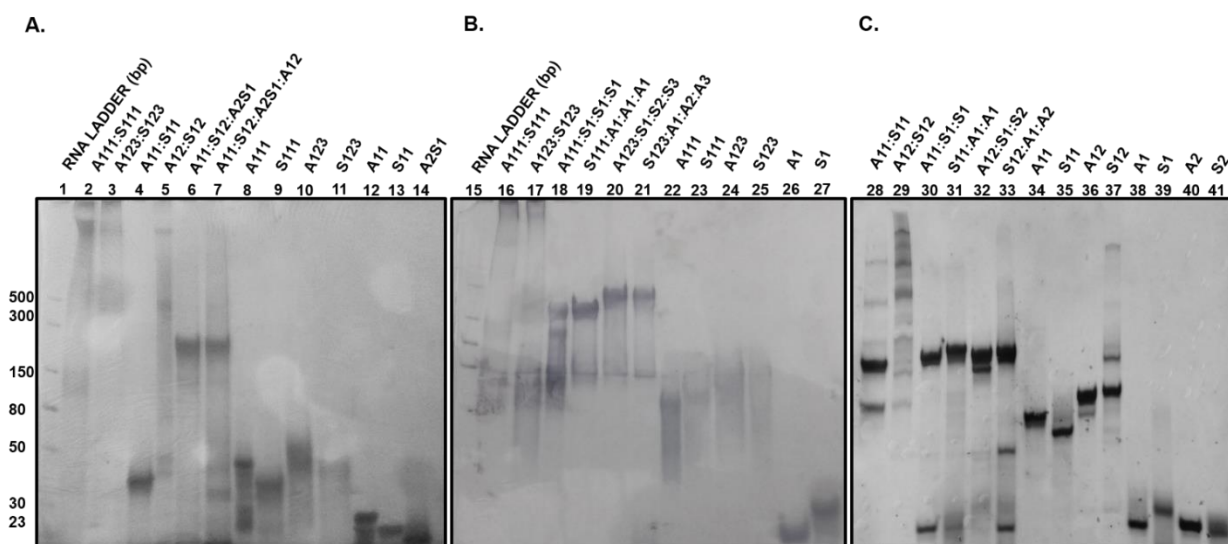


Figure 2.4 siRNA self-assembly. Native, non-denaturing 16% PAGE. **(A)** V-shape (lanes 12-14) and Y-shape (lanes 8-11) RNA templates and the self-assembled V- (lanes 4-7) and Y-shape (lanes 2-3) siRNA hybrids. **(B)** Linear (lanes 26, 27), Y-shape (lanes 22-25) RNA templates and the self-assembled Y-shape (lanes 16-21) siRNA hybrids. **(C)** Linear (lanes 38-41), V-shape (34-37) RNA templates and the self-assembled V-shape (lanes 28-33) siRNA hybrids. The RNA ladder (23-500bp) was used to track the relative sizes of the siRNA hybrids on the gels (lanes 1 and 15). Reprinted with permission: Patel MR, Kozuch SD, Cultrara CN, Yadav R, Huang S, Samuni U, Koren J 3rd, Chiosis G, Sabatino D. *Nano Lett.* **2016**, 16(10), 6099–6108. Copyright 2016 American Chemical Society.

In order to study the structural properties of hybrid siRNAs, CD spectroscopy was used to assess changes (if any) in the typical A-type helical structure anticipated from double-stranded RNA hybrids. The A-type RNA helices contain a minimum peak at 240 nm and a broad maximum in between 250-290 nm.³³ In the case of the self-assembled V- and Y-shape siRNA hybrids (**Figure 2.5**), the A-type broad maximum and minimum bands were observed

in between 250-290 nm and 240 nm, respectively, albeit with a decrease in the amplitudes of the molar ellipticities at these characteristic wavelengths. In these cases, minor distortions in the A-type helical trajectory were observed with the V- and Y-shape siRNA hybrids, presumably due to the conformational constraints imparted by the branchpoint synthon.^{11,20} Despite this change, the self-assembled V- and Y-shape siRNA hybrids maintained CD signatures that were consistent with the A-type RNA helix (**Figure 2.3**).

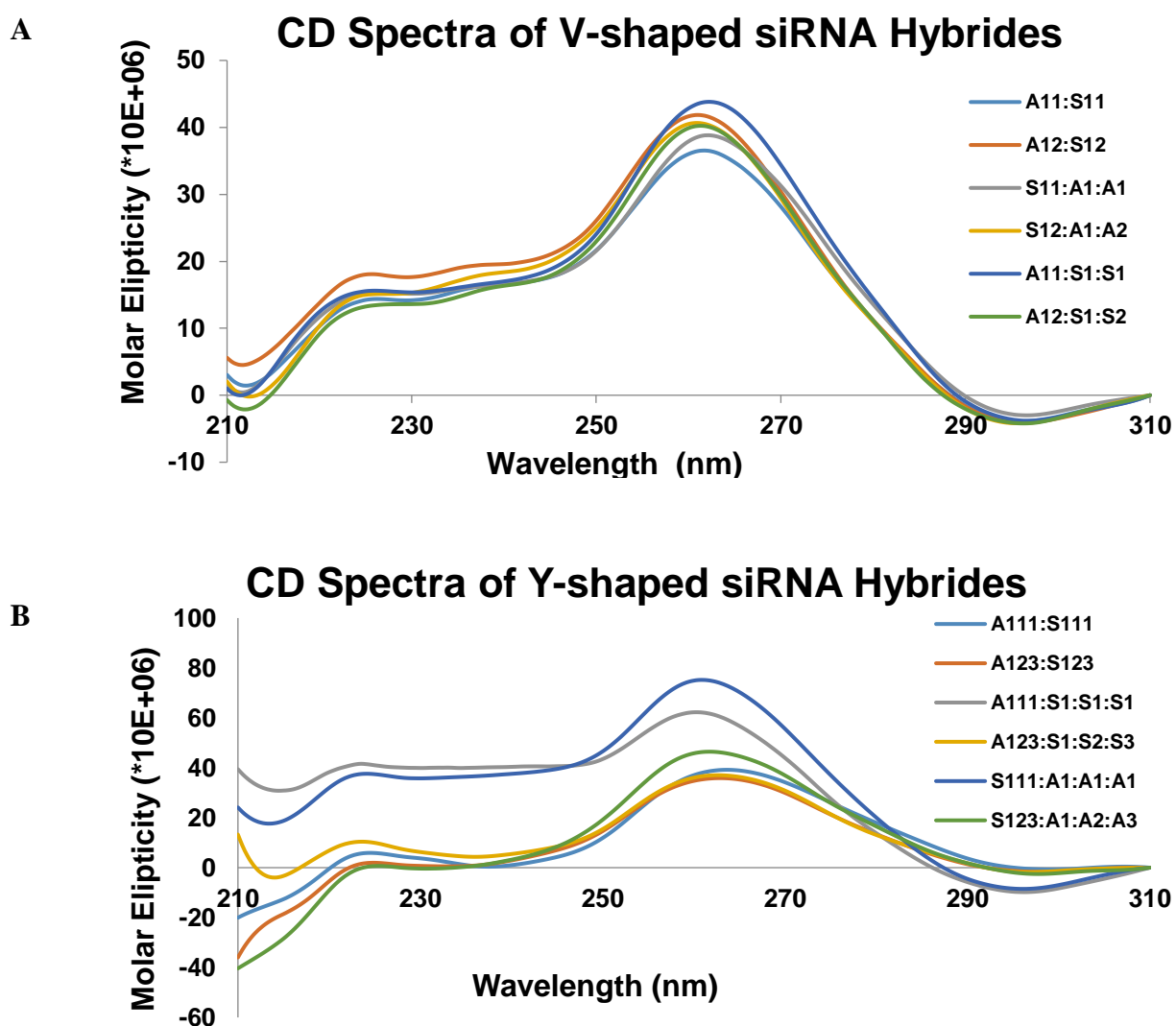


Figure 2.5 Circular dichroism spectroscopy of V- and Y-shaped siRNAs. All hybrid siRNA samples were prepared by annealing equimolar quantities (0.75 nM) of antisense V-shaped (**A**) or Y-shaped (**B**) RNA templates with their complementary linear or V- or Y-shaped RNA sequences. Samples were hybridized in annealing buffer (10 mM Tris, 50 mM NaCl, 1 mM EDTA, pH 7.5–

8.0, 13-15 μL) by pre-heating at 95 $^{\circ}\text{C}$ (3-5 min) followed by slow cooling to rt over 1 h and overnight storage at 4 $^{\circ}\text{C}$ prior to CD analyses. All samples were diluted in annealing buffer (1 mL) and the CD analysis was observed from 205-310 nm. Reprinted with permission: Patel MR, Kozuch SD, Cultrara CN, Yadav R, Huang S, Samuni U, Koren J 3rd, Chiosis G, Sabatino D. *Nano Lett.* **2016**, 16(10), 6099–6108. Copyright 2016 American Chemical Society.

siRNA hybrid stabilities were then measured by thermal denaturation (T_m) (**Figure 2.4**). In this assay, the observed melting temperature (T_m) reflects the temperature at which 50% of the hybrids have denatured into single strands. Consequently, the higher the T_m the more thermally stable the siRNA hybrid. In this study, the siRNA hybrids based on the V-shape RNA templates were found to be very stable, with high T_m values for the A11:S11 ($T_m = 84^{\circ}\text{C}$) and A12:S12 ($T_m = 78^{\circ}\text{C}$). The V-shaped RNA templates hybridized with their complementary linear strands showed good thermal stabilities (A11:S1S1, $T_m = 76^{\circ}\text{C}$ and A12:S1S2, $T_m = 77^{\circ}\text{C}$). Similarly, the siRNA hybrids, A111:S111 and A123:S123, based on the Y-shape RNA templates were also found to be stable, $T_m = 69^{\circ}\text{C}$ and $T_m = 63^{\circ}\text{C}$, respectively. The Y-shaped RNA template hybridized to its complementary linear RNA strands formed siRNA hybrids which maintained good thermal stabilities (A111:S1S1S1, $T_m = 62^{\circ}\text{C}$ and A123:S1S2S3, $T_m = 68^{\circ}\text{C}$). Taken together, the linear, V- and Y-shape siRNA hybrids maintained good thermal stability, indicating their potential applicability to cell biology under physiologically relevant conditions (pH~7, T: 37 $^{\circ}\text{C}$).

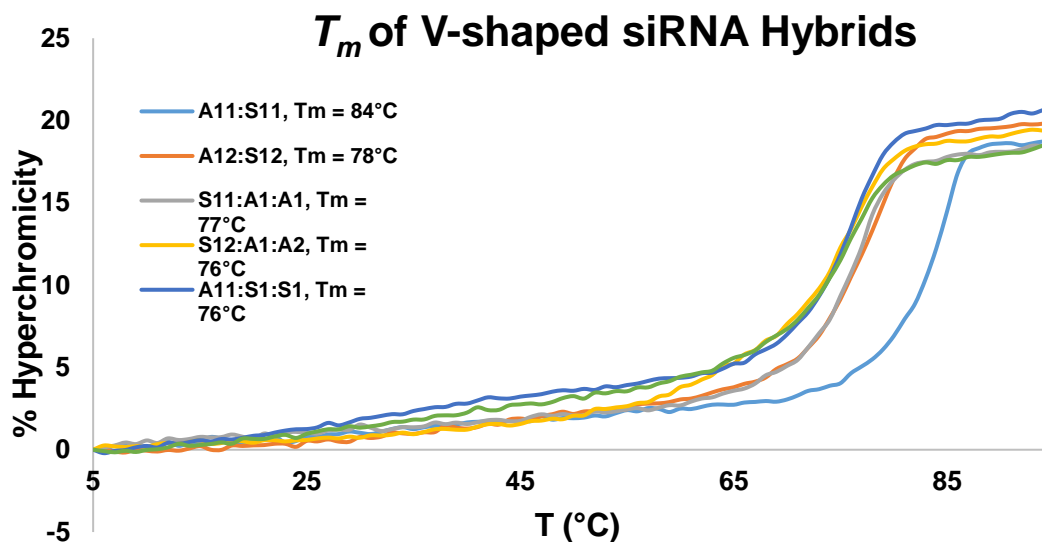
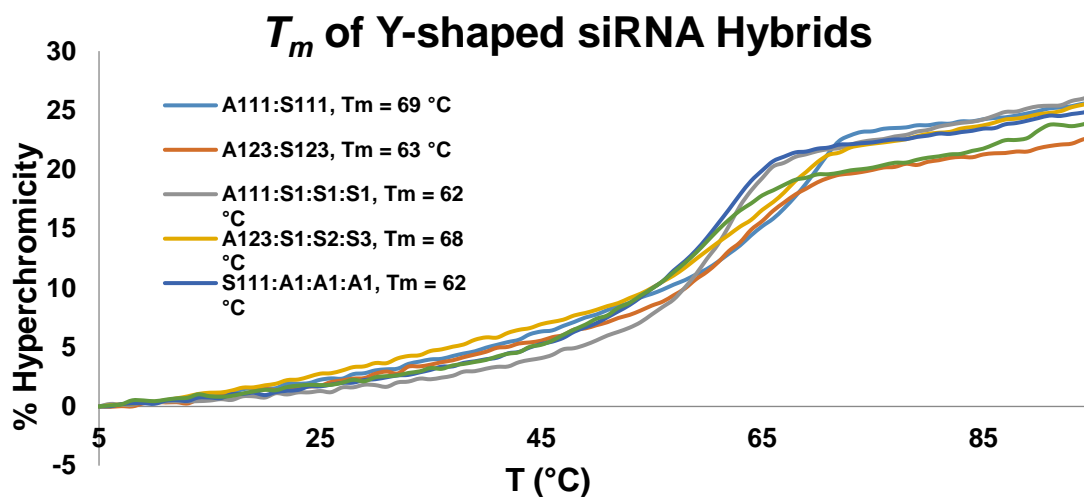
A.**B.**

Figure 2.6 Thermal denaturation of V- and Y-shaped siRNAs. All sample hybrids were prepared by annealing equimolar quantities ($0.75\ \mu\text{M}$) of antisense V-shaped (**A**) or Y-shaped (**B**) RNA to their complementary single or V- or Y-shaped RNA template strands. Samples were hybridized in annealing buffer (10 mM Tris, 50 mM NaCl, 1 mM EDTA, pH 7.5–8.0, 13–15 μL) by pre-heating at 95°C followed by slow cooling to rt over 1 h and overnight storage at 4°C prior to T_m analyses. Before running T_m , all samples were diluted in annealing buffer (1 mL) and the T_m analyses were observed at 260 nm between temperatures of 5– 95°C . Reprinted with permission: Patel MR, Kozuch SD, Cultrara CN, Yadav R, Huang S, Samuni U, Koren J 3rd, Chiosis G, Sabatino D. *Nano Lett.* **2016**, 16(10), 6099–6108. Copyright 2016 American Chemical Society.

2.4.4 RNAi activity of GRP-targeting siRNA hybrids in human cancer cell lines

In collaboration with Drs. Gabriela Chiosis and John Koren 3rd, the RNAi activity of the siRNA hybrids were studied in human cancer cell lines at the Memorial Sloan Kettering Cancer Center (MSKCC) in New York, NY. The GRP overexpressing human cervical HeLa,²⁷ endometrial AN3CA³⁴⁻⁴⁰ and breast MDA-MB-231⁴¹ cancer cells in addition to a nontumorigenic lung fibroblast MRC5⁴² cell line displaying normal GRP function were used as representative models to assess the influence of the glucose regulated chaperones, GRP-75, 78 and 94 on cell viability. The most potent anticancer effects were observed with the tri-functional Y-shape siRNA targeting GRP-75, 78 and 94. In this case, potent (50-95%) knockdown was observed in all cancer cell lines which translated to significant levels of tumor cell cycle arrest (50-80%) and cancer cell death (50-60%). In comparison, the multiple GRP78-targeting Y-shape siRNA (A123:S1S2S3) triggered only about 10% AC3CA cell death whereas the GRP-75, 78 and 94 targeting Y-shape siRNA produced a 5-fold increase (50%) in cytotoxicity at low doses of 5 nM. Moreover, GRP knockdown with the GRP-75, 78 and 94 targeting Y-shape siRNA had a more pronounced effect on tumor cell growth inhibition (50-80%) and death (50-60%) when compared to the control, non-tumorigenic MRC5 cell line which displayed modest growth inhibition (10-30%) and death (10-20%) (Figure 2.5). These results correlate an addiction of human cancer cells to the overexpressed glucose regulated chaperone which may contribute towards cancer treatment selectivity.⁴³ Therefore, the self-assembled siRNA hybrids targeting multiple GRPs proved useful in screening these important oncogene targets for elucidating their role on cancer cell biology while improving siRNA therapeutic efficacy and specificity in cancer.

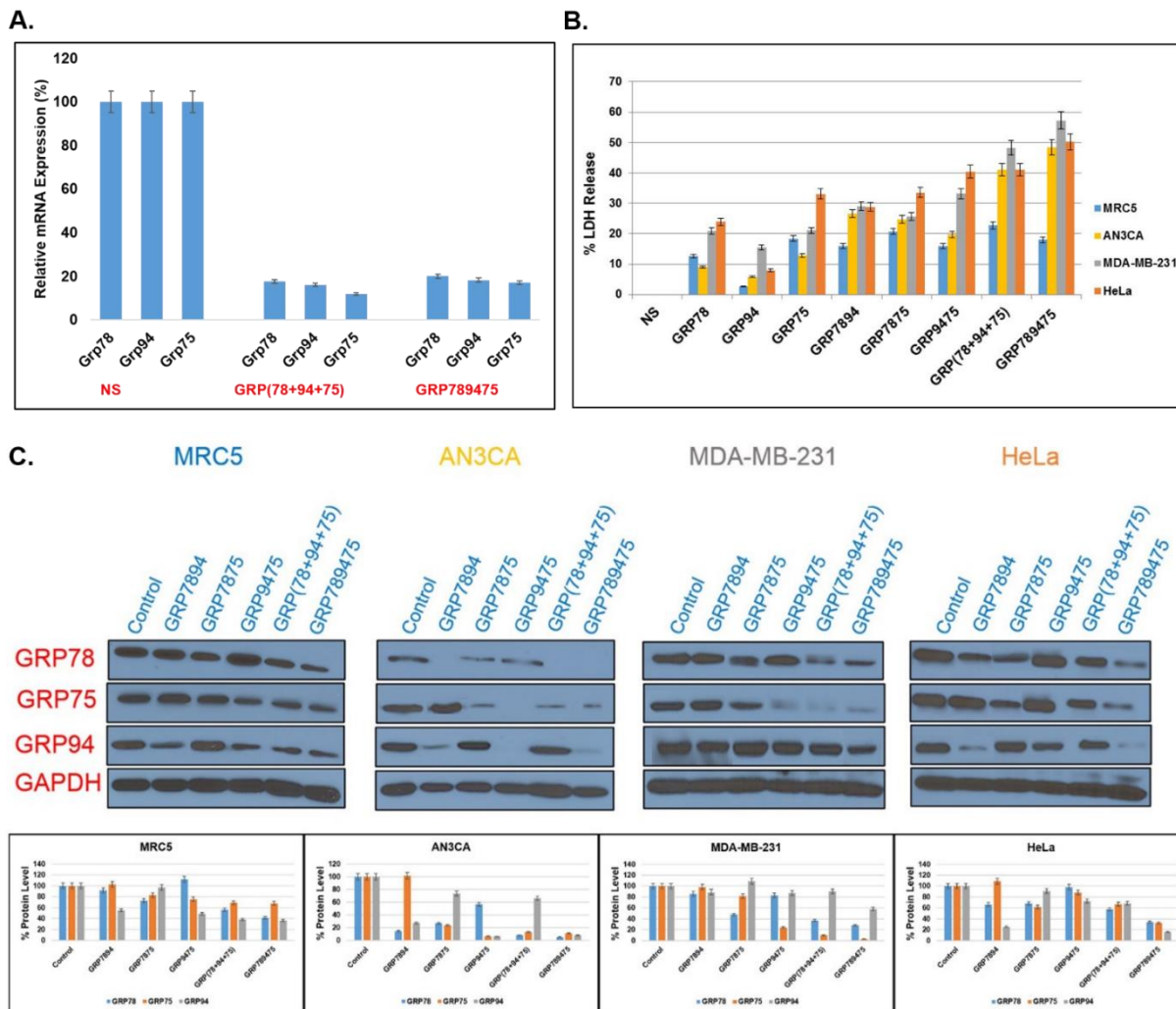


Figure 2.7 RNAi screening. (A) GRP mRNA levels detected by RT-PCR. HeLa cells were transfected with NS RNA, linear GRP(78+94+75) and Y-shape GRP(789475) siRNA (5 nM) using RNAiMAX™ (7 μL). GRP78, GRP94, GRP75, and GAPDH mRNA levels were normalized according to GAPDH and quantitated with respect to NS RNA. (B) LDH Release Assay. The % LDH released was measured following transfections of all treated cell lines (MRC5, AN3CA, MDA-MB-231 and HeLa). The LDH levels were quantitated and normalized according to the NS RNA. (C) Western blots measuring GRP78, GRP94 and GRP75 (% protein) levels following siRNA (5 nM) transfections in normal lung, MRC5, endometrial, AN3CA, breast, MDA-MB-231 and cervical, HeLa cancer cells. The GRP78, GRP94 and GRP75 levels were normalized according to GAPDH and quantified with respect to the NS RNA. Data represents knockdown efficiency of V-shape siRNAs (GRP7894, GRP7875, GRP9475), Y-shape siRNA (GRP789475) and the linear siRNAs (GRP78+GRP94+GRP75) added in combination. All experiments were replicated in triplicates with average values presented with their standard deviations about the mean. Statistical analyses produced error bars with acceptable variance ±SEM; N = 3, p < 0.05. Reprinted with permission: Patel MR, Kozuch SD, Cultrara CN, Yadav R, Huang S, Samuni U, Koren J 3rd, Chiosis G, Sabatino D. *Nano Lett.* **2016**, 16(10), 6099–6108. Copyright 2016 American Chemical Society.

2.5. Conclusions

This study demonstrated the rational design and applications of RNA templates in the self-assembly of higher order siRNA hybrids for RNAi screening of the GRP oncogenes and cancer gene therapy applications. The novel V- and Y-shape siRNA hybrids described in this thesis chapter were shown, through thermal denaturation and CD spectroscopy respectively, to confirm the prerequisite siRNA hybrid stabilities and A-type helices for invoking RNAi activity. In an RNAi screen across a panel of GRP overexpressing cancer cell lines and a non-tumorigenic control cell line displaying normal levels of GRP, the multi-functional Y-shape siRNAs targeting GRP-75, 78 and 94 mRNA oncogenes displayed synergistic anticancer effects which superseded the siRNAs targeting GRP78 alone. The RNAi screen also revealed the influence of GRP activity on cell viability. The GRP overexpressing cancer cells were sensitized to GRP-75, 78 and 94 knockdown resulting in greater tumor cell cycle arrest and cytotoxicity relative to the non-tumorigenic control. In conclusion, these novel siRNA motifs encompass a new class of bio-probes for studying RNAi activity in cancer and for screening important (single or multiple) oncogene targets for successful applications in cancer gene therapy.

2.6 Experimental

2.6.1 General Methods

Chemical synthesis reagents and solvents were obtained from ChemGenes, Glen Research, Aldrich and VWR and used as received. Solid phase oligonucleotides synthesis reagents and materials were obtained from ChemGenes or Glen Research Inc. and also used without further purification. HPLC grade solvents for chromatography were purchased from EMI Biosciences. Analytical thin-layer chromatography (TLC) was performed on aluminum-backed silica gel plates (Merck 60 F254). TLCs were visualized under UV shadowing (260 nm) or staining (10%

H₂SO₄/MeOH). Compound purification using silica gel chromatography was performed on 230-400 mesh silica (Sorbent Technologies). Molecular weights for **2.2-2.5** were measured as direct injections on a Hewlett Packard series 1100 MSD equipped with ESI as ion-source in positive mode using 50/50 v/v MeOH/H₂O at a flow-rate of 1 mL/min. Nuclear magnetic resonance spectra (¹H, ¹³C, ³¹P COSY, HMQC NMR) were recorded on an Varian NMR AS500 spectrophotometer. The NMR spectra were obtained at ambient temperature using either an indirect pulse-field gradient (ID-PFG) or a switchable pulse-field gradient (SW-PFG) probe. The obtained data was processed using VNMRJ software (version 2.2). The ¹H and ¹³C assignments were based on gCOSY and gHMQC NMR correlation experiments.

2.6.2 Synthesis

5'-O-levulinyl ribouridine (2.2): Levulinic acid (7.5 mL, 74 mmol) and *N,N*-dicyclohexylcarbodiimide (DCC) in dichloromethane (DCM, 15.2g) were stirred together in 150 mL of anhydrous diethyl ether to generate levulinic anhydride (Lv₂O). The reaction was run at room temperature (22 °C) under N₂ atmosphere for 5 hours. The byproduct (DCU) was removed by vacuum filtration and the filtrate was evaporated into viscous oil. In a second flask, ribouridine (3.0 g, 12.3 mmol) was vacuum dried for 5 hours and flushed with nitrogen before being suspended in 50 mL of anhydrous dioxane with resin-bound lipase enzyme, *Candida Antarctica* 435 (3 g). Crude Lv₂O was dissolved in dioxane (150 mL) and added to the flask containing the ribouridine and enzyme in dioxane. The chemo-enzymatic reaction was run for 3-4 hours at 22 °C (room temperature) under N₂. The reaction progress was monitored by TLC (10% MeOH in DCM) which confirmed ~90% conversion of starting material to product and the appearance of two non-polar products (R_f: 0.83 and 0.724). The resin-bound lipase was filtered, washed (MeOH) and recycled

for additional use. The filtrate was concentrated and purified by silica gel column chromatography (1-10% MeOH: DCM) to isolate the product in 60% yield.

^1H NMR (**2.2**, 500 MHz, DMSO- d_6): δ 11.31 (1H, s, NH), 7.88 (1H, d, $J = 10$ Hz, H6), 5.77 (1H, d, $J = 7$ Hz, H5), 5.64 (1H, d, $J = 9$ Hz, H1'), 5.37 (1H, d, $J = 7.5$ Hz, H5'), 4.14 (1H, dd, $J = 12$, 7.5 Hz, H5''), 4.06 (1H, t, $J = 10$ Hz, H2'), 3.95 (1H, bs, H3'), 3.32 (1H, s, H4'), 2.69 (2H, s, Lv CH₂), 2.37 (2H, s, Lv CH₂), 2.09 (3H, s, Lv CH₃); ^{13}C NMR (**2.2**, 500 MHz, DMSO- d_6): δ 207.2 (CO), 172.7 (CO), 163.6 (CO), 151.1 (CO), 146.0 (C6), 107.2 (C5), 89.05 (C1'), 81.57 (C4'), 73.31 (C2'), 70.16 (C3'), 64.12 (C5'), 37.76 (CH₂), 29.8 (CH₂), 27.90 (CH₃); ESI-MS [M]⁻: Calcd. for C₁₄H₁₈N₂O₈ : 341.3, found : 341.0.

5'-O-levulinyl 2'-O-monomethoxytrityl ribouridine (2.4) and 5'-O-levulinyl 3'-O-monomethoxytrityl ribouridine (2.3): A tritylation reaction was conducted using nucleoside **2.2** (2.52 g, 7.37 mmol), monomethoxytrityl chloride, MMT-Cl (2.73 g, 10.6 mmol) and silver nitrate (1.5 g, 10.6 mmol) which were dried under vacuum overnight before dissolving the reagents in pyridine (6.5 mL) under nitrogen at room temperature (22 °C). The reaction was run for 3 h and tracked by TLC (20:80 MeCN:DCM) which confirmed the presence of the 2' and 3'-OMMT regioisomers, R_f(**2.4**): 0.5 and R_f(**2.3**): 0.36, respectively. The reaction mixture was then diluted with ethyl acetate (EtOAc) (60 mL) and washed twice with saturated sodium bicarbonate (NaHCO₃) (60 mL). The organic layer was separated and dried using anhydrous sodium sulfate (Na₂SO₄). The solvent was evaporated and the crude product purified by silica gel column chromatography (5-50% MeCN:DCM). The presences of pyridine in the reaction complicated the spotting on TLC, so a TLC plate pre-stained with 10% sulfuric acid in methanol was used to detect the product by detritylating the yellow colored MMT⁺ group. The 5'-O-levulinyl 2'-O-monomethoxytrityl ribouridine, **2.4**, eluted first and was dried as a white foam in yields of 30%.

The identity of the 3'-OMMT regioisomer was confirmed by ^1H - ^1H COSY NMR which indicated a correlation cross-peak between the 3'H and 3'-OH in **2.4**.

^1H NMR (**2.4**, 500 MHz, DMSO- d_6): δ 11.32 (1H, s, NH), 7.52-6.81 (14H, m, MMT), 7.14 (1H, d, $J = 8$ Hz, H6), 5.92 (1H, d, $J = 7$ Hz, H1'), 5.43 (1H, dd, $J = 8$ Hz, H5), 5.22 (1H, d, $J = 7$ Hz, 3'OH), 4.21 (1H, t, $J = 6$ Hz, H2'), 4.0 (2H, m, H5'), 3.88 (1H, dd, $J = 12$ Hz, H4'), 3.71 (3H, s, OMe), 3.03 (1H, td, $J = 6.5$ Hz, H3'), 2.69 (2H, t, $J = 7$ Hz, Lv CH₂), 2.38 (2H, td, $J = 6.5$ Hz, Lv CH₂), 2.09 (3H, s, CH₃); ESI-MS [M]⁻: Calcd. for C₃₄H₃₄N₂O₉⁻ : 613.7, found: 613.3.

5'-O-levulinyl 2'-O-monomethoxytrityl 3'-O-phosphoramidous ribouridine (2.5) Isolated tritylated nucleoside **2.4** was reacted separately in a phosphitylation reaction by first drying the tritylated nucleoside (1.31 g, 2.13 mmol) overnight prior to reaction. Dry tetrahydrofuran (THF) (15 mL) was added to the nucleoside under a flow of nitrogen and *N,N*-diisopropylethylamine (DIEA) (1.48 mL, 8.50 mmol) and the phosphitylating reagent, Cl-P(OCEt)N(*i*-Pr)₂ (650 μ L, 2.34 mmol) was to the flask. The reaction was stirred for 3 h at room temperature and monitored by TLC (45% Acetone: Hexanes) until the formation of the phosphoramidite diastereomers was observed, R_f(**2.5**) 0.60. A white precipitate, EtNH(*i*Pr)₂⁺ Cl⁻, was also observed as an indication of reaction completion. Upon reaction completion, EtOAc (60 mL) was added to the reaction mixture prior to washing twice with saturated NaHCO₃ (30 mL). The organic phase was dried over Na₂SO₄ and concentrated to a yellowish foam. The crude product was purified by silica gel chromatography (20-45% Acetone: Hexanes). Product **2.5** was collected, dried as a white foam in yields of 60%. ^{31}P NMR (**2.5**, 400 MHz, DMSO- d_6): 151.56 and 148.35; ESI-MS [M]⁻: Calcd. for C₄₃H₅₁N₄O₁₀P: 813.87, found: 813.3.

2.6.3 Solid phase RNA synthesis

RNA was synthesized on an automated ABI 3400 synthesizer. Reagents for the synthesis cycle were as follows: *detritylation reagent* (3% solution of dichloroacetic acid in dichloromethane), *coupling reagent* (0.25 M ethylthiotetrazole in acetonitrile), *capping reagent* (Cap A: 1:1:8 v/v/v acetic anhydride:pyridine:tetrahydrofuran, Cap B: 16% *N*-methyl imidazole in tetrahydrofuran), *oxidation reagent* (0.02 M iodine in 75:20:5 v/v/v tetrahydrofuran:pyridine:water) and *acetonitrile wash* (Biotech grade purchased from EMI). Oligonucleotide syntheses were performed on a 1 μ mol scale using 1000 - 2000 Å LCAA CPG. RNA phosphoramidites were prepared as 0.15 M solutions in anhydrous acetonitrile with coupling times of 10 min. For the synthesis of branch RNA, the branchpoint phosphoramidites (**2.5**) were also prepared as 0.2 M solutions in MeCN and coupled with an extended reaction time of 20 min.

RNA syntheses were performed using the following synthesis cycle: *Detritylation*: Dichloromethane wash (30s) followed by delivery of 3% dichloroacetic acid in dichloromethane (120s); *Coupling*: delivery of RNA phosphoramidites with activator (0.25 M ethylthiotetrazole in acetonitrile), *Capping*., delivery of Cap A and Cap B (14 sec) and *Oxidation*: delivery of oxidizing solution (0.02 M iodine in 75:20:5 v/v/v tetrahydrofuran:pyridine:water) for 20 sec followed by a wait period of 20 sec. Single stranded RNA sequences were extended in the 3' \rightarrow 5' orientation on solid-phase until completion.

V- and Y-shape RNA were first grown in the 3' \rightarrow 5' position followed by coupling of the branchpoint phosphoramidite **2.5**. The branchpoint phosphoramidite was coupled for 20 min, followed by a manual decyanoethylation step (2:3 v/v triethylamine:acetonitrile, 90 min) prior to the 2'-OMMT detritylation. The oligonucleotide bound CPG was washed with acetonitrile (30 mL) and replaced on the synthesizer to complete 3' \rightarrow 5' RNA synthesis of the antiparallel

complimentary strand. The terminal 5'-OH was then capped with automated delivery of Cap A and Cap B (14 sec). Following V-shape RNA synthesis, **2.9**, the 5'-levulinyl protecting group was removed by flushing the column with 0.5 M hydrazine hydrate buffered in 3:2 v/v pyridine:acetic acid (20 min). Following delevulation, the CPG-bound V-shape RNA was cleaved and deprotected from the solid support for analysis and purification. For Y-shape RNA, automated RNA synthesis was continued from the branchpoint 5'-OH to yield branch RNA **2.10**.

2.6.4 Cleavage and deprotection of RNA

Cleavage and deprotection of the synthesized RNA was performed after drying the synthesizer columns under Ar_(g) for 10 min. CPG-bound RNA was then transferred into autoclaved screw-cap microtubes (1.5 mL) and treated with a 1 mL solution of 3:1 v/v ammonium hydroxide in absolute ethanol at 55 °C for 16 to 20 hrs. RNA samples were then evaporated *in-vacuo* and the CPG was washed twice with autoclaved distilled water (500 µL). Crude oligonucleotides were re-suspended in a mixture of 1:1.5 v/v dimethylsulfoxide:triethylamine trihydrofluoride (150 µL) to complete the 2'-desilylation reaction at 65 °C for 2 hr. The crude RNA samples were subsequently precipitated from the reaction mixture with 3 M NaOAc (25 µL) in n-BuOH (1 mL). Precipitation was completed in freezer (-80 °C) on dry ice for 30min prior to centrifugation (12,000 rpm) leaving the crude oligonucleotides as a solid white pellet. The collected RNA samples were dried in a Speedvac concentrator and re-suspended in autoclaved water (1 mL) for yield determination using UV absorbance measurements at 260 nm.

2.6.5 Polyacrylamide gel electrophoresis (PAGE)

siRNA samples (**Table, 2.1, sequences 1-26**) were analyzed using denaturing PAGE. Analytical samples were prepared by drying 0.1 OD (A₂₆₀) overnight and re-suspending the sample

in a denaturing formamide solution (80% formamide in 10X TBE buffer) prior to loading on the gel. Samples were loaded (20 μ L/well) along with dye solution (5 μ L of 10 mL formamide mixed with trace amounts of bromophenol blue and xylene cyanol) to track gel migration. The gels were run at 300 V, 100 mA and 12 W for 3 h in 1X TBE running buffer on a 7 M urea (21 g), 24% polyacrylamide gel. Gels were visualized under short range (265 nm) UV-shadowing and subsequently placed in a Stains-All[®] (Sigma) solution (25 mg Stains-All[®], 50 mL isopropyl alcohol, 25 mL formamide, 125 mL water). After 2 h, the gel was removed from the stain solution and exposed to light for analyses.

Pure siRNAs (**Table, 2.1, sequences 1-26**) were analyzed by native PAGE. Purified complementary RNA strands were combined in equimolar quantity (20 μ M) and mixed in annealing buffer (25 μ L, 10 mM Tris, 50 mM NaCl, 1 mM EDTA, pH 7.5–8.0) to afford the hybrid mixtures. The resulting mixtures were heated to 95°C for 7 minutes on a heating block, slowly cooled to room temperature (22°C) over 1 h and stored in the fridge overnight at 4 °C prior to analysis. The hybridized siRNA samples were suspended in 30% sucrose loading buffer (15 μ L in 1X TBE). Samples were then loaded on a 16% native, non-denaturing PAGE and run at 300 V, 100 mA and 12 W for 2.5 h. Following electrophoresis, the siRNA bands were visualized under UV shadowing (260 nm) and stained with a Stains-All (Sigma-Aldrich[™]) solution.

2.6.6 Ion pairing reverse phase HPLC (IP RP HPLC)

All samples (**Table, 2.1, sequences 1-26**) were analyzed by IP RP HPLC to determine purity. HPLC was performed on a Waters[®] 2695 Alliance Separations Module. Crude samples were dissolved in autoclaved water (0.1 OD for analytical) and injected into a Waters Symmetry C-18 reverse phase column (4.6 x 150 mm, 5 μ m particle size, 120 Å) using a gradient of 5-95% (20% acetonitrile in 0.1 M triethylammonium acetate) at 60 °C with a flow rate of 1 mL/min over

26 min at 260 nm. Peak areas were calculated to determine percent purity of samples. IP RP HPLC was used to confirm siRNA purities >90% following purification.

2.6.7 Electrospray ionization mass spectrometry (ESI MS)

siRNA samples (0.1-0.4 μ M) were dissolved in autoclaved water and analyzed by mass spectrometry. Samples were analyzed by Dr. Mark Hail at Novatia LLC, Newton, PA, utilizing Oligo HTCS equipped ESI/MS in negative mode. The data was obtained and deconvoluted using ProMass software. Theoretical molecular weights were calculated by entering each sequence identity on IDT OligoAnalyzer. <https://www.idtdna.com/calc/analyzer>

2.6.8 CD Spectroscopy

siRNA samples were hybridized in annealing buffer (0.75 μ M, 10 mM Tris, 50 mM NaCl, 1 mM EDTA, pH 7.5–8.0, 1 mL) as previously described. Samples were then transferred to fused quartz cells (1 cm path length) incubated at 10 °C under N₂ for 5 min prior to spectral acquisition. CD spectra were collected using an AVIV 62A DS CD spectrophotometer as an average of 3 scans with a 1.0 nm band width interval and a 0.5 nm step interval. CD spectra were analyzed in between 210 and 310 nm, blank corrected and smoothed prior to analyses. The raw data was exported into Microsoft Excel™ and plotted as changes in molar ellipticities (θ) with increasing wavelengths (210 – 310 nm).

2.6.9 Thermal Denaturation (*T_m*) studies

All siRNA hybrids were prepared as previously described in annealing buffer (0.75 μ M, 10 mM Tris, 50 mM NaCl, 1 mM EDTA, pH 7.5–8.0, 1 mL). Thermal denaturation of the siRNA hybrids was performed using a CARY 3E, UV-Vis spectrophotometer, from 5 – 95 °C, with temperature ramping of 0.5 °C /min. The changes in absorption at 260 nm as a function of

temperature were collected and the first derivative plot was used to determine the melting temperatures (T_m) of the siRNA samples. Data was subsequently transferred and plotted in Microsoft Excel™ as changes in the hyperchromicities (% H) observed at 260 nm as a function of temperature (5 – 95 °C).

2.6.10 Cell Culture

The human normal lung cells MRC5 (ATCC® CCL-171™), endometrial cancer cells AN3CA (ATCC® HTB-111™), breast cancer cells MDA-MB-231 (ATCC® HTB-26™) and cervical cancer cells HeLa (ATCC® CCL-2™) were purchased from ATCC. MDA-MB-231, HeLa and MRC5 cells were cultured in Dulbecco's Modified Eagle medium (DMEM) while AN3CA cells were in Minimum Essential Medium (MEM) supplemented with 10% (v/v) Fetal Bovine Serum (FBS) and 1% (v/v) Penicillin/streptomycin (P/S) under 5% CO₂ at 37 °C. For passaging cells were detached with 0.25% trypsin and re-suspended with complete culture medium.

2.6.11 siRNA Transfections in AN3CA Cells

Briefly, the AN3CA endometrial cancer cells (ATCC® HTB-111™), 1×10^5 , were plated in 6-well culture plates containing MEM culture media with 10% FBS. Cells were cultured for 48 h in a humidified incubator set at 37 °C with 5% CO₂. Prior to transfections, the siRNA hybrids (5 μ L, 2.5-12.5 μ M, in DMEM, 250 μ L) were mixed with the transfection reagents (Lipofectamine 2000™, Silentfect™ or RNAiMAX™, 2.5 – 7 μ L in DMEM, 250 μ L) according to the manufacture's recommendation. The mixtures were incubated (10 min, 22°C) then added to the AN3CA cell culture and incubated at 37 °C with 5% CO₂ over a three-day period. Cell growth over time (65-72 h) was monitored in an Incucyte™ (Essen BioScience).

2.6.12 RNA isolation and quantitative RT-PCR

GRP mRNA was isolated from the HeLa cervical cancer cell lines using the manufacturer's protocol (TRIzol[®], ThermoFisher Scientific). The RNA pellet was dissolved in diethylpyrocarbonate-treated H₂O. The total mRNA levels were quantitated by measuring the absorbance of collected RNA samples at 260 nm. The isolated RNAs (1.5 µg of each sample) were treated with gDNA Wipeout buffer at 42 °C to eliminate residual genomic DNA. These samples were then reverse-transcribed using Quantiscript reverse transcriptase, Quantiscript RT Buffer, and RT Primer Mix according to manufacturer's protocol (QIAGEN). Additionally, the samples were incubated with RNaseH to remove RNA, and the resulting cDNAs were then diluted to 100 µL with distilled water. Each quantitative PCR consisted of 5 µL of cDNA template, 12.5 µL of PerfCta SYBR Green Supermix, Low ROX (Quanta Biosciences, Beverly, MA), and 500 nM of forward and reverse primers in a final volume of 25 µL. For human GRP78, the primer sequences were 5'-ACCTCCAACCCCGAGAACA-3' (forward) and 5'-TTCAACCACCTTGAACGGC-3' (reverse). For human GRP94, 5'-ACTGTTGAGGAGCCCATGGAGG-3' (forward) and 5'-GCTGAAGAGTCTCGCGGGAAAC-3' (reverse). For human GRP75, 5'-AGCTGGAATGGCCTTAGTCAT-3' (forward) and 5'-CAGGAGTTGGTAGTACCCAAATC-3' (reverse). For GAPDH, the primer sequences were 5'-ACCACAGTCCATGCCATCAC-3' (forward) and 5'-TCCACCACCCTGTTGCTGTA-3' (reverse). The reactions were carried out on an ABI PRISM 7000 sequence detection system (Applied Biosystems, Foster City, CA) for 30 cycles (95 °C for 15 sec, 60 °C for 45 sec) after an initial 3 min of incubation at 95 °C. The fold change in the expression of each gene was calculated using the standard curve method, with GAPDH used as an internal control for normalization.

2.6.13 Western Blots

The cell media was aspirated from the transfected culture and washed with PBS buffer for 2-3 min, twice. The cells were lysed using cell lysis buffer (1% Tween-20, 50 mM Tris, 130 mM NaCl, 5 mM EDTA) containing protease inhibitors and phosphatase inhibitors (Protease inhibitor, PSMF, Phos2, Phos3). Protein concentration of lysates were determined using the BSA protein assay reagent (ThermoFisher Scientific Inc.). Proteins samples (15-20 mg, 20 μ L) were dissolved in 5X loading buffer, boiled for 5-7 min, and resolved in 10% sodium dodecyl sulfate polyacrylamide gel electrophoresis (SDS-PAGE). The proteins were electrotransferred onto a polyvinylidene difluoride membrane (Bio-Rad Laboratories), which was blocked in Tris-buffered saline, pH 8.0, Tween-20, 5% (w/v) skimmed milk (TBST solution) for 1 h at room temperature (22 °C). Membranes were then probed with the indicated primary antibodies (anti-PARP p85 fragment pAb, Promega Inc. and anti-GRP78 pAb, Cell Signaling Inc.) in TBST solution at 4 °C overnight. Next day, membranes were washed with TBST solution (3X, 10 min each) and incubated with horseradish peroxidase (HRP) conjugated secondary antibodies (1:3000) at room temperature for 1 h followed by washing with TBST solution (3X, 10 min each). Immunoblotted protein bands were visualized by enhanced chemiluminescence reagent (ThermoFisher Scientific) and quantified using NIH imager (ImageJ)

2.6.14 Cell Cytotoxicity

Following transfection with GRP78 specific siRNAs, a cytotoxicity assay was performed with all cells using the Cytotoxicity Detection Kit (ThermoFisher Scientific Inc.). With this kit, the rate of cell lysis is monitored by determination of the LDH amount released into the culture medium and quantified at 492 nm by the detection of the red formazan chromophore.

2.7 References

1. Naldini, L. *Nature* **2015**, 526, 351-360.
2. Ajith, T. A. *J. Exp. Ther. Oncol.* **2015**, 11, 33-39.
3. Masiero, M.; Nardo, G.; Indraccolo, S.; Favaro, E. *Mol. Aspects Med.* **2007**, 28, 143-166.
4. Lam, J. K.; Chow, M.Y.; Zhang, Y.; Leung, S. W. *Mol. Ther. Nucleic Acids.* **2015**, 4, e252.
5. Gaglione, M.; Messere, A. *Mini Rev. Med. Chem.* **2010**, 10, 578-595.
6. Guo, P. *Nat. Nanotechnol.* **2010**, 5, 833-842.
7. Shukla, G. C.; Haque, F.; Tor, Y.; Wilhelmsson, L. M.; Toulmé, J. J.; Isambert, H.; Guo, P.; Rossi, J. J.; Tenenbaum, S. A.; Shapiro, B. A. *ACS Nano.* **2011**, 5, 3405-3418.
8. Afonin, K. A.; Viard, M.; Kagiampakis, I.; Case, C. L.; Dobrovolskaia, M. A.; Hofmann, J.; Vrzak, A.; Kireeva, M.; Kasprzak, W. K.; KewalRamani, V. N.; Shapiro, B. A. *ACS Nano.* **2015**, 9, 251-259.
9. Afonin, K. A.; Viard, M.; Koyfman, A. Y.; Martins, A. N.; Kasprzak, W. K.; Panigaj, M.; Desai, R.; Santhanam, A.; Grabow, W. W.; Jaeger, L.; Heldman, E.; Reiser, J.; Chiu, W.; Freed, E. O.; Shapiro, B. A. *Nano Lett.* **2014**, 14, 5662-5671.
10. Nakashima, Y.; Abe, H.; Abe, N.; Aikawa, K.; Ito, Y. *Chem. Commun.* **2011**, 47, 8367-8369.
11. (a) Maina, A.; Blackman, B. A.; Parronchi, C. J.; Morozko, E.; Bender, M. E.; Blake, A. D.; Sabatino, D. *Bioorg. Med. Chem. Lett.* **2013**, 23, 5270-5274., (b) Maina, A. Branching into RNAi: Synthesis, Characterization and Biology of Branch and Hyperbranch siRNAs. *Ph.D. Thesis* **2014**, Seton Hall University, South Orange, New Jersey.
12. Lee, A.S. *Curr. Opin. Cell Biol.* **1992**, 4, 267-273.
13. Zhang, L. H.; Zhang, X. *J. Cell Biochem.* **2010**, 110, 1299-1305.
14. Roller, C.; Maddalo, D. *Front Pharmacol.* **2013**, 4, 10.
15. Chang, Y. J.; Huang, Y. P.; Li, Z. L.; Chen, C. H. *PLoS One.* **2012**, 7, e35123.
16. Dejeans, N.; Glorieux, C.; Guenin, S.; Beck, R.; Sid, B.; Rousseau, R.; Bisig, B.; Delvenne, P.; Buc, Calderon, P.; Verrax, J. *Free Radic. Biol. Med.* **2012**, 52, 993-1002.
17. Yi, X.; Luk, J.M.; Lee, N.P.; Peng, J.; Leng, X.; Guan, X.Y.; Lau, G.K.; Beretta, L.; Fan, S.T. *Mol. Cell Proteomics.* **2008**, 7, 315-25.
18. Firczuk, M.; Gabrysiak, M.; Barankiewicz, J.; Domagala, A.; Nowis, D.; Kujawa, M.; Jankowska-Steifer, E.; Wachowska, M.; Glodkowska-Mrowka, E.; Korsak, B.; Winiarska, M.; Golab, J. *Cell Death Dis.* **2013**, 4, e741.
19. Lee, A. S. *Nat. Rev. Cancer* **2014**, 14, 263-276.
20. (a) Patel MR, Kozuch SD, Cultrara CN, Yadav R, Huang S, Samuni U, Koren J 3rd, Chiosis G, Sabatino D. *Nano Lett.*, **2016**, 16, 6099–6108., (b) Patel, M.R.. RNAi Nanotechnology: A Platform for siRNA Screening and Gene Therapy. *Ph.D. Thesis* **2016**, Seton Hall University, South Orange, New Jersey.
21. Kirk, O.; Christensesn, M.W. *Org. Proc. Res. Dev.*, **2002**, 6, 446–451.
22. Chen, J.W.; Wu, W.T.; *J Biosci and Bioeng.* **2003**, 95, 466-469
23. Wilkinson, K.A.; Merino, E.J.; Weeks, K.M. *Nature* **2006**, 1, 1610-1616.
24. Vedejs, E.; Fuchs, P.L. *J. Org. Chem.*, **1971**, 36, 366–367.
25. Iwai, S.; Sasaki, T.; Ohtsuka, E. *Tetrahedron* **1990**, 46, 6673-6688.
26. (a) Damha, M.J.; Braich, R.S. *Tetrahedron Lett.* **1998**, 39, 3907-3910, (b) Braich, R.S.; Damha, M.J. *Bioconjugate Chem.* **1997**, 8, 370-377.
27. Suzuki, T.; Lu, J.; Zahed, M.; Kita, K.; Suzuki, N. *Arch. Biochem. Biophys.* **2007**, 468, 1-14.

28. Saar Ray, M.; Moskvovich, O.; Iosefson, O.; Fishelson, Z. *J. Biol. Chem.* **2014**, 289, 15014-15022.
29. Porterfield, J.Z.; Zlotnick, A. *Virology.* **2010**, 407, 281-288.
30. (a) McCarthy, S.M.; Gilar, M.; Gebler, J. *Anal. Biochem.* **2009**, 390, 181-188, (b) Noll, B.; Seiffert, S.; Vornlocher, H.-P.; Roehl, I., *J. Chromatogr. A* **2011**, 1218, 5609-5617.
31. Beverly, M.; Hartsough, K.; Machemer, L.; Pavco, P.; Lockridge, J., *J. Chromatogr. B* **2006**, 835, 62-70.
32. (a) Petrov, A.; Tsa, A.; Puglisi J.D. *Methods Enzymol.* **2013**, 530, 301-313, (b) Petrov, A.; Wu, T.; Puglisi, E.V.; Puglisi, J.D. *Methods Enzymol.* **2013**, 530, 315-30.
33. Gray, D.M.; Hung, S.H.; Johnson, K.H. *Methods Enzymol.* **1995**, 246, 19-34.
34. Gray, M. J.; Mhawech-Fauceglia, P.; Yoo, E.; Yang, W.; Wu, E.; Lee, A. S.; Lin, Y. G. *Int. J. Cancer.* **2013**, 133, 21-30.
35. Bifulco, G; Miele, C; Di Jeso, B; Beguinot, F; Nappi, C; Di Carlo, C; Capuozzo, S; Terrazzano, G; Insabato, L; Ulianich, L. *Gynecol. Oncol.* **2012**, 125, 220-225.
36. Ulianich, L; Insabato, L. *Front. Med.* **2014**, 1, 55-60.
37. Matsuo, K; Gray, M. J; Yang, D. Y; Srivastava, S. A; Tripathi, P. B; Sonoda, L, A; Yoo, E. I; Duebeau, L; Lee, A. S; Lin, A. S. *Gynecol. Oncol.* **2013**, 128, 552-559.
38. Luvsandagya, B.; Nakamura, K.; Kitahara, Y.; Aoki, H.; Murata, T.; Ikeda, S.; Minegishi, T. *Gynecol. Oncol.* **2012**, 126, 132-139.
39. Wang, H.; Liu, Z.; Gou, Y.; Qin, Y.; Xu, Y.; Liu, J.; Wu, J. Z. *Int. J. Nanomedicine* **2015**, 10, 5505-5512.
40. Calì, G; Insabato, L; Conza, D; Bifulco, G; Parrillo, L; Mirra, P; Fiory, F; Miele, C; Raciti, G. A; Di Jeso, B; Terrazzano, G; Beguinot, F; Ulianich, L. *J. Cell. Physiol.* **2014**, 229, 1417-1426/
41. Dejeans, N.; Glorieux, C.; Guenin, S.; Beck, R.; Sid, B.; Rousseau, R.; Bisig, B.; Delvenne, P.; Buc Calderon, P.; Verrax, J. *Free Radic. Biol. Med.* **2012**, 52, 993-1002
42. Rubporn, A.; Srisomsap, C.; Subhasitanont, P.; Chokchaichamnankit, D.; Chiablaem, K.; Svasti, J.; Sangvanich, P. *Cancer Genomics Proteomics.* **2009**, 6, 229-237.
43. Taldone, T.; Ochiana, S.O.; Patel, P.D.; Chiosis, G. *Trends Pharmacol. Sci.* **2014**, 35, 592603.

CHAPTER 3: FLUORESCENTLY LABELED SiRNAs AND THEIR THERANOSTIC APPLICATIONS IN CANCER GENE THERAPY

3.1 Abstract

Gene therapy has emerged as a promising precision nano-medicine strategy in the targeted detection and therapy of cancer. The integration of therapy and diagnostics “theranostics” have gained significant traction in the development of new and improved gene therapeutics that effectively diagnose and treat cancers at the onset of the disease. At the forefront of its pre-clinical and clinical applications are the short-interfering RNA (siRNA), that have silenced oncogenic mRNA expression of oncoproteins leading to cancer cell death through the RNA interference (RNAi) mechanism. Our research program focuses on the development of siRNAs designed to target and silence the expression of the Glucose Regulated Proteins (GRPs). The GRPs are a class of chaperone proteins assisting in protein folding events within the endoplasmic reticulum. Under physiological or pathological stress conditions, some GRPs translocate to the cell surface where they function as receptors signaling oncogenic activity. Therefore, the GRPs have been classified as clinically viable therapeutic targets. In the theranostic approach presented in Chapter 3 of this thesis, the covalent attachment of a fluorophore, fluorescein isothiocyanate (FITC), is applied for monitoring cell uptake, co-localization and biological activity of a wide range of GRP-silencing siRNAs, including those adopting linear, V-shape and Y-branch nanostructures. The incorporation of the FITC reporter did not perturb the requisite A-type helix structure required for siRNA activity as verified by CD spectroscopy. Furthermore, FITC did not inhibit hybrid duplex stability, verified by T_m , although some degree of fluorescence quenching relative to the unlabeled siRNA was detected by spectrofluorimetry. In an attempt to overcome the quenching effect, the higher-order V- and Y-shape siRNAs enabled the incorporation of multiple FITC reporters; however, the

incorporation of multiple FITC probes did not overcome the quenching effects *in vitro*. In cells, the silencing efficiency of the FITC-labeled siRNAs within a prostate cancer cell line (PC-3, ATCC® CRL-1435™) was determined via RT-PCR. In all cases, FITC-siRNA hybrids (50nM) exhibited less mRNA knockdown (~10-30%) when compared to their non-labeled counterparts (~40-80%). Conjugation of the FITC probe to the sense strand of the siRNAs re-established mRNA knockdown (~50-<90%) efficiency which also translated to more potent cell death over a 72 hr period (~20-95%). Cell uptake of the multi FITC-labeled V- and Y-shape siRNAs was monitored via flow cytometry which revealed rapid cell internalization (2-4 hrs) and enhanced fluorescent signaling which remained present within the cells post transfection (72 hrs). Western blot analysis of the lead Y-shaped FL-siRNA showed protein level silencing of GRP78 and GRP75 (~40%), while qRT-PCR showed mRNA silencing of GRP78 and 94 (~40-60%). Taken together, the data presented within this chapter outlines the potential utility of FL-siRNAs as potent theranostic agents for cancer gene therapy.

3.2 Introduction

3.2.1 SiRNAs as Theranostic Agents

“Theranostics” is a term that refers to the simultaneous integration of diagnosis and therapy in the detection and treatment of a wide range of diseases, including cancer.¹ Nano-theranostics characterizes nanoparticle formulations that have gained widespread utility in the development of nano-medicine strategies for advanced theranostic applications. Ultimately, the purpose is to diagnose and treat diseases at their earliest stages, when they are most likely curable or at least treatable. Nano-theranostic approaches can be promising treatment options, even for the most lethal or difficult to treat diseases such as cancer, cardiovascular diseases and AIDS.^{2,3} Advanced theranostic nano-medicines are multifunctional in nature, capable of diagnosis and delivery of

therapy to the diseased cells with the incorporation of targeting ligands, biomarkers and reporter probes that enable detection.⁴⁻⁶ (**Figure 3.1**) The therapeutic agent can encompass a small molecule synthetic drug or complex natural product, synthetic, semi-synthetic and recombinant biologics, toxins and suicide substrates or irreversible inhibitors. The diagnostic agent can include a fluorescent reporter, a radionuclide, near IR sensors and contrast agents that have also received widespread use in pre-clinical and clinical applications (**Figure 3.1**). Theranostic nano-medicines are robust, biocompatible and non-toxic delivery platforms that can sustain controlled release, targeted delivery and higher transport efficiency by receptor mediated endocytosis at the target site.⁷ For example, stimulus responsive delivery agents have led to the development of triggered release (*i.e.*, smart delivery)⁸ and synergistic performance in combination therapy strategies (*i.e.* siRNA co-delivery with other therapeutics).⁹

Acting as a multimodal therapy strategy, siRNA based theranostics have been shown to greatly improve the diagnosis and therapy of many disease types, including cancer.⁹ In this multimodal approach, iron oxide nanoparticles were developed for simultaneous *in vivo* imaging and siRNA delivery into tumors by high resolution MRI and near infrared (NIR) *in vivo* optical imaging.¹⁰ The siRNA, coupled with aminated dextran particles, myristoylated polyarginine peptide, a membrane translocation peptide, and the NIR dye Cy5.5 were all conjugated to the surface of an iron oxide nanoparticles. Tracking these probes *in vivo* by MRI and NIR fluorescence optical imaging, the delivery of siRNA and its silencing efficiency of Survivin genes in glioma tumors was monitored for 48 h by dextran coated iron oxide nanoparticles. Drug loaded quantum dots have also been used as theranostic agents in which solid lipid nanoparticles were combined with the chemotherapeutic paclitaxel, also known as Taxol®, and Bcl-2 targeted siRNA into human lung carcinoma cells.¹¹ The prepared solid lipid nanoparticles loaded with the combined

paclitaxel/siRNA complexes exhibited synergistic anticancer activities by triggering caspase-mediated apoptosis. The strong fluorescence intensity of quantum dots within solid lipid nanoparticles enabled *in situ* visualization and intracellular translocation of solid lipid nanoparticles in A549 lung cancer cells.

Theranostic approaches to cancer treatment have also shown to be successful in silencing oncogene expression in aggressive forms of cancers.¹² In this application, a near-infrared (NIR) fluorescent polymer capable of *in vivo* siRNA delivery was used to simultaneously track tumor accumulation by noninvasive NIR imaging. Systemic siRNA delivery using the polyPCPDTBT polymer-NIR nanoparticle formulation resulted in efficient silencing of V-Raf expression of murine sarcoma viral oncogene homolog B (BRAF) in anaplastic thyroid cancer (ATC) tumor tissues and significantly suppresses tumor growth and metastasis in an orthotopic mouse model.

Carbon dots (Cdots) are currently emerging as a class of promising fluorescent probes because of their low photobleaching and optical blinking, tunable photoluminescence, versatile surfaces, and excellent biocompatibility.^{13,14} Cdot based nanocarriers have been developed to deliver siRNA against anti-apoptotic protein, Survivin, in human gastric cancer cell line MGC-803.¹⁵ It is well known that Survivin plays an important role in regulating cell division, apoptosis, and checkpoint mechanisms of genomic integrity.^{16,17} In addition, Survivin expression is often upregulated in human cancers, as it can be treated as a specific tumor marker with prognostic and therapeutic implications from studies of gastric carcinomas.¹⁸ The siRNA-Cdot complex was rapidly accumulated into the MGC-803 cells within 2 h. Blue fluorescence from Cdots and red fluorescence from labeled siRNA increase significantly in a time dependent manner. SiRNA-Cdots complexes, which target Survivin, exhibited potent mRNA and protein knockdown which induced

apoptosis and cell cycle arrest in G₁ phase in human gastric cancer cells MGC-803. The resulting Cdots-based delivery system may be used to advance the field of siRNA therapeutics.

SiRNAs conjugated to dual-purpose superparamagnetic iron oxide nanoparticles (SPIONs) were evaluated as theranostic agents against pancreatic ductal adenocarcinoma (PDAC).¹⁹ Multifunctional theranostic probes comprising of dextran-coated SPIONs that were easily detected by MRI imaging. These probes were functionalized with: (i) the non-immunogenic ligand EPPT1²⁰ specifically targeting the tumor antigen under glycosylated MUC1 (uMUC1), which is a hallmark of early pancreatic tumorigenesis and abundantly and ubiquitously expressed in PDAC; (ii) myristoylated polyarginine peptides (MPAPs)²¹ to enhance cellular uptake and mediating the endosomal escape of siPLK1 into the cytoplasm; and (iii) siPLK1, for selective silencing of siPLK1 to halt cell cycle progression selectively in the tumor.²² Administrations of these complexes in tumor-bearing mice allows monitoring of the delivery agent to the tumor site by MRI resulting in efficient silencing of the target gene, PLK1. This approach can significantly advance the therapeutic potential of siRNAs by providing an effective way to shuttle siRNAs to target sites and to non-invasively access therapeutic efficacy of the siRNAs by monitoring tumor growth.

SiRNAs have also been designed to target Pim-1, a serine/threonine kinase that phosphorylates heterochromatin protein HP1 γ and several other targets, for example, cdc25 and c-Myb²⁴⁻²⁶ is involved in the induction of B cell lymphoma when co-expressed together with c-Myb.²⁷ In addition, Pim-1 seems to play a role in cell survival, differentiation, and proliferation.^{28,29} SiRNAs targeting Pim-1³⁰ exhibited excellent silencing efficiency of a Pim1-green fluorescent protein (GFP) fusion gene at low nanomolar concentrations (5 nM). PsiR4 was labeled with Cy3 at the 5' -end of the sense strand to investigate cellular uptake and localization in

living COS-7 and F-11 cells. Cellular uptake of the Cy3-labeled siRNA by lipofection was observed in more than 90% of the cells post transfection (4-6 hr). Fluorescence imaging revealed strong inhibition of Pim1-GFP expression at a concentration of 10 nM, with nearly complete Pim-1 silencing at a concentration of 50 nM, while western blot analysis confirmed the knockdown of Pim-1 with PsiR4-Cy3 at the protein level. These results show that PsiR4-Cy3 is a useful molecule to study siRNA uptake and localization in living cells.

Fluorescently labeled siRNAs have also been used to optimize knockdown efficacy.³⁰ SiRNA labeled with FITC at either the 5'-end of the sense or the antisense strand were compared with un-transfected or mock transfected cells with unlabeled siRNA. In this instance, distinct intracellular fluorescence staining was observed in cells transfected with FITC labeled siRNA. These signals showed intracytoplasmic and perinuclear localization, in accordance with the current notion of RNAi occurring as a post-transcriptional process. No qualitative difference was observed between sense and antisense-labeled siRNA molecules.

Taken together, these selected examples serve to highlight the fruitful applications of theranostic siRNA formulations that have enabled detection and treatment in difficult to treat cancers *in vitro* and *in vivo* by selectively targeting and silencing oncogenic mRNA expression. Moreover, the theranostic siRNA formulation can be fine-tuned to incorporate noninvasive reporter probes for tracking biological activity in live cancer cells and within *in vivo* xenograft models, as well as chemotherapeutics, which potentiates the anti-cancer effects when used in combination treatment regimens. As such, the multifunctional siRNA theranostic formulations have shown success in difficult to treat tumors, while also minimizing relapse and the evolution of treatment resistance. The latter is a primary goal in the development of effective precision medicine approaches.

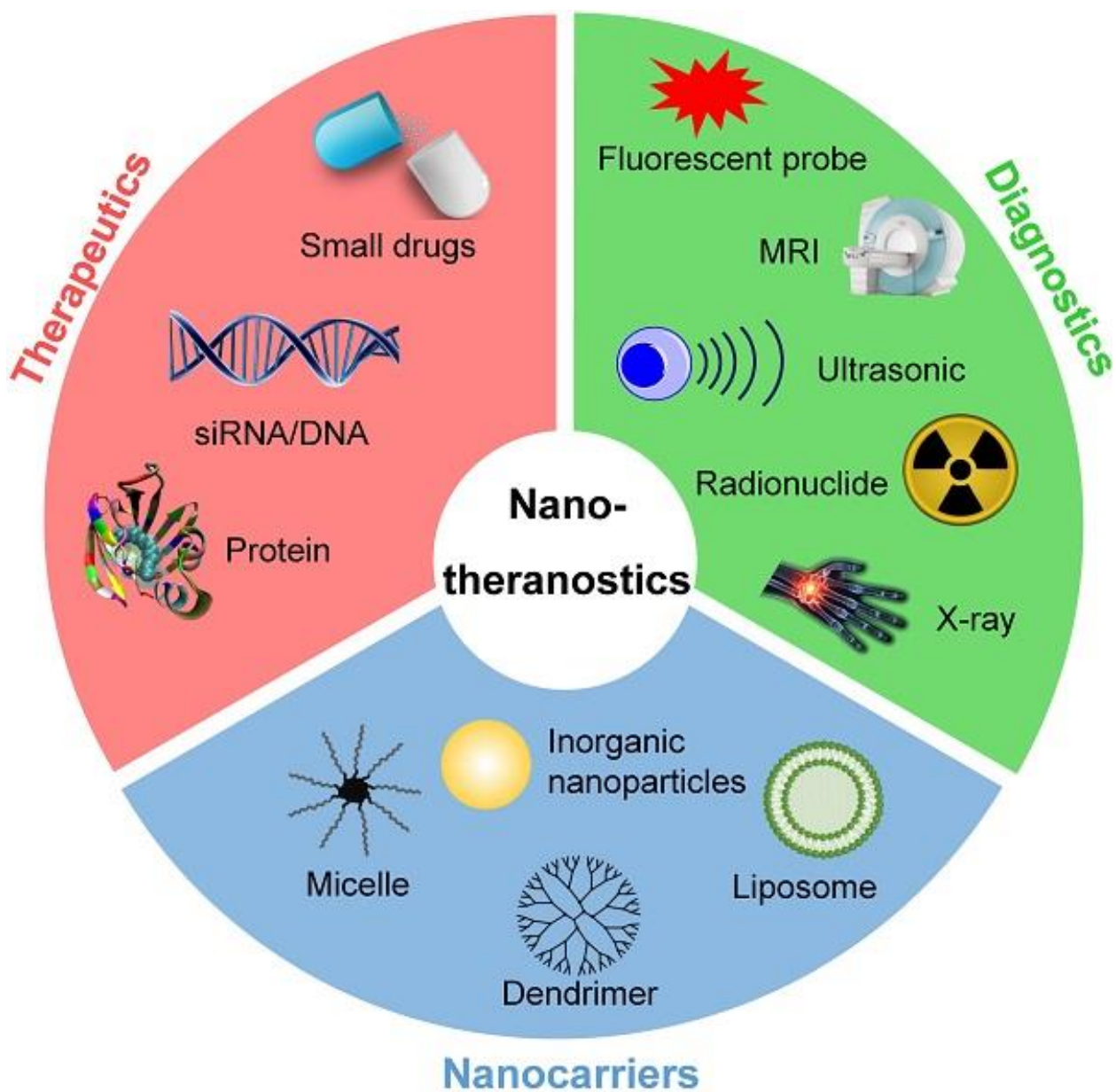


Figure 3.1 Multifunctional applications of theranostic agents. Wang, J.; Cui, H. *Theranostics*. 2016, 6 (9), 1274-76.³¹

3.2.2 The Glucose Regulated Proteins as Therapeutic Targets

The glucose-regulated protein (GRPs) are chaperone proteins that serve as the main sensors for misfolded proteins in the endoplasmic reticulum (ER) and trigger the unfolded protein response

(UPR) under physiological and pathological cellular stress conditions.³² GRPs are found in the lumen of the ER or the mitochondria where they own important functions in the regulation of protein folding events that are necessary for cell homeostasis and survival. As chaperones, GRPs are subcellularly localized in the ER where they chaperone protein folding activity, in the mitochondria where they interact with pro-apoptotic executors and at the cell surface where they direct cell signaling.³³ Cell surface GRPs have been found on a variety of cancer cells but not on normal ones, thereby making them valuable biomarkers for the development of targeted forms of cancer therapy (Table 3.1).³⁴⁻³⁷

Glucose-regulated protein 78 (GRP78), also known as the immunoglobulin heavy chain binding protein (BiP), is a member of the heat-shock protein (HSP) family of chaperones that mainly resides in endoplasmic reticulum (ER).³⁸ GRP78 is an important regulator of ER homeostasis due to its role in protein folding and assembly while targeting misfolded proteins for degradation.³⁹ Numerous studies have shown that cells under physiological or pathological ER stress, such as hypoxia, acidosis and glucose deprivation, elicit upregulation of GRP78.^{40,41} Upregulation of GRP78 is commonly associated with tumor cell apoptosis resistance,⁴² drug resistance,⁴³ tumor adhesion, migration and metastasis.⁴⁴ Furthermore, studies have shown that downregulation of GRP78 can promote apoptosis and inhibit tumor growth.^{45,46} Our group has shown that targeting and silencing GRP78 expression in HepG2 liver cancer cells resulted in noticeable albeit minimal (5-15%) cell death.⁴⁷ More importantly, cancer cell surface GRP78 is associated with pathological stress induced conditions that are typically associated with the tumor microenvironment.^{48,49} In addition, the cell surface GRP78 often presents in the form of clustering or punctate aggregates associated with carcinogenesis.⁵⁰ Taken together, cell surface GRP78 has

been classified as a biomarker which serves as a receptor for oncogenic signaling and as a target for GRP78-dependent gene therapy in cancer cells exhibiting GRP78 overexpression.

Similarly, GRP94 has been found to maintain ER Ca^{2+} homeostasis and confer cancer cells protection from apoptosis.⁵¹ Alternatively, GRP94 suppression or knockdown in patient derived multiple myeloma samples was found to trigger apoptosis by inhibition of the WNT–survivin pathway.⁵² Furthermore, in the absence of GRP94, the multiple myeloma cells were found to undergo mitotic destruction, which resulted in cell death and correlated with a decreased expression of Survivin.⁵³ Therefore, GRP94 might promote survival and progression of multiple myeloma as well as in other, related tumors. For example, induction of GRP94 in HeLa cells was observed following transfection with 2'-O-methyl-modified siRNA targeting GRP78 mRNA. GRP94 induction was hypothesized to play a compensatory role in maintaining UPR activity.

GRP75, a homologue of HSP70 has been found to interact with the tumor suppressor p53, leading to the inhibition of p53 function and induction of apoptosis.⁵⁴ Furthermore, cell surface GRP94 and GRP170 function in antigen presentation, and their secreted forms have the ability to stimulate immune responses, which could be useful in the development of cancer vaccines.⁵⁵ In cancer cells, GRP170 is upregulated by hypoxia and by drugs such as celecoxib (a non-steroidal anti-inflammatory drug) and proteasome inhibitors, and knockdown of GRP170 activated the expression of the UPR pro-apoptotic factor CHOP and stimulated apoptosis.⁵⁶ Therefore, GRP170 might also protect cancer cells against cell death by blocking ER Ca^{2+} release or delaying the onset of the UPR by binding to the ER stress sensors.⁵⁷ Therefore, the GRPs encompass an important class of tumor-promoting genes whose downregulation has been found to confer potent anti-cancer effects in a panel of cancer cell lines.⁵⁸ Towards this effect, we have demonstrated that silencing

GRP 75, 78 and 94 in endometrial, cervical and breast cancer resulted in potent GRP knockdown and cell death relative to a non-tumorigenic cell line which displayed normal GRP expressions.

Type of Cancer	GRP78	GRP94	GRP75
Bladder	+		
Brain	+		+
Breast	+	+	+
Colorectal	+	+	+
Endometrial	+		
Esophageal	+	+	
Gastric	+	+	
Head and Neck	+	+	
Leukemia	+		+
Liver	+	+	+
Lung	+	+	+
Melanoma	+		
Multiple myeloma	+	+	
Nasopharyngeal		+	
Oral	+	+	
Osteosarcoma		+	
Ovarian	+		+
Pancreatic	+	+	+
Prostate	+		
Renal	+		
Thyroid			

Table 3.1 Overexpression of GRPs in different cancer types. Adapted with permission from Springer Nature: Lee, A.S. *Nat. Rev. Cancer* **2014**, *14*, 263-276.

3.3 Project Objectives

In an effort to build on previous work from our group, this chapter describes the design, synthesis, characterization and biological evaluation of fluorescently labeled siRNA nanostructures within human cancer cells. The project objectives for this study begins with the selection of the lead linear, V- and Y-shaped siRNAs that elicited the most potent silencing efficiency when targeting one or two sites of oncogenic GRP78 and those related to the GRP-75 and 94 mRNA sequences. The solid-phase RNA synthesis strategy based on our previous study⁴⁷ was used to generate V-shape and Y-branch RNA templates using the ribouridine branch-point synthon (**Figure 3.2**). The lead linear, V- and Y-shaped RNAs were functionalized with an amino modified hexamethylene linker, which facilitated conjugation of the reporter fluorescent probe. The amino modified sequences were then coupled to fluorescein isothiocyanate (FITC) following a previously reported method.⁵⁹ Following coupling, RP-IP-HPLC and ESI-MS were used to characterize the purity and identity of the RNA templates. The hybrid fluorescently-labeled siRNAs (FL-siRNA) were characterized by Polyacrylamide Gel Electrophoresis (PAGE), Thermal Denaturation (T_m) and Circular Dichroism Spectroscopy (CD). Fluorescence emissions and quantum yields (ϕ) of the FL-siRNA constructs were also determined in order to evaluate the overall efficacy of the functionalized siRNAs as molecular beacons. Biological evaluation and uptake efficiency of the linear, V- and Y-shaped FL-siRNA constructs were determined within the PC-3 human prostate cancer cell line. Silencing efficiency of the siRNA constructs was determined at the mRNA and protein levels by qRT-PCR and western blot, respectively. Whereas, time-dependent cellular uptake efficiency was evaluated by flow cytometry and fluorescence microscopy. To assess the toxicity effects of the fluorescently labeled siRNAs, cell viability was determined using propidium iodide (PI) staining.

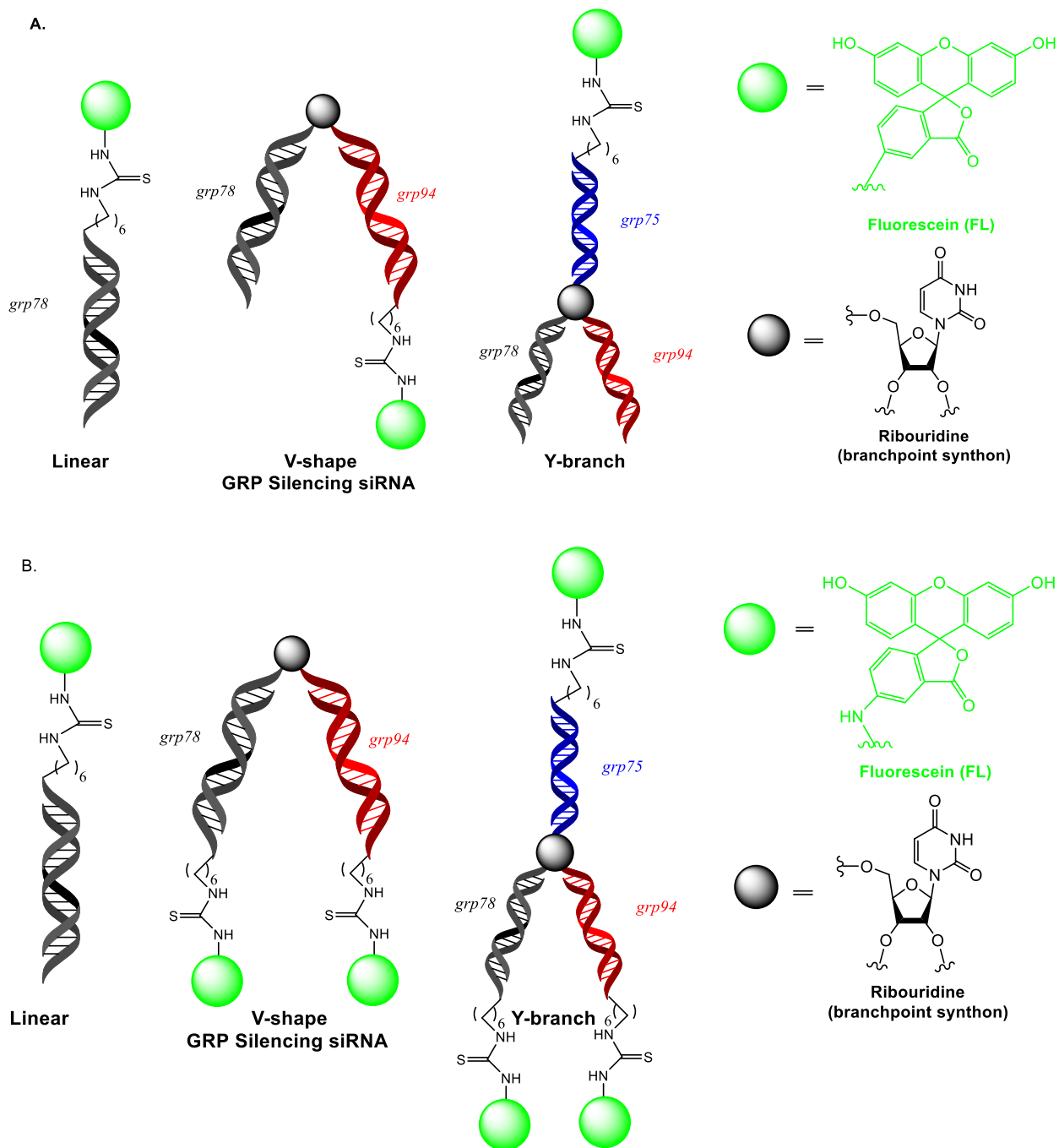
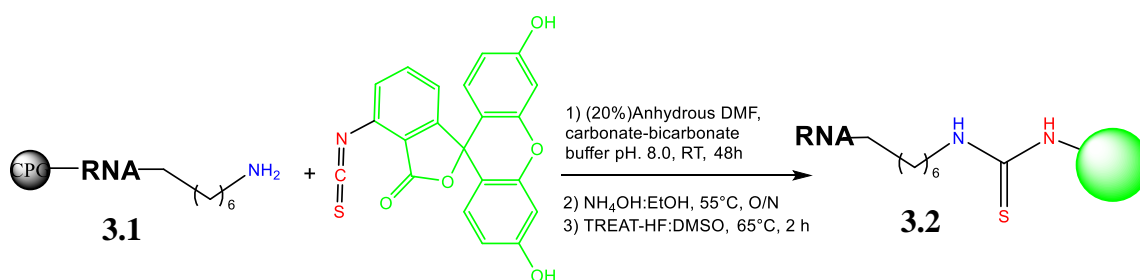


Figure 3.2. Rational design of FL-siRNA bioconjugates. Linear, V-shape and Y-branch GRP silencing siRNAs with **A)** single and **B)** multiple FITC probes. Drawn in ChemDraw.

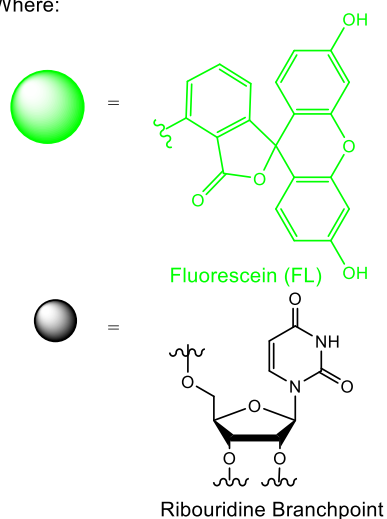
3.4 Results and Discussion

3.4.1 FITC Solid Phase RNA Bioconjugation

As a representative example, the amino functionalized RNA template, **3.1**, was subjected to a solid-phase bioconjugation reaction for the attachment of the fluorescent probe, fluorescein isothiocyanate (FITC). Based on literature precedence,⁵⁹ the attachment of FITC was achieved by reacting FITC in 20% aqueous DMF mixed in 0.1M carbonate-bicarbonate buffer (pH 8.5) onto the amino modified RNA template bound to the solid support (**Scheme 3.1**). Following reaction, FL-RNA sample, **3.2**, was cleaved and deprotected from the solid support for analysis and purification.



Where:



RNA	% Conversion ^a
a) GRP78	58%
b) GRP78 GRP94	40%
c) GRP78 GRP94 GRP75	<5%

^aConversions based on RP IP HPLC analysis at 260 and 488 nm

Scheme 3.1 Solid phase bioconjugation of linear, V- and Y- shape FITC-RNA bioconjugates. Drawn in ChemDraw.

3.4.2 Analysis and Purification of FITC-RNA Templates

The RNA templates described in this study (**Table 1**) are based on the target sequences for downregulating GRP-75, 78 and 94 expression in human cancer cells.^{46,60} The linear, V- and Y-shaped RNA templates were synthesized by semi-automated solid phase RNA synthesis following our previously reported procedure.⁴⁷ The RNA templates were purified by Reverse-Phase Ion-Pairing High Performance Liquid Chromatography (RP IP HPLC) in $\geq 95\%$ purities and their identities were confirmed by electrospray ionization mass spectrometry (ESI MS) (**Table 3.2**). Purified FL-RNA templates were then quantitated by UV-Vis spectroscopy at 260 nm which also confirmed the absorption of FITC (460-490 nm). Denaturing PAGE analysis of the purified RNA templates suggested some degradation, however, RP IP HPLC re-analysis of the sequences confirmed pure RNA samples. Presumably, denaturing PAGE conditions produced some sample degradation, albeit minimal (**Figure 3.4**). Moreover, UV shadowing of the gel revealed FITC fluorescence for the labeled RNA templates (**Figure 3.4B**). However, the analysis did reveal that the FITC-Y shaped RNA was not present. The reaction was conducted multiple times in an effort to obtain the FITC-Y shaped siRNA, however, none were successful. To address this problem, attachment of the FITC probe to the corresponding complementary linear sense strands was achieved in high yields and purities $>95\%$, allowing further characterization to be conducted with the fluorescently-labeled Y-shape siRNA hybrid.

Name	Sequence ^a	Percent Yield (%) ^b	Percent Purity (%) ^c	Mass ^d
1 GRP78A1	5'-AUC AGA AUC UUC CAA CAC U-3'	91	>99%	5949.6 (5949.9)
2 GRP78S1	5'-AGU GUU GGA AGA UUC UGA U-3'	92	>99%	6103.7 (6103.9)
3 GRP94S1	5'-GAA GAA GCA UCU GAU UAC C-3'	90	>99%	6068.8 (6069.0)
4 GRP75S1	5'-ACU GAC UCG GAG AAU ACA A-3'	91	>99%	6091.8 (6092.2)
5 V-78A194A1	2'-3'-CUU CUU CGU AGA CUA CUG G-5' rU 3'-5'-AUC AGA AUC UUC CAA CAC U-3'	83	>99%	12929.7 (12929.9)
6 V-78A178A2	2'-3'-CCU CGC GUA AUC AUG AUC U-5' rU 3'-5'-AUC AGA AUC UUC CAA CAC U-3'	81	>98%	12275.4 (12276.6)
7 Y-78A194A175A1	2'-3'-CUU CUU CGU AGA CUA CUG G-5' 5'-UUG UA UCU CCG AGU CAG U-3'-5'-rU 3'-5'-AUC AGA AUC UUC CAA CAC U-3'	62	>98%	18335.9 (18357.2)
8 FITC-78A1	FITC-NH-(CH ₂) ₆ -5'-AUC AGA AUC UUC CAA CAC U-3'	52	>97%	6516.7 (6518.5)
9 FITC-78S1	FITC-NH-(CH ₂) ₆ -5'-AGU GUU GGA AGA UUC UGA U-3'	48	>98%	6670.8 (6672.5)
10 FITC-94S1	FITC-NH-(CH ₂) ₆ -5'-GAA GAA GCA UCU GAU UAC C-3'	51	>97%	6635.9 (6636.8)
11 FITC-75S1*	FITC-NH-(CH ₂) ₆ -5'-ACU GAC UCG GAG AAU ACA A-3'	N/A	>99%	6629.3 (6628.8)
12 FITC-V-78A194A1	2'-3'-CUU CUU CGU AGA CUA CUG G-5'-(CH ₂) ₆ -NH-FITC rU 3'-5'-AUC AGA AUC UUC CAA CAC U-3'	22	>95%	13013.1 (12884.6)
13 FITC-V-78A178A2	2'-3'-CCU CGC GUA AUC AUG AUC U-5'-(CH ₂) ₆ -NH-FITC rU 3'-5'-AUC AGA AUC UUC CAA CAC U-3'	20	>95%	12969.1 (12843.9)

Table 3.2. ^aLinear, V- and Y-shaped RNA sequences designed to target GRP-78, 94 and 75. ^bDetermined by UV-Vis Spectroscopy. ^c Obtained by RP-IP-HPLC using 0.1 mM TEAA in 0-45% MeCN, pH: 7.2 over 20 min. ^d Calculated mass (observed mass) by ESI-MS in negative mode (Novatia LLC, Newton, PA). * Sample purchased from ChemGenes (Wilmington, MA)

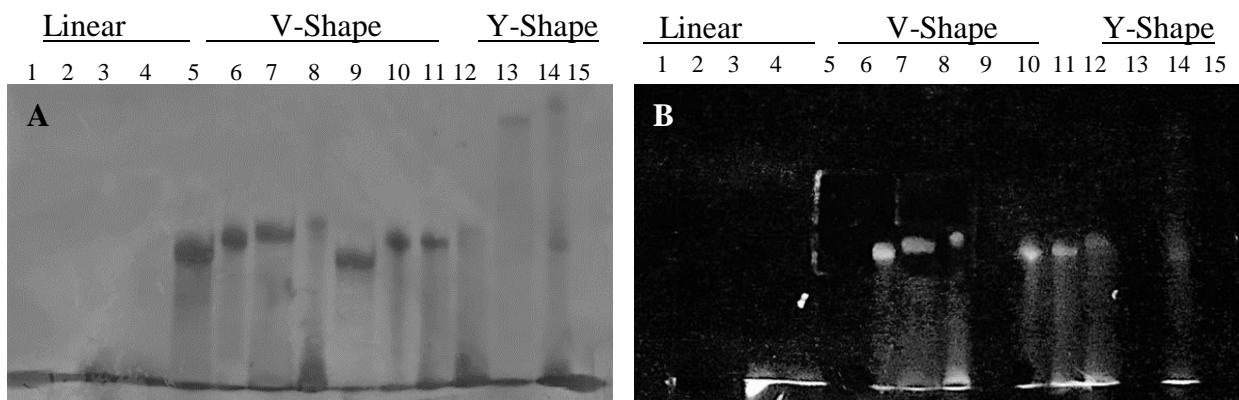


Figure 3.3 Denaturing PAGE of FITC-labeled siRNAs. Sequences in green represent FITC labeled sequences: Lane 1: Dye; Lane 3 GRP78A1; Lane 4 FITCGRP78-A1; Lane 5 V-78A194A1; Lane 6 FITC-C₆-V-78A194A1; Lane 7 FITC-V-78A194A1 (peak1); Lane 8 FITC-V-78A194A1 (peak2); Lane 9 V-78A178A2; Lane 10 FITC-V-78A178A2; Lane 11 FITC-V-78A194A1 (peak1); Lane 12 FITC-V-78A194A1 (peak2); Lane 13 Y-78A194A175A1; Lane 14 FITC-Y-78A194A175A1; Lane 15 Dye.

3.4.3 FITC-siRNA Hybridization and Native PAGE

The RNA templates were hybridized with their complementary strands in the annealing Tris buffer buffer (10 mM Tris, 50 mM NaCl, 1 mM EDTA, pH 7.5 – 8.0) conditions. siRNA hybridization and self-assembly was confirmed by a native, non-denaturing 16% polyacrylamide gel electrophoresis (PAGE). In this assay, (**Figure 3.5A**) the lower molecular weight linear hybrids migrated fastest on the gel while the V-and Y-shaped RNA templates hybridized to their complementary RNA single strands (**Figure 3.5A**, lanes 4-9 and lanes 10-13, respectively) migrated slower on the gels. Long wave UV shadowing, **Figure 3.5B** revealed the FITC-labeled siRNA hybrids (**Figure 3.5B**, lanes 5-6, 8-9 and 11-13).

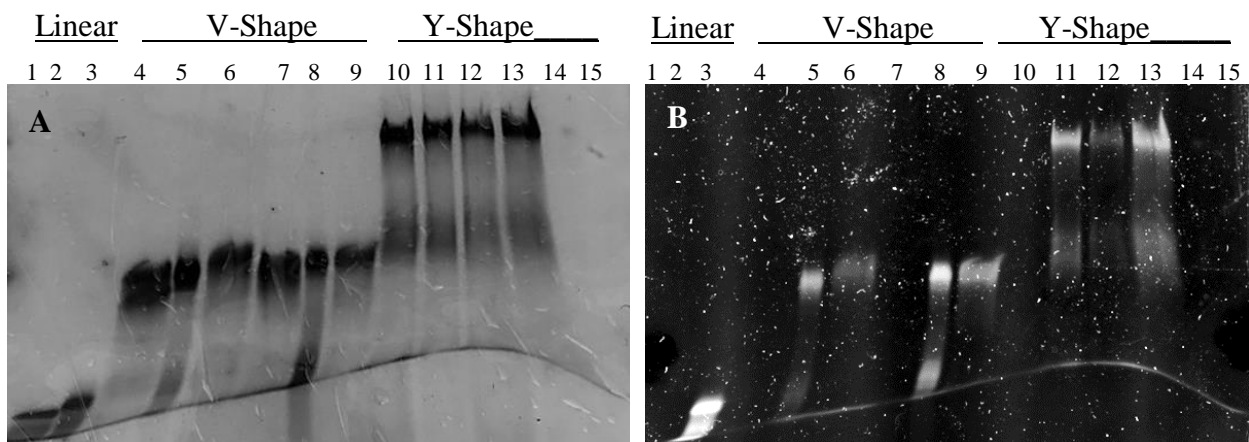


Figure 3.4 Native PAGE of FITC-labeled siRNAs. Sequences in green represent FITC labeled sequences Lane 1: Dye; Lane 2 A1:S1; Lane 3 **FL-A1**:S1; Lane 4 V-78A194A1:78S194S1; Lane 5 **FL-V-78A194A1**:78S194S1; Lane 6 V-78A194A1:78S1**FL-94S1**; Lane 7 V-78A178A2:78S178S2; Lane 8 **FL-V-78A178A2**:78S178S2; Lane 9 V-78A178A2:**FL-78S1**78S2; Lane 10: Y-78A194A175A1:78S194S175S1; Lane 11 Y-78A194A175A1:**FL-78S1**94S175S1; Lane 12 Y-78A194A175A1:78S1**FL-94S1**75S1; Lane 13 Y-78A194A175A1:**FL-78S1FL-94S1**75S1; Lane 15 Dye.

Native PAGE of multi-FITC siRNA samples also confirmed successful hybridization, (**Figure 3.4 A, B**). In this assay, (**Figure 3.6A**) the lower molecular weight linear hybrids migrated fastest on the gel while the V- and Y-shaped RNA templates hybridized to their complementary RNA single strands which contained the FITC-label (**Figure 3.4A**, lanes 5-9 and lanes 10-13, respectively) were more retained on the gel. Long wave UV shadowing, **Figure 3.5 B** revealed the brilliant multi-FITC-labeled siRNA hybrids (**Figure 3.5B**, lanes, 7-8 and 11-13).

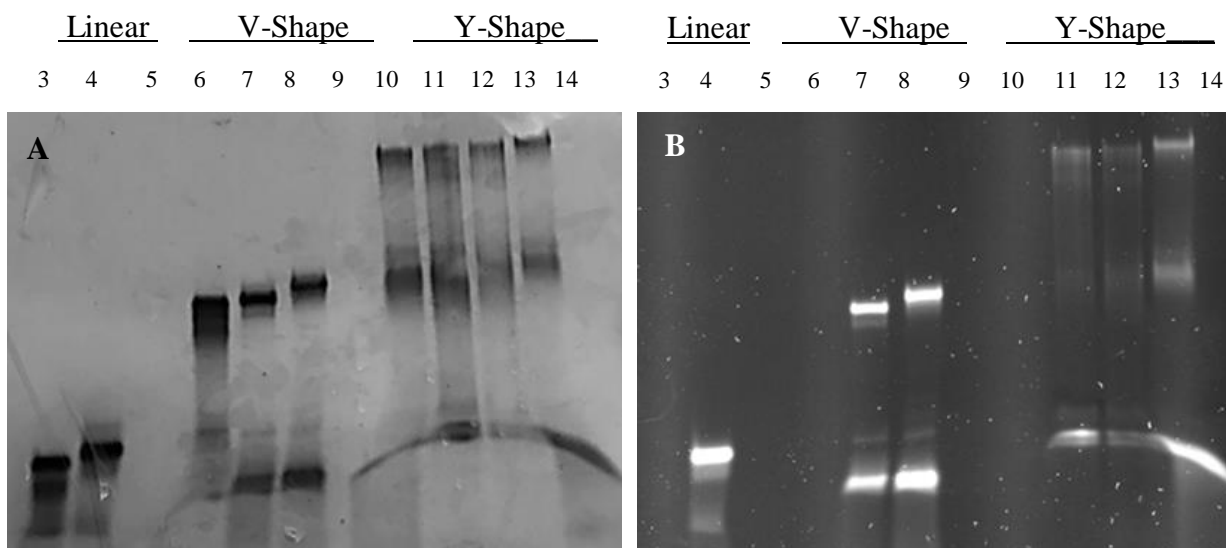


Figure 3.5 Native PAGE of multi-FITC-labeled siRNAs. Sequences in green represent FITC labeled sequences. Lane 1 Dye; Lane 2 empty; Lane 3 A1:S1; Lane 4 78A1:FL-78S1; Lane 5 empty; Lane 6 V78A194A1:78S194S1; Lane 7 V-78A194A1:FL-78S194S1; Lane 8 V-78A194A1:FL-78S1FL-94S1; Lane 9 empty; Lane 10 Y-78A194A175A1:78S194S175S1; Lane 11 Y-78A194A175A1:78S194S1FL-75S1; Lane 12 Y-78A194A175A1:78S1FL-94S1FL-75S1; Lane 13 Y-78A194A175A1:FL-78S1FL-94S1FL-75S1; Lane 14 empty; Lane 15 Dye.

3.4.4 Circular Dichroism (CD) Spectroscopy of siRNA Hybrids

Circular dichroism (CD) spectroscopy was used to explore whether the siRNA hybrid structures maintained the prerequisite A-type helix geometry for RNAi applications.⁶¹ The linear siRNAs displayed typical CD profiles for A-form helices, with a minimum peak at 240 nm and a broad maximum in between 250-290 nm.⁶² In all cases, the FITC-linear, V- and Y-shaped template siRNA hybrids (**Figure 3.6A**), retained the A-type broad maximum and minimum bands were observed between 250-290 nm and 240 nm, respectively, albeit with a decrease in the amplitudes of the molar ellipticities at these characteristic wavelengths. The multi-FITC labeled siRNAs (**Figure 3.6B**), produced more pronounced deviations from the A-type RNA helix. In most cases, the maximum peak at 260 nm remained; however, with notable changes in molar ellipticities at the characteristic maxima and minima within the 210-250 nm range. Taken altogether, the FITC-

labeled template siRNA hybrids were found to maintain A-type helices within their higher-ordered structure formulations while incorporation of multiple FITC probes within the siRNA hybrids was found to distort the A-type helix.

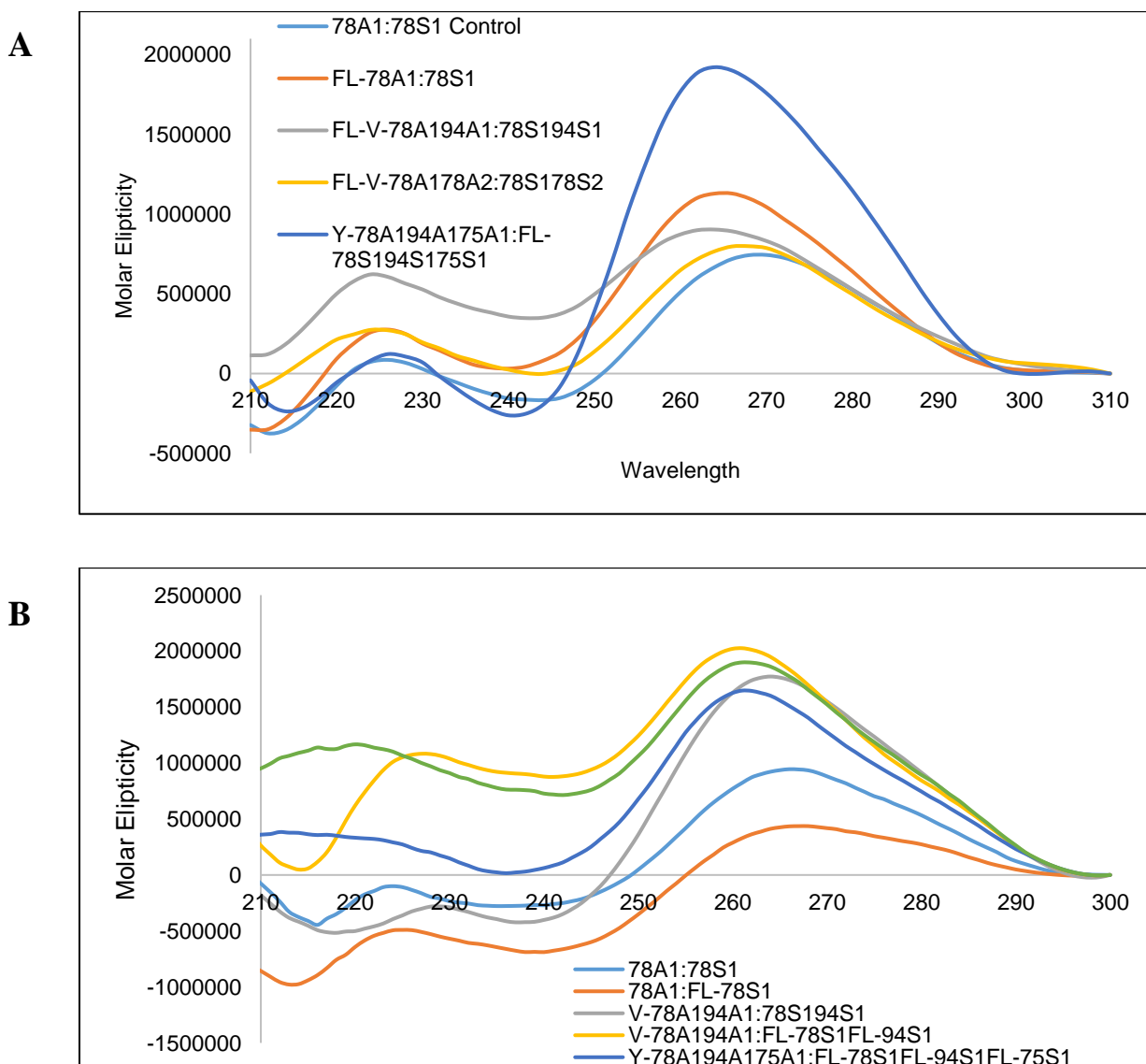


Figure 3.6 Circular dichroism spectroscopy of (A) FITC-templated siRNAs and (B) multi-FITC labeled siRNAs. All hybrid siRNA samples were prepared by annealing equimolar quantities (1.25 nM) of antisense RNA templates with their complementary linear sequences. Samples were hybridized in annealing buffer (10 mM Tris, 50 mM NaCl, 1 mM EDTA, pH 7.5 – 8.0) by pre-heating at 95 °C (7 min) followed by slow cooling to room temperature over 1 h and overnight storage at 4 °C prior to CD analyses. All samples were diluted in annealing buffer (1 mL) and the CD analysis was observed from 210-310 nm.

3.4.5 Thermal Denaturation (T_m) analysis of siRNA Hybrids by UV-Spectroscopy

SiRNA hybrid stabilities were measured by thermal denaturation (T_m) **Figure 3.7 A-C**. The addition of the FITC probe at the 5' terminus of the antisense strand had little to no effect on hybrid stability. (**Figure 3.7 B**) For example, FITC-GRP78A1:S1 maintained similar hybrid stabilities (T_m : 63°C) to the native A1:S1 (T_m : 62°C). Likewise, the FITC-V78A194A1:78S194S1 (T_m : 58→60 °C) and FITC-V78A178A2:78S178S2 (T_m : 55→62°C) showed a very slight increase in thermal hybrid stabilities. The Y-shaped hybrids elicited a weaker hybrid stability, (T_m : 52 °C), however, like seen previously, incorporation of the FITC label had little to no effect on siRNA hybrid thermal stability. In the case of the multi-FITC siRNAs, the V-shape RNA template hybridized with two FITC-linear RNAs showed a slight increase in hybrid stability (T_m : 58→65 °C) while the Y-shape hybridized with three FITC-linear RNAs exhibited a significant increase in hybrid stability (T_m : 52→68 °C). (**Figure 3.7 C**) Taken together, this data shows that attachment of the FITC probe into the template V- and Y-shape RNAs has little effect on the hybrid stability of the siRNAs, however, incorporation of multiple FITCs within a single siRNA construct shows enhanced stability of the siRNA duplex, which may improve their applications in biology.

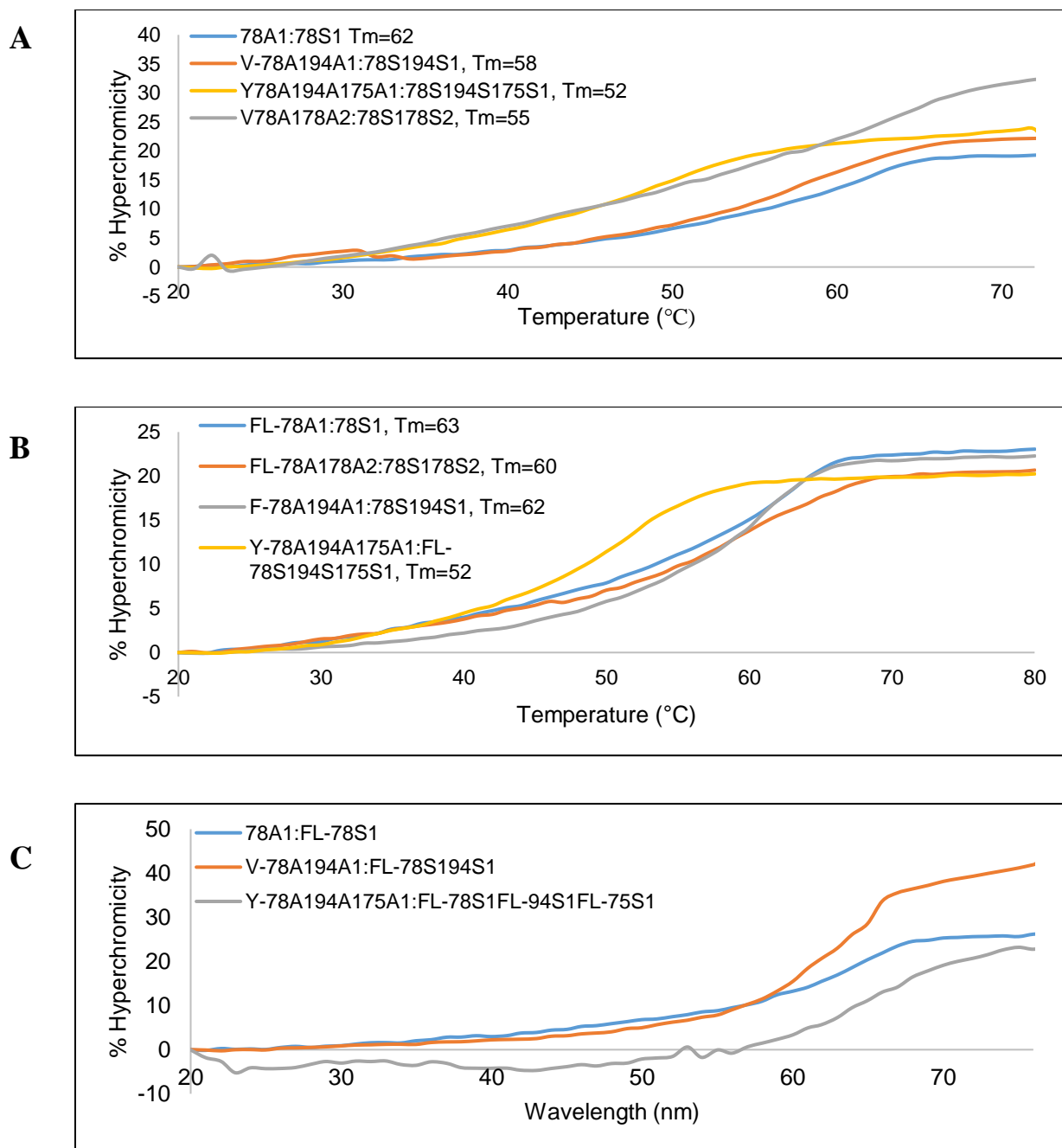
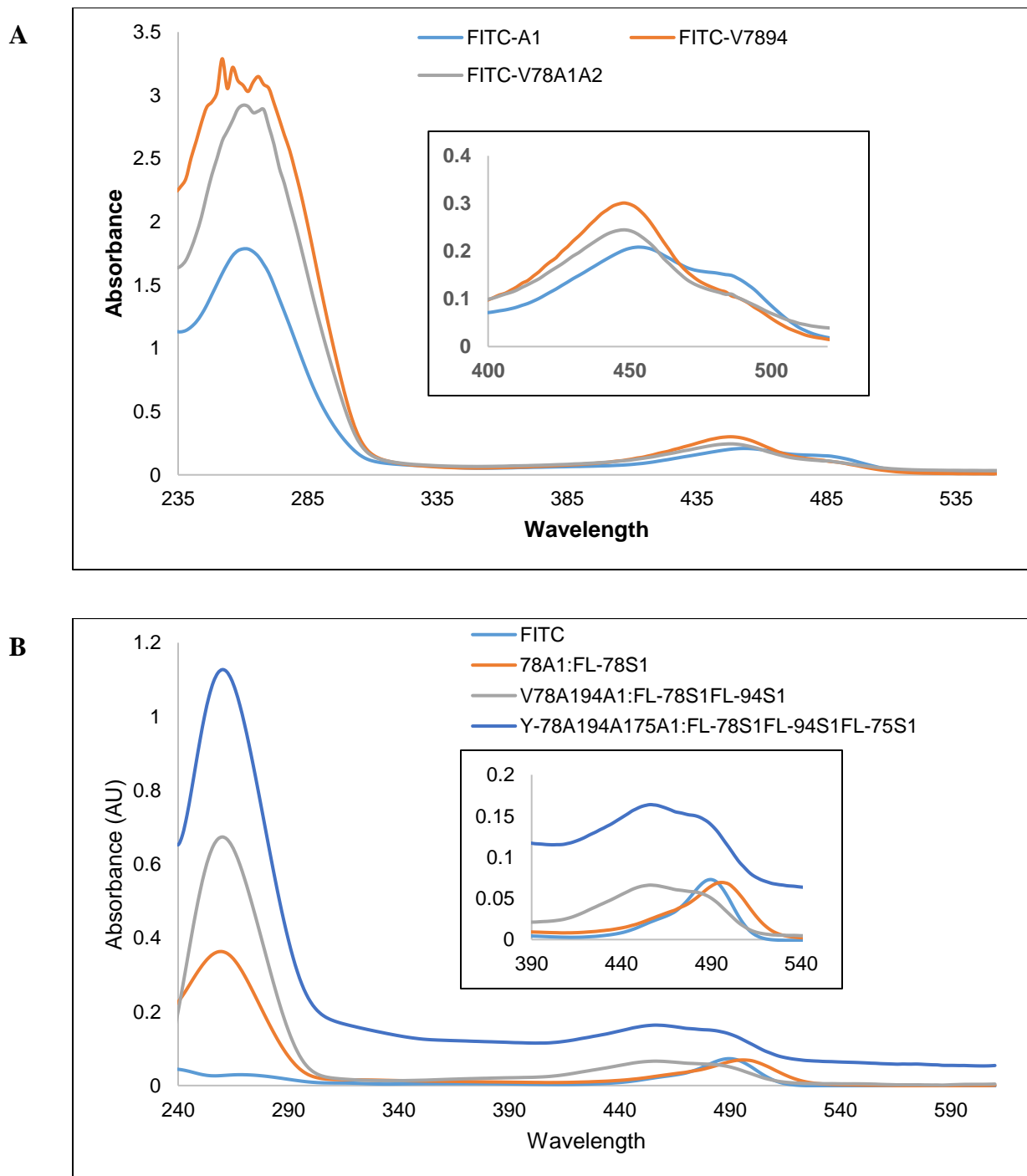


Figure 3.7 Thermal denaturation, T_m , of non-labeled, (A), FITC-labeled siRNAs, (B), and multi-FITC-labeled siRNAs, (C). All hybrid siRNA samples were prepared by annealing equimolar quantities (1.25 nM) of antisense RNA templates with their complementary linear sequences. Samples were hybridized in annealing buffer (10 mM Tris, 50 mM NaCl, 1 mM EDTA, pH 7.5 – 8.0) by pre-heating at 95 °C (7 min) followed by slow cooling to room temperature over 1 hr and overnight storage at 4 °C prior to T_m analyses. Before running T_m , all samples were dissolved in annealing buffer (1 mL) and the T_m analyses were observed at 260 nm and plotted as observed changes in percentage hyperchromicity (%H) as a function of temperature, 20-80 °C.

3.4.6 UV Absorption and Fluorescence Emission Spectra

Spectrofluorimetry was used to determine whether the siRNA hybrid structures had any effect on fluorescence intensity and quantum yields of the FITC probe. Previous studies on fluorescently labeled oligonucleotides have illustrated that covalent conjugation decreases fluorescence efficiency.⁴⁸ FITC-siRNA hybrids (**Figure 3.9**) were prepared as described in the previous characterization studies. UV absorbance measurements were initially conducted to maintain absorption ranges of 0.1 – 0.01 (**Figure 3.8**) to limit inner filter effects that may be caused by more concentrated samples.⁶³



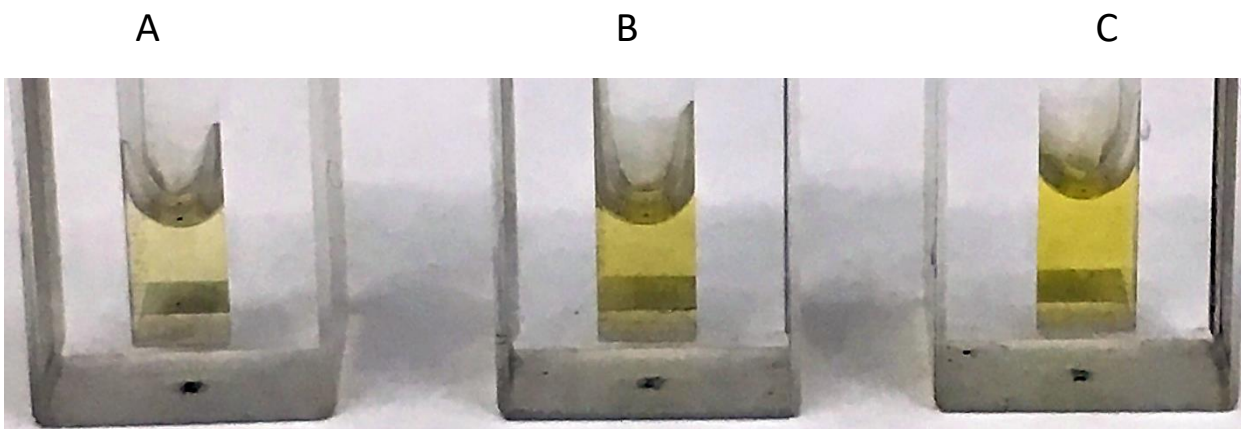


Figure 3.9 Multi-FITC siRNA samples pre dilution for fluorescence spectroscopy analysis. Linear 78A1:FL-78S1 (A), V-78A194A1:FL-78S1FL-94S1 (B) and Y78A194A175A1:FL-78S1FL-94S1FL-75S1 (C).

Upon conjugation of FITC with the siRNA sequences, a blue shift (485 – 445 nm) was observed due to a variety of effects that can be contingent on temperature, environment and oligonucleotide length, sequence and conformation, which must be determined for each experiment.⁶⁴ UV absorption studies revealed an overlap of the FITC-labeled siRNA samples, with an observed excitation peak selected at 460 nm. Upon excitation (λ_{ex} : 460 nm), the emission spectrum was monitored (λ_{em} : 470-650 nm) for the FL-siRNA hybrids (**Figure 3.10A**). Interestingly, the linear FITC-78A1:S1 sample yielded comparable fluorescence emission intensity ($\phi = 1.3$) as the FITC fluorescent probe alone ($\phi = 0.93$). Furthermore, a notable blue shift in the fluorescence emission maxima, λ_{em} : 515nm to 520nm was noted for the FL-siRNAs vs FITC alone. The V- ($\phi = 0.28$, 0.14) and Y-shaped ($\phi=0.15$) FITC-labeled siRNAs displayed a significant quenching (70-85%) when compared to the linear FL-siRNA and the FITC control. The latter is presumably due to the nature of the extended sequence composition and higher-order structures of the V- and Y-shape siRNAs, which effects FITC fluorescence efficiency when compared to the linear FITC-labeled

siRNA hybrid duplex. In order to overcome this limitation, multiple FITC-labeled complementary sense strand RNAs were hybridized to the template V and Y-shape RNA templates. The fluorescence emission spectra of the FITC-labeled V- and Y-shape siRNAs which incorporated two and three FITC fluorescent probes was found to increase fluorescence emission intensity by ~5-fold (**Figure 3.10B**) although with still observable quenching effects (FL-S1 $\phi = 0.66$, V-2FL-S1 $\phi = 0.17$, Y-3FL-S1 $\phi = 0.24$) when compared with the siRNA with the incorporation of a single FITC probe (**Figure 3.10A**). The latter results underscore the potential utility of the self-assembled higher-order V- and Y-shape siRNA motifs, facilitating the incorporation of multiple fluorescent probes for enhancing fluorescence detection and signaling for biological applications.

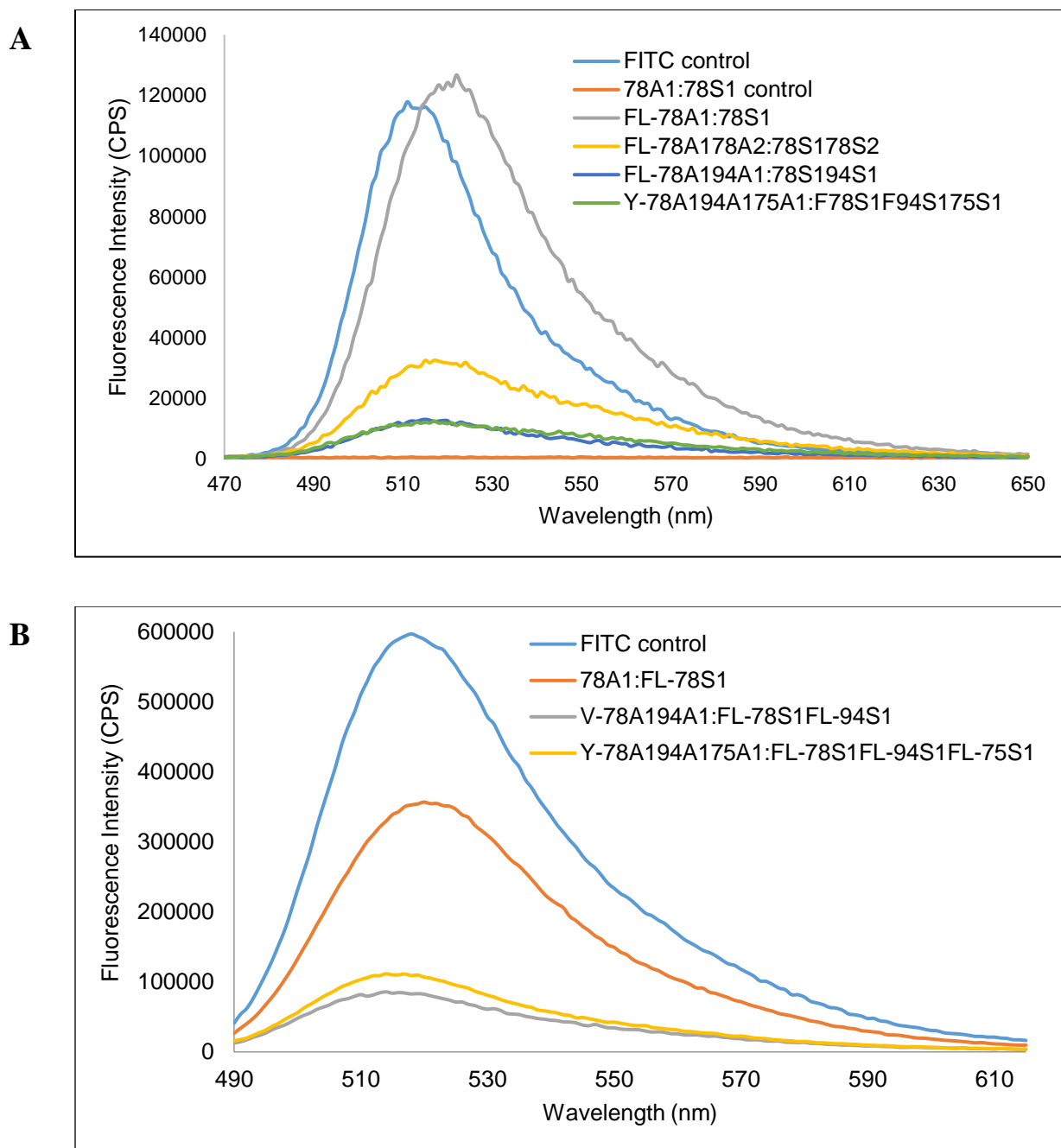


Figure 3.10 Fluorescence emission of (A) FITC-labeled siRNAs and (B) multi-FITC labeled siRNAs. All siRNA hybrids were prepared as previously described in annealing buffer (1.25 μ M, 10 mM Tris, 50 mM NaCl, 1 mM EDTA, pH 7.5 – 8.0, 1 mL). Absorbance readings were within the 0.1 – 0.01 range necessary for accurate fluorescence emission measurement. (A) UV absorbance of anti-sense FL-siRNA hybrids was conducted to determine the absorbance at the wavelength of excitation, 460 nm. Excitation of 460 nm and emission window of 470–650 nm. (B) UV absorbance of siRNA hybrids was conducted to determine the absorbance at the wavelength of excitation, 486 nm. Excitation of 486 nm and emission window of 490–610 nm.

3.4.7 Transfection and RT-PCR in PC3 Cells

The PC-3 prostate cancer cell line (ATCC® CRL-1435™) was used as a model, GRP overexpressing cell line to determine the knockdown efficiency of the FITC-labeled siRNA constructs.⁶⁵ SiRNA transfections (10µM) were conducted with the *TransIT-X2*® Dynamic Delivery System transfection reagent within the PC-3 cell culture and incubated over a three-day (72h) period. RT-PCR of the isolated GRP mRNA sequences indicated that upon GRP78 mRNA knockdown a sharp upregulation of GRP94 was observed with a lower effect on GRP75 mRNA levels (**Figure 3.11A**). Presumably, this compensatory effect may be linked to the maintenance of the UPR under the stress-induced conditions, potentially linking the activity of these GRP chaperones.⁴⁶ A similar trend was observed for the V-shaped siRNA targeting GRP78 and 94 mRNA, with a noticeable upregulation of GRP75, albeit to a smaller extent. The Y-shaped siRNA targeting all three GRP chaperone proteins displayed the most synergistic mRNA knockdown (40-70%). Analysis of the FITC-labeled siRNA constructs demonstrated GRP knockdown (20-70 %) albeit at a loss when compared to the non-FITC-labeled siRNAs (40-80 %). (**Figure 3.11A**) The decrease in GRP silencing activity of the FL-labeled siRNAs can be partially attributed to detrimental effects of functionalizing the 5' terminus of the antisense siRNA strand which may inhibit incorporation into RISC and mRNA processing as part of the RNAi pathway.⁶⁶ Interestingly, when the sense strands were FITC-labeled and hybridized to the complementary Y-shaped RNA template, the FITC-labeled Y-shape siRNA displayed comparable GRP knockdown efficiency (55-95%) as the non-FITC-labeled Y-shape siRNAs (40-80 %). (**Figure 3.11B**) The latter proves that RNAi activity can be restored within the higher-order V- and Y-shape siRNAs by FITC-labeling the complementary sense strands followed by siRNA hybridization into functional siRNA nanostructure formulations.⁶⁷⁻⁶⁹

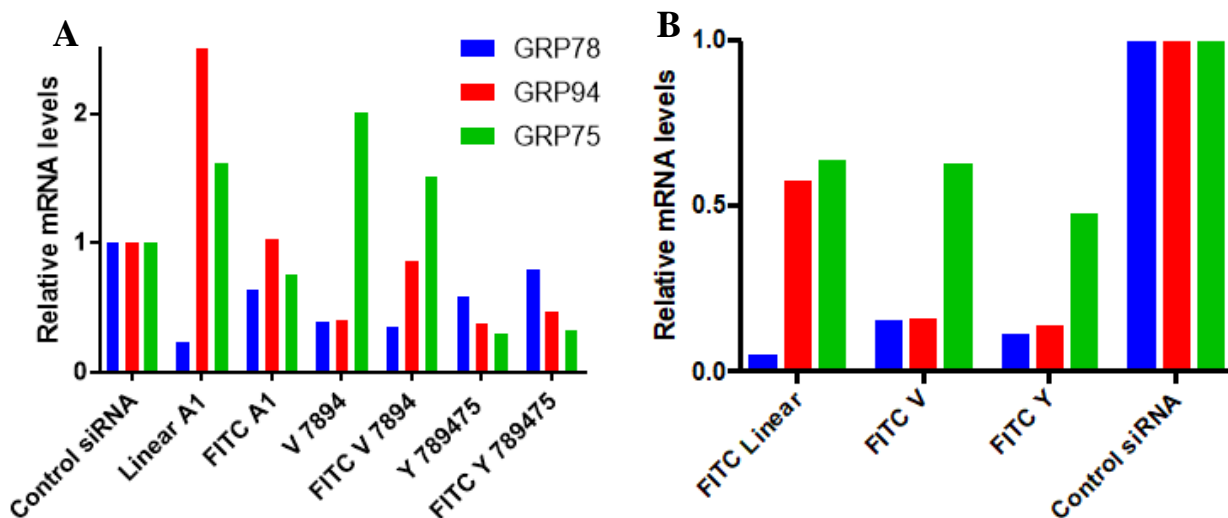


Figure 3.11 qRT-PCR analysis of GRP75, 78 and 94 gene knockdown. 50nM siRNA samples were transfected into PC-3 cells and relative mRNA levels were normalized to a control siRNA. (A) Total mRNA levels were analyzed 72 h post transfection of the antisense FL-siRNA constructs. (B) Total mRNA levels were analyzed 48 h post transfection of the sense-strand FL-siRNA constructs containing 1, 2 and 3 FITC probes (B).

3.4.8 Internalization Efficiency via Flow Cytometry and Fluorescent Microscopy

Incorporation of the FITC within the siRNA constructs provided the ability to monitor cellular uptake quickly and efficiently. PC-3 cells were treated with FL-siRNA and cell uptake measurements were determined by flow cytometry 3 h post transfection. Analysis of the linear, V- and Y-shaped FITC-labeled siRNA revealed a slight shift in fluorescence intensity *vs* the total gated cell population post transfection (**Figure 3.13A**). This data suggested that 3 hours may not be sufficient for complete siRNA uptake. To determine the optimal cell uptake time, a new set of siRNA samples were prepared (50 nM). PC-3 cells were transfected as previously described analyzed 20 hours post transfection by flow cytometry and revealed that FL-siRNA treatment at higher concentrations (100 nM) and treatment time (20 h) elicited the greatest shift in cell-based fluorescence intensity (**Figure 3.12A**). Interestingly, multiple incorporation of FITC upon

hybridization of complementary FL-sense strand RNA to V- and Y-shape RNA templates produced multi-FL probes which increased cell signaling in a time dependent (3-72 h) uptake experiment (**Figure 3.12B**). Fluorescent microscopy was used to validate internalization and verified the visualization of the FITC-siRNAs up to 24 h post transfection. (**Figure 3.14**) Therefore, the V- and Y-shape RNA templates efficiently enable the incorporation of multiple fluorescent probes for improving cell signaling and detection, while maintaining potent RNAi activity.

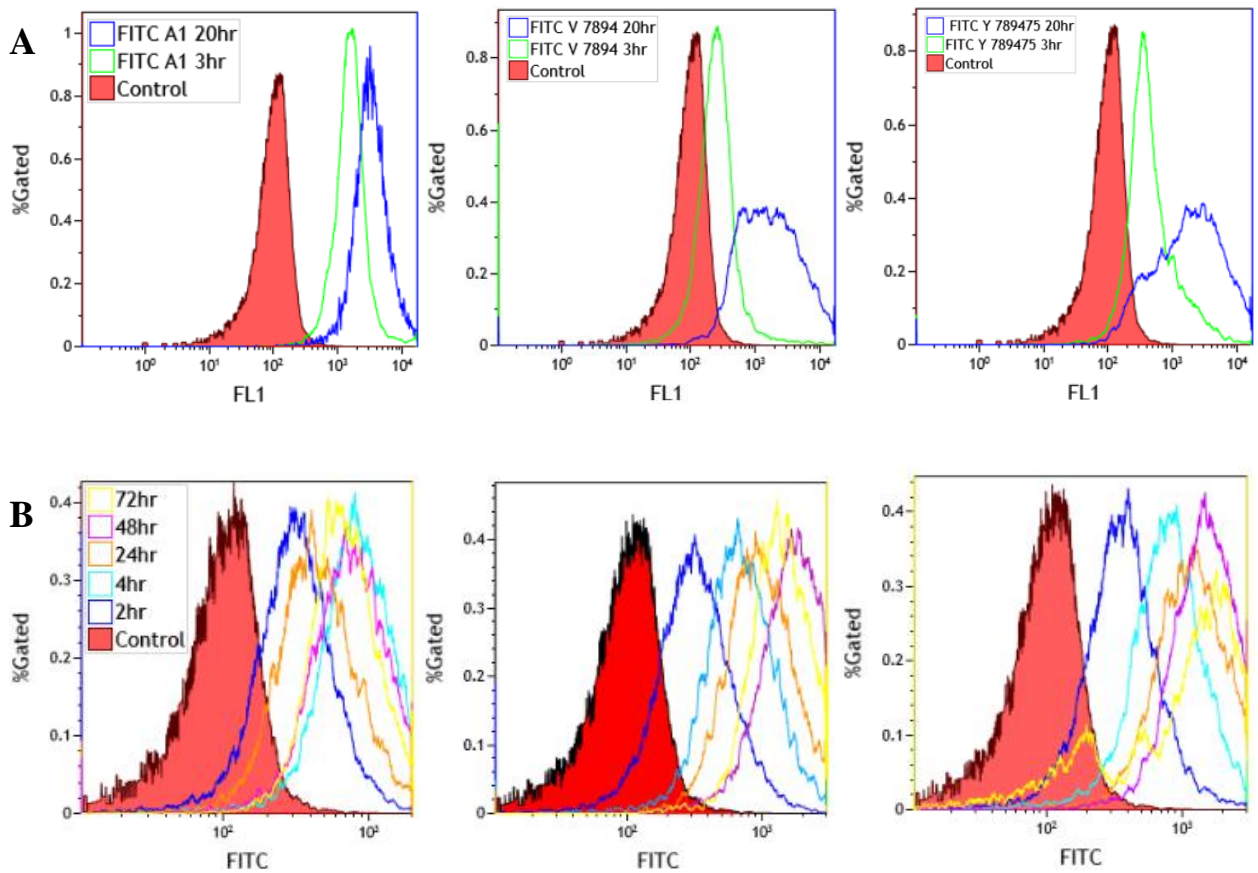
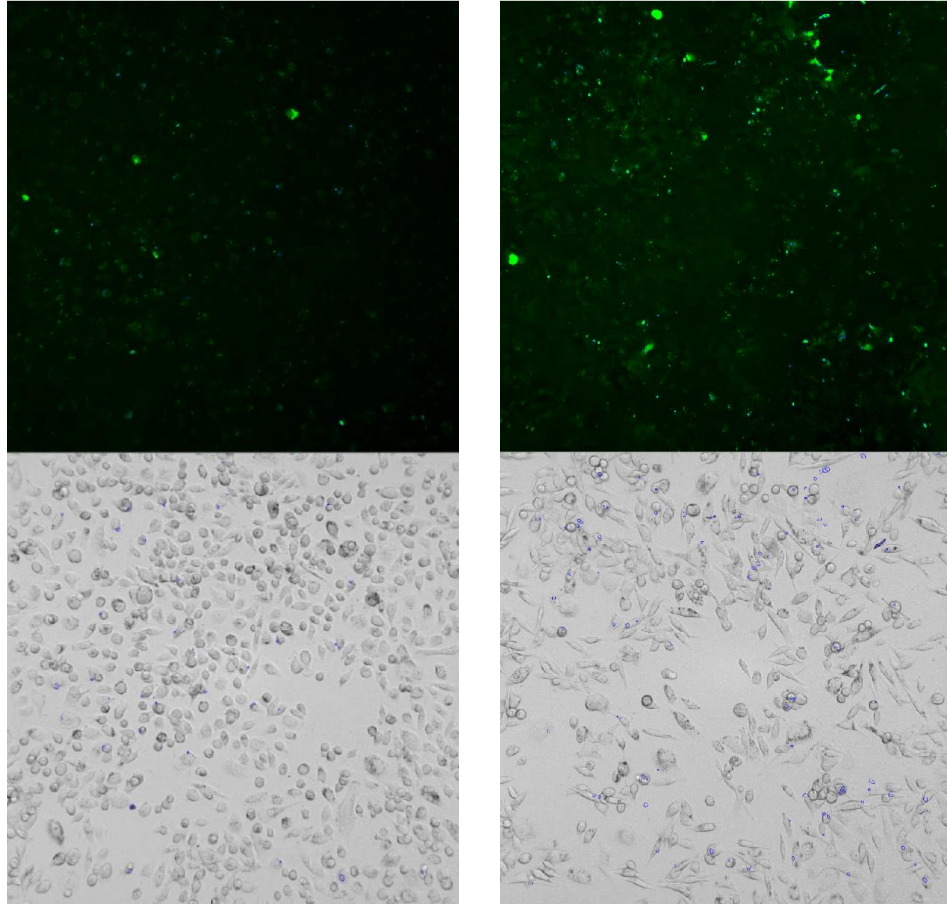


Figure 3.12 Uptake efficiency monitored by flow cytometry of 50nM FL-siRNA transfection at 3 and 20 h. (**A**) internalization efficiency of linear, V- and Y-shaped siRNA containing 1 FITC probe. (**B**) Time dependent internalization efficiency of linear, V- and Y-shaped siRNA containing 1, 2 or 3 FITC probes, respectively.

A

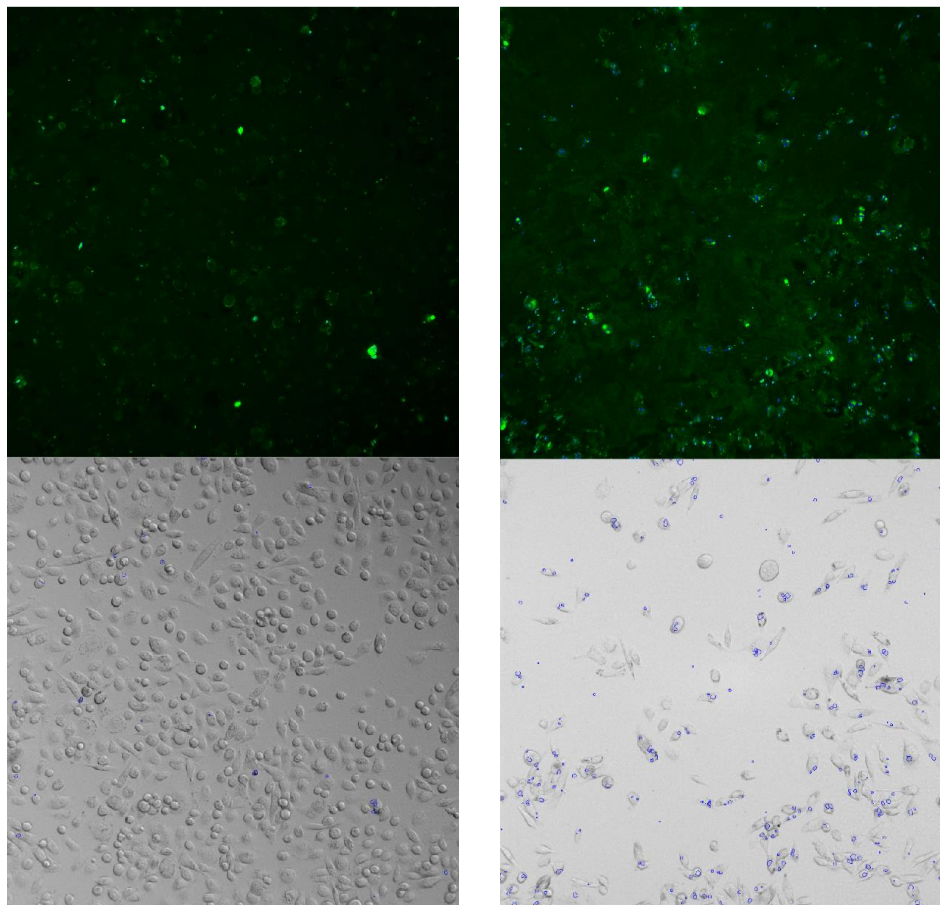


FL-linear siRNA

4 hours post transfection

24 hours post transfection

B

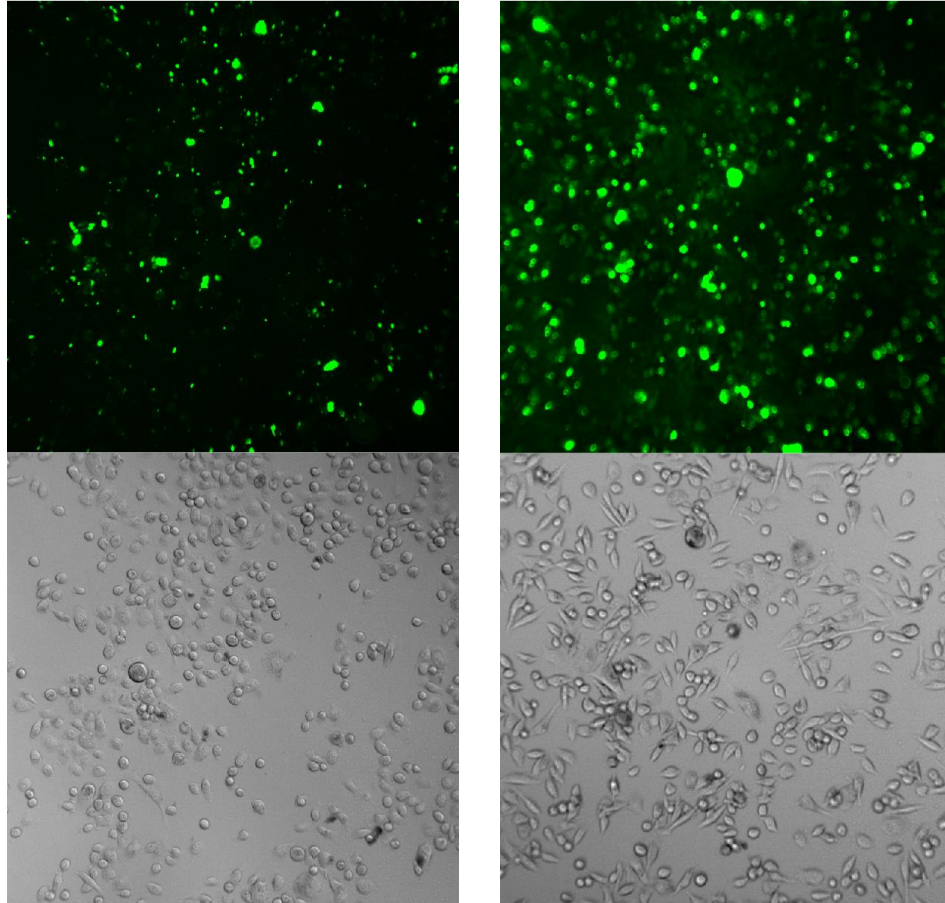


V-FL-siRNA

4 hours post transfection

24 hours post transfection

C



Y-FL-siRNA

4 hours post transfection

24 hours post transfection

Figure 3.13 Fluorescent microscope images of FL-siRNA transfected PC-3 cells at 4 and 24 hours post transfection. (A) FL-linear, (B) V-FL-siRNA containing 2 FITC probes, (C) Y-FL-siRNA containing 3 FITC probes

3.4.9 Western Blot

Following the qRT-PCR screening analysis of the FITC-siRNA samples, the lead Y-shaped siRNA containing three FITC probes was selected for further analysis. The Y-shaped siRNA sample (50nM) was prepared and transfected into PC-3 cells as described earlier. Cells were collected 72 h post transfection and subjected to qRT-PCR and western blot. RT-PCR showed mRNA knockdown of GRP78 (~40%), increased knockdown of GRP94 (~60%) and no visible knockdown of GRP75. However, western blot indicated protein level knockdown of GRP78 and 75 (~30-35%) in both instances, but no visible knockdown of GRP94 at the protein level, which is known to vary from the mRNA transcript levels.

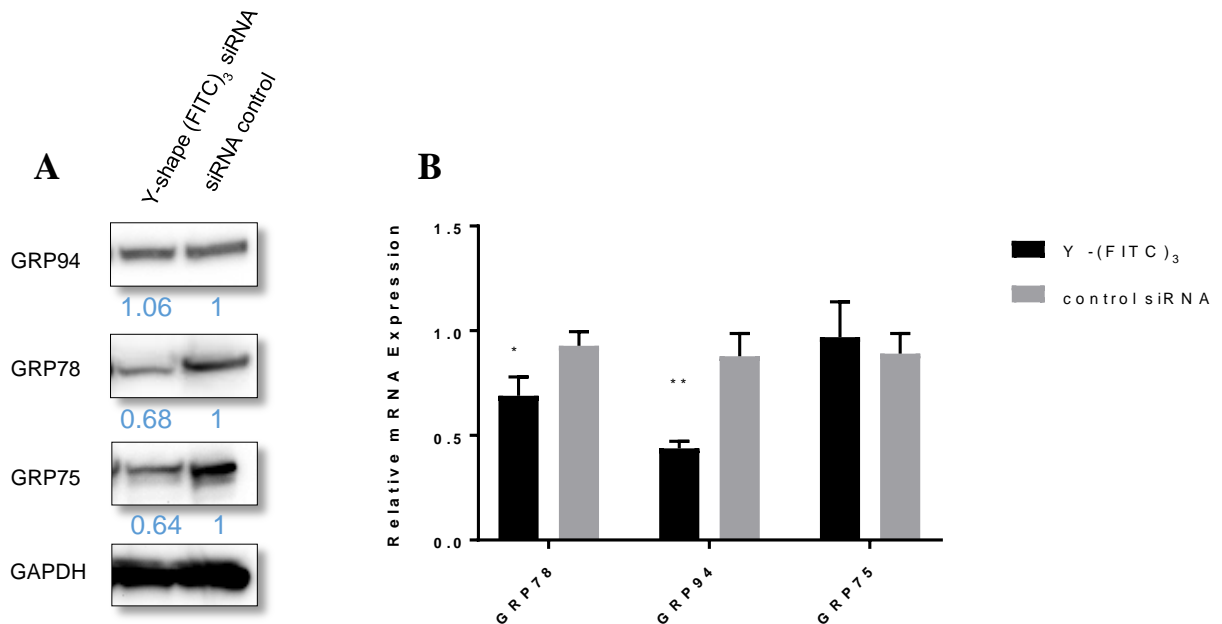


Figure 3.14 Protein and mRNA knockdown levels of GRP75, 78 and 94 determined by Western Blot (A), and RT-PCR (B). *P<0.05 in PC-3 cells and *P<0.01 in PC-3 cells.

3.4.10 Cell Viability

Cell viability of the FITC-labeled siRNAs treated PC-3 cells was measured using propidium iodide (PI) staining. PI is a fluorescent intercalating agent that stains dead cells and is commonly used in flow cytometry to evaluate cell viability. PI cannot cross the membrane of live cells, making it useful to differentiate necrotic, apoptotic and healthy cells.⁷⁰ PC-3 cell viability was determined at 24, 48 and 72 h post transfection to determine which construct exhibited the most potent cell death activity. (Figure 3.15 A, B) Following the 24 h incubation, it was noted that the supernatant contained PC-3 cells, as an initial indicator of cell death due to loss in adhesion. Both the supernatant cells as well as the cells still adhered to the bottom of the well were tested for viability. PI staining showed an increase in cell death over a 72h period for all samples. The Y-shape targeting all three GRPs elicited the most potent cell death in both cases.

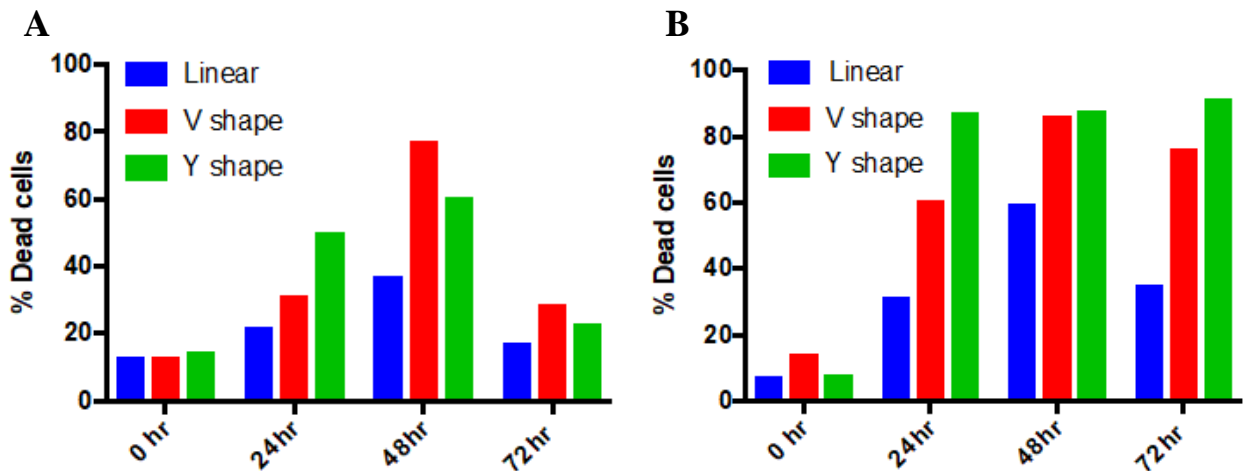


Figure 3.15 Cell viability determined using PI on flow cytometry, adhered cells (A) and supernatant cells (B)

3.5 Conclusions

In the theranostic approach described in Chapter 3 of this thesis, the covalent attachment of a fluorophore, fluorescein isothiocyanate (FITC), has been developed for monitoring cell uptake, co-localization and biological activity within PC-3 prostate cancer cells. A wide range of GRP-silencing siRNAs, including those adopting linear, V-shape and Y-branch structures allowed the incorporation of multiple FITC reporter probes. Although FITC-labeling had some effect on the requisite A-type helix structure required for RNAi activity, the fluorescent probe did not inhibit hybrid duplex stability according to thermal denaturation studies. Fluorescence quenching was observed in the higher-order V- and Y-shape siRNAs which enabled the incorporation of multiple FITC reporter probes, albeit with greater intensities of fluorescence emissions detected when compared to the siRNAs containing a single FITC. Upon transfection within the PC-3 prostate cancer cells, the FITC-labeled siRNAs triggered GRP mRNA and protein knockdown via RT-PCR and western blot, respectively, which resulted in loss of cell-based adhesion and cell death within the PC-3 cells. Flow cytometry and fluorescent microscopy also revealed the presence of the FITC-labeled siRNA within PC-3 cells up to 72 hrs. Therefore, the V- and Y-shape multi-FITC labeled siRNA encompass a new class of theranostic agents with enhanced cell-based detection and RNAi activity in cancer.

3.6 Experimental Section

3.6.1 Materials and Methods.

Chemical synthesis reagents and solvents were obtained from ChemGenes, Aldrich and VWR and used as received. Solid phase RNA synthesis reagents were obtained from ChemGenes or Glen Research Inc. and also used without further purification. Analytical thin-layer chromatography (TLC) was performed on aluminum-backed silica gel plates (Merck 60 F254).

TLCs were visualized under UV shadowing (260 nm) or staining (10% H₂SO₄/MeOH). Compound purification using silica gel chromatography was performed on 230-400 mesh silica (Sorbent Technologies). Molecular weights for the branchpoint uridine phosphoramidite was measured by direct injections on a Hewlett Packard series 1100 MSD equipped with ESI as ion-source in positive mode using 50/50 v/v MeOH/H₂O at a flow-rate of 0.5 mL/min. Nuclear magnetic resonance spectra (¹H, ¹³C, ³¹P COSY NMR) were recorded on a Varian NMR AS500 spectrophotometer. NMR spectra were obtained at ambient temperature using an indirect pulse-field gradient (ID-PFG) probe. The obtained data was processed using VNMRJ software (version 2.2). Materials for cell biology were obtained from Thermofisher Scientific, Cell Signaling, Biologend, Mirus and Invitrogen Life Technologies.

3.6.2 FITC bioconjugation of linear, V- and Y-shape siRNAs

Linear, V- and Y-shaped siRNAs were selected to target the GRP chaperones (GRP-75, 78 and 94) and the requisite RNA templates were synthesized as previously reported⁵⁸ and summarized in chapter 2. Following synthesis, a 5'-DMS(O)-MT-Amino C6 modifier (Glen Research Inc.) was coupled to the 5' terminal hydroxyl group using an extended 15-minute coupling time on an ABI 3400 DNA/RNA Synthesizer. The solid phase oligonucleotide synthesis cycle was continued with the coupling step (0.25 M ethylthiotetrazole in acetonitrile), capping (Cap A: 1:1:8 v/v/v acetic anhydride:pyridine:tetrahydrofuran, Cap B: 16% *N*-methyl imidazole in tetrahydrofuran) and oxidation (0.02 M iodine in 75:20:5 v/v/v tetrahydrofuran:pyridine:water) followed by removal of the DMS(O)MT protecting group with a detritylation step (3% solution of dichloroacetic acid in dichloromethane). The amino functionalized RNA templates were then subjected to a solid-phase bioconjugation reaction for the attachment of the fluorescent probe, fluorescein isothiocyanate (FITC). Following a previously reported method⁵⁹ attachment of FITC

was achieved by reacting FITC (75 eq., 30 mg) dissolved in 20% aqueous *N,N*-dimethylformamide (DMF) in 0.1M carbonate-bicarbonate buffer (pH 8.5) to the deprotected amino modified RNA templates. The reaction was agitated at room temperature for 48 hours on a benchtop shaker. Following the reaction, the CPG bound RNA was washed with DMF and acetonitrile (MeCN) until no visible orange color remained in the supernatant. The sample was then cleaved and deprotected using 3:1 v/v NH₄OH: EtOH at 55 °C for 12-14 hours. The 2'-TBDMS protecting groups were desilylated using 1:1.5 v/v trimethylamine-trihydrofluoride TEA-3HF:DMSO at 65 °C for 2 h. The crude FL-RNA was precipitated in 3M NaOAc (25 μL) and n-BuOH (1 mL) and dissolved in diethyl pyrocarbonate (DEPC) treated Millipore water, RNase-free, for analysis and purification.

3.6.3 RP IP HPLC

The crude RNA templates were analyzed by Reverse Phase Ion Pairing High Performance Liquid Chromatography (RP-IP-HPLC) to determine crude purities. Briefly, HPLC analyses (0.1 OD) and purifications (1 OD) were performed on a Waters[®] 2695 Alliance Separations Module. Crude RNA templates were dissolved in autoclaved water (1 mL) and injected into a Waters[®] SymmetryShield™ RP-8 column (4.6 X 250 mm, 5μm particle size, 100Å) heated at 60 °C. HPLC analyses and purifications were conducted using a gradient of 4-90% eluent B (50% acetonitrile in 0.1 M triethylammonium acetate, TEAA) in eluent A (0.1 M TEAA). The HPLC flow rate was set at 1 mL/min, with run times of 25 min and with dual absorbance detection at 260 and 488 nm using a Waters[®] 2489 UV/Visible detector. Retention times (min.) and peak areas (% area) were integrated with Empower II software (Waters[®]) and used to confirm RNA purities ≥95% following sample purifications.

3.6.4 Mass Spectrometry

RNA templates (300-1300 pmol) were dissolved in RNase-free millipore water (50-200 μ L) and analyzed by Dr. Mark Hail at Novatia LLC, Newtown, PA. Samples were analyzed on an Oligo HTCS equipped ESI/MS in negative mode. The data was obtained and deconvoluted using ProMass software. Theoretical molecular weights were calculated by entering each sequence identity on IDT OligoAnalyzer. <https://www.idtdna.com/calc/analyzer>

3.6.5 Denaturing Polyacrylamide Gel Electrophoresis

Purified template RNAs (300pmol) were loaded on a 24% denaturing PAGE (7M Urea) run at 300 V, 100 mA and 12 W for 3 hr. Following electrophoresis, the RNA bands were visualized under UV shadowing and stained with a Stains-All (Sigma-Aldrich™) solution.

3.6.6 siRNA Hybridization

Purified complementary RNA strands were combined in equimolar quantities (200 pmol) and mixed in annealing buffer (35 μ L, 10 mM Tris, 50 mM NaCl, 1 mM EDTA, pH 7.5–8.0) to afford the hybrid mixtures. The resulting mixtures were heated to 95°C for 7 minutes on a heating block, slowly cooled to room temperature (22°C) over 1 h and stored in the fridge overnight at 4°C prior to analysis.

3.6.7 Non-denaturing, Native Polyacrylamide Gel Electrophoresis (PAGE)

The hybrid siRNA samples (10 μ M) in annealing buffer (10 mM Tris, 50 mM NaCl, 1 mM EDTA, pH 7.5–8.0) were concentrated to minimal volume (~10 μ L) and suspended in 30% sucrose loading buffer (15 μ L in 1X TBE). Samples were loaded on a 16% native, non-denaturing PAGE

and run at 300 V, 100 mA and 12 W for 2.5 hr. Following electrophoresis, the siRNA bands were visualized under UV shadowing and stained with Stains-All (Sigma-Aldrich™) solution.

3.6.8 Circular Dichroism (CD) Spectroscopy

siRNA samples were hybridized in annealing buffer (1.25 μ M, 10 mM Tris, 50 mM NaCl, 1 mM EDTA, pH 7.5–8.0, 1 mL) as previously described. Samples were then transferred to fused quartz cells (1 cm path length) and incubated at RT under N₂ for 2 minutes prior to spectral acquisition. CD spectra were collected on an Olis DSM 1000 Spectrophotometer as an average of 3 scans with a 1.0 nm bandwidth interval and a 0.5 nm step interval. CD spectra were analyzed in between 210 and 310 nm, blank corrected with annealing buffer and smoothed prior to analyses. The raw data was exported into Microsoft Excel™ and plotted as changes in molar ellipticities (θ) with increasing wavelengths (210 – 310 nm).

3.6.9 Thermal Denaturation (T_m)

All siRNA hybrids were prepared as previously described in annealing buffer (1.25 μ M, 10 mM Tris, 50 mM NaCl, 1 mM EDTA, pH 7.5 – 8.0, 1 mL). Thermal denaturation of the siRNA hybrids was performed using a CARY 3E, UV-Vis spectrophotometer, from 20 – 80 °C, with temperature ramping of 0.5 °C /min. The changes in absorption at 260 nm as a function of temperature was collected and the first derivative plot was used to determine the melting temperatures (T_m) of the siRNA samples. The data was transferred and plotted in Microsoft Excel™ as changes in the hyperchromicities (%H) observed at 260 nm as a function of temperature (20 – 80 °C).

3.6.10 Fluorescence Emission and Quantum Yield (ϕ) Determination

All siRNA hybrids were prepared as previously described in annealing buffer (1.25 μ M, 10 mM Tris, 50 mM NaCl, 1 mM EDTA, pH 7.5 – 8.0, 1 mL). UV absorbance measurements on a HP 8452A PDA spectrophotometer were initially conducted to determine FL-siRNA absorbances at the wavelengths of excitation, λ_{ex} : 460 and λ_{em} : 486 nm. Absorbance readings within the 0.1 – 0.01 A.U. range were recovered from serial dilution measurements necessary for accurate fluorescence emission measurements. Fluorescence emission and quantum yields were determined on a Horiba Fluorolog 3 spectrophotometer using FluorEssence V3.5 with an excitation of λ_{ex} : 460 and emission window λ_{em} : of 470-650 nm. Quantum yield values determined mathematically: $\left(\frac{Abs\ of\ FITC}{Abs\ of\ Sample}\right) * \left(\frac{Max\ intensity\ of\ Sample}{Max\ intensity\ of\ FITC}\right) * (0.93)$

3.6.11 Cell Culture

Prostate cancer cell line PC-3 (ATCC®) were cultured in RPMI 1640 complete growth medium supplemented with 10% (v/v) fetal bovine serum (FBS), and 1% (v/v) penicillin/streptomycin (P/S) under 5% CO₂ at 37 °C. For passaging, PC-3 cells were detached with 0.25% trypsin and re-suspended with complete culture medium.

3.6.12 SiRNA Transfections in PC-3 Cells and Cellular Uptake via Flow Cytometry and Fluorescence Microscopy

PC-3 prostate cancer cells (ATCC® CRL-1435™), 9.0×10^4 , were plated in 24-well culture plates containing RPMI complete culture media with 10% FBS. Cells were cultured in a humidified incubator set at 37 °C with 5% CO₂. Prior to transfections, the siRNA hybrids (7.5 μ L, 10 μ M, in Opti-MEM, 133.5 μ L) were mixed with the transfection reagent (*TransIT-X2*® Dynamic Delivery System, 9 μ L, in Opti-MEM, 250 μ L) according to the manufacture's recommendation.

The mixtures were incubated (15 min, 22 °C) then added to the PC-3 cell culture and incubated at 37 °C with 5% CO₂ over a three-day (72 h) period. Samples were tested at 3 h and 20 h post-transfection to determine internalization efficiency. Cells were removed from the well using trypsin and diluted in RPMI-1640 media. Samples were quantified using a Cytomics FC 500 flow cytometer. Time-dependent uptake for linear, V- and Y-shaped siRNAs containing one, two and three FITC probes was determined using CellInsight™ CX5 High Content Screening (HCS) Platform (ThermoFisher Scientific). Cells were visualized 2, 4, 8, 24, 48 and 72 hours post transfection. Images were analyzed using Thermo Scientific™ HCS Studio™ Cell Analysis Software.

3.6.13 Gene Knockdown via Quantitative Real-Time Polymerase Chain Reaction (qRT-PCR)

Total RNA was isolated following transfections (48 h) from TriZol (Ambion) preserved cells using a TriRNA Pure Kit (Geneaid), following the manufacturer's instructions. The collected RNA was then quantitated on a Qubit 3.0 fluorimeter using the Qubit Broad Range (BR) assay kit (Thermo Fisher Scientific). RNA (200 ng) was reversed transcribed into cDNA using a high capacity cDNA kit (Applied Biosystems). RT-PCR was performed using pre-developed TaqMan™ gene expression primer-probes for GRP78 (assay ID Hs99999174_m1), GRP94 (assay ID Hs00437665_g1), GRP75 (Hs00269818_m1), and GAPDH (Hs99999905_m1) and TaqMan™ fast advanced master mix. qPCR fast assay was carried out on a StepOnePlus (Applied Biosystems). Fold changes were calculated with the $\Delta\Delta C_t$ method using GAPDH as endogenous control and the negative siRNA as the control sample.

3.6.14 Western Blot

Total protein was isolated from the cell cultures following transfection (78 h). Protein lysates were prepared by lysing the cells in ice-cold RIPA buffer (G-Biosciences) supplemented with protease and phosphatase inhibitors (Millipore Sigma) which were diluted 1:10 as per the manufacturer's recommendations. Cell debris was removed by centrifugation at 16,000g at 4°C and protein concentrations were determined using a Pierce™ BCA kit (Thermo Fisher Scientific). A sample (20-35 mg) of the supernatant protein was mixed with LDS buffer and DTT, incubated at 70 °C for 10 min and resolved on a 4-12% Bis-Tris PAGE gradient gel before being transferred to a PVDF membrane. Following transfer, the membrane was blocked in 5% skim milk for 1 h, washed and incubated at 4 °C overnight with a rabbit 1° mAb against human GRP78, GRP94, GRP75 or GAPDH (all purchased from Cell Signaling Technology) at a 1:1000 dilution. The membrane was subsequently washed and incubated with an anti-rabbit HRP-conjugated 2° Ab (Cell Signaling Technology) for 1 h at room temperature at 1:2000 dilution. The bands were visualized using a SignalFire™ ECL reagent (Cell signaling Technology) on a ProteinSimple FluorChem E imager.

3.6.15 Cell Viability

Cell viability was determined in 24-well plates with PC-3 cells cultured in RPMI complete growth media and then incubated in the presence or absence of FITC-siRNA (50 μ M) for 72 h at 37 °C. After 24, 48 and 72 hrs, the supernatant was collected and the remaining cells were removed using trypsin. Cell samples were pelleted and re-suspended in 1% BSA in PBS (1 mL) and stained using PI (100 μ L) according the manufacturer's recommendation. Samples were quantified using a Cytomics FC 500 flow cytometer (Beckman Coulter). Data was processed with Kaluza® (Beckman Coulter) flow analysis software.

3.7. References

1. Sumer, B; Gao, J. *Nanomedicine (Lond)*. **2008**; 3(2):137-40.
2. Deveza L; Choi J; Yang F. *Theranostics*. **2012**; 2(8):801–814.
3. Janib SM; Moses AS; MacKay JA. *Adv Drug Deliv Rev*. **2010**; 62(11):1052–1063.
4. Yu MK; Park, J; Jon, S. *Theranostics* **2012**; 2(1):3–44.
5. Xie J; Lee S; Chen X. *Adv Drug Deliv Rev* **2010**; 62(11):1064–79.
6. Ye Y; Chen X. *Theranostics*. **2011**; 1:102–126.
7. Muthu MS; Singh S. *Nanomedicine (Lond)* **2009**; 4(1):105–118.
8. Muthu MS; Rajesh CV; Mishra A. et al. *Nanomedicine (Lond)* **2009**; 4(6):657–667.
9. Zhao J; Mi Y; Feng SS. *Nanomedicine (Lond)* **2013**; 8(6):859–862.
10. Medarova Z; Pham W; Farrar C; Petkova V; Moore A *Nat Med*. **2007**; 13(3):372-377.
11. Bae KH; Lee JY; Lee SH; Park TG; Nam YS *Adv Healthc Mater*. **2013**; 2(4):576-584.
12. Liu, Y; Gunda, V; Zhu, X; Xu, X; Wu, J; Askhatova, D; Farokhzad, OC; Parangi, S; Shi, J. *PNAS* **2016**; 113 (28) 7750-7755
13. Baker SN; Baker GA. *Angew Chem Int Ed* **2010**, 49:6726–6744.
14. Li H; Kang Z; Liu Y; Lee S-T. *J Mater Chem* **2012**, 22:24230–24253.
15. Wang, Q; Zhang, C; Shen, G; Liu, H; Fu, H; Cui, D. *Journal Of Nanobiotechnology* **2014**; 12(1):1-24.
16. Yang D; Welm A; Bishop JM. *Proc Natl Acad Sci* **2004**, 101:15100–15105.
17. Suzuki A; Hayashida M; Ito T; Kawano H; Nakano T; Miura M; Akahane K; Shiraki K. *Oncogene* **2000**, 19:3225–3234.
18. Lu CD; Altieri DC; Tanigawa N. *Cancer Res* **1998**, 58:1808–1812.
19. Mahajan UM; Teller S; Sandler M; et al. *Gut*. **2016**; 65(11):1838-1849.
20. Mukherjee P, Ginardi AR, Madsen CS, et al. *Glycoconj J* **2001**; 18:931-42.
21. Medarova Z, Pham W, Farrar C, et al. *Nat Med* **2007**; 13:372-7.
22. Song B, Liu XS, Rice SJ, et al. *Mol Cancer Ther* **2013**; 12:58-68.
23. Koike, N; Maita, H; Taira, T; Ariga, H; Iguchi-Ariga, SM. *FEBS Lett* **2000** 467, 17–21.
24. Mochizuki, T; Kitanaka, C; Noguchi, K; Muramatsu, T; Asai, A; Kuchino, Y. *J. Biol. Chem.* **1999** 274, 18659–18666.
25. Winn, LM; Lei, W; Ness, SA. *Cell Cycle* **2003** 2, 258–262.
26. Van Lohuizen, M; Verbeek, S; Krimpenfort, P; Domen, J; Saris, C; Radaszkiewicz, T; Berns, A. *Cell* **1989** 56, 673–682.
27. Konietzko, U; Kauselmann, G; Scafidi, J; Staubli, U; Mikkers, H; Berns, A; Schweizer, M; Waltereit, R; and Kuhl, D. *EMBO J*. **1999** 18, 3359–3369.
28. Wang, Z; Bhattacharya, N; Weaver, M; Petersen, K; Meyer, M; Gapter, L; Magnuson, NS. *J Vet Sci* **2001** 2, 167–179.
29. Grünweller, A; Gillen, C; Erdmann, VA; Kurreck, J. *Oligonucleotides*. **2003**;13(5):345-52.
30. Ocker, M; Neureiter, D; Lueders, M; Zopf, S; Ganslmayer, M; Hahn, EG; Herold, C; Schuppan, D. *Gut* **2005**; 54:1298-1308.
31. Wang, J., Cui, H. *Theranostics* **2016**; 6(9): 1274-1276.
32. Lee, A.S. *Nat. Rev. Cancer* **2014**, 14, 263-276.
33. Wu, J. & Kaufman, R. J. *Cell Death Differ*. **2006** 13, 374–384.

34. Kim, Y; Lillo, AM; Steiniger, SC; Liu, Y; Ballatore, C; Anichini, A; Mortarini, R; Kaufmann, G; Zhou, B; Felding-Habermann, B; Janda, KD. *Biochemistry* **2006**, 45, 9434.
35. Liu, Y; Steiniger, SC; Kim, Y; Kaufmann, GF; Felding-Habermann, B. Janda, KD. *Mol. Pharm.* **2007** 4, 435-447.
36. Yoneda, Y; Steiniger, SC; Capková, K; Mee, JM; Liu, Y; Kaufmann, G.F.; Janda, K.D. *Bioorg. Med. Chem. Lett.* **2008**, 18, 1632.
37. Arap MA; Lahdenranta J; Mintz PJ; Hajitou A; Sarkis AS; Arap W; Pasqualini R. *Cancer Cell.* **2004** 6(3):275-84.
38. Lee AS. *Trends Biochem Sci.* **2001** 26(8):504-510.
39. Li Z; Li Z. *Biochim Biophys Acta.* **2012** 1826(1):13-22.
40. Lee AS. *Cancer Res.* **2007** 67(8):3496-3499.
41. Fernandez PM; Tabbara SO; Jacobs LK; Manning FC; Tsangaris TN; Schwartz AM; Kennedy KA; Patierno SR. *Breast Cancer Res Treat.* **2000** 59(1):15-26.
42. Chang YJ; Huang YP; Li ZL; Chen CH. *PLoS One.* **2012** 7(4):e35123
43. Mhaidat NM; Alzoubi KH; Almomani N; Khabour OF. *Cancer Biomark.* **2015** 15(2):197-203.
44. Zhang L; Li Z; Fan Y; Li H; Li Z; Li Y. *Int J Biochem Cell Biol.* **2015** 64:202-211.
45. Pi L; Li X; Song Q; Shen Y; Lu X; DI B. *Oncol Lett.* **2014** 7(3):685-692.
46. Suzuki, T.; Lu, J.; Zahed, M.; Kita, K.; Suzuki, N. *Arch. Biochem. Biophys.* **2007**, 468, 1-14
47. Maina, A; Blackman, BA; Parronchi, CJ; Morozko, E; Bender, ME; Blake, AD; Sabatino, D. *Bioorg. Med. Chem. Lett.* **2013** 23, 5270-5274.
48. Gonzalez-Gronow M; Selim MA; Papalas J; Pizzo SV. *Antioxid Redox Signal.* **2009** 11(9):2299-306.
49. Quinones QJ; de Ridder GG; Pizzo SV. *Histol Histopathol.* **2008** 23(11):1409-16.
50. Li Z; Zhang L; Zhao Y; Li H, Xiao H; Fu R; Zhao C; Wu H; Li Z. *Int J Biochem Cell Biol.* **2013**; 45(5):987-94.
51. Reddy, RK; Lu, J; Lee, AS. *J. Biol. Chem.* **1999** 274, 28476–28483.
52. Hua, Y. *et al. Clin. Cancer Res.* **2013** 19, 6242–6251.
53. Wadhwa, R. *et al. J. Biol. Chem.* **1998** 273, 29586–29591.
54. Wadhwa, R. *et al. Exp. Cell Res.* **2002** 274, 246–253.
55. Luo, B; Lee, A. S. *Oncogene* **2013** 32, 805–818.
56. Gao, YY. *et al. J. Clin. Endocrinol. Metab.* **2010** 95, E319–E326.
57. Sanson, M. *et al. Cell Death Differ.* **2008** 15, 1255–1265.
58. Patel, MR; Kozuch, SD; Cultrara, CN; Yadav, R; Huang, S; Samuni, U; Koren, J; Chiosis, G; Sabatino, D. *Nano Letters* **2016** 16 (10), 6099-6108.
59. Murakami, A; Nakaura, M; Nakatsuji, Y; Nagahara, S; Tran-Cong, Q; Makino, K. *Nucleic Acids Research*, **1991** 19(15), 4097-4102.
60. Saar Ray, M; Moskovich, O; Iosefson, O; Fishelson, Z. *J. Biol. Chem.* **2014**, 289, 15014-15022.
61. Chiu, YL; Rana, TM. *RNA.* **2003**, 9, 1034-1048.
62. Gray, DM; Hung, SH; Johnson, KH. *Methods Enzymol.* **1995**, 246, 19-34.
63. Fonin AV, Sulatskaya AI, Kuznetsova IM, Turoverov KK. *PLoS ONE* **2014** 9(7): e103878.
64. Sjöback, R; Nygren, J; Kubista, M. *Biopolymers* **1998**, 46, 445-453.

65. Misra UK; Payne S; Pizzo SV. *J Biol Chem.* **2011** 14;286(2):1248-59.
66. Pham JW, Sontheimer EJ. *J Biol Chem* **2005** 280: 39278–39283.
67. Hamada, M; Ohtsuka, T; Kawaida, R; Koizumi, M; Morita, K; Furukawa, H; Imanishi, T; Miyagishi, M; and Taira, K. *Antisense Nucleic Acid Drug Dev.* **2002** 12, 301–309.
68. Amarzguioui, M; Holen, T; Babaie, E; Prydz, H. *Nucleic Acids Res.* **2003** 31, 589–595.
69. Harborth, J; Elbashir, S.M; Vandenbruch, K; Manninga, H; Scaringe, SM; Weber, K; Tuschl, T. *Antisense Nucleic Acid Drug Dev.* **2003** 13, 83–105.
70. Lecoer H. *Exp. Cell Res.* **2002** 277 (1): 1–14.

CHAPTER 4: CONCLUSIONS AND CONTRIBUTIONS TO KNOWLEDGE

4.1 Conclusions and Contributions to Knowledge made in this Thesis

4.1.1 Development of Higher-Order siRNA hybrids for RNAi Mediated Cancer Gene Therapy

With the rapid expansion and advances that have been made in the field of RNA nanotechnology, the ability to design single siRNA nanostructures that can deliver multiple siRNAs presents an intriguing opportunity for screening of a wide range of oncogene targets while potentiating cancer gene therapy effects. Chapter 2 described the optimization of the synthesis strategy of a branchpoint amidite, for the incorporation within the solid phase synthesis of novel V- and Y-shaped RNAs. The solution-phase synthesis of the requisite branchpoint amidite, 5'-O-levulinyl (Lv) 2'-O- monomethoxytrityl (MMT) ribouridine phosphoramidite was based on an optimized 3-step synthesis strategy featuring: (a) synthesis of levulinic anhydride followed by chemo-enzymatic levulination of the 5' ribouridine hydroxyl group using lipase acrylic resin from *Candida antarctica*; (b) tritylation of the 2' hydroxyl group and (c) phosphitylation of the remaining 3' hydroxyl group (**Scheme 2.1**). The branchpoint amidite was used to develop a library (26) of siRNAs designed to target multiple GRP chaperone proteins and elicit a more potent, synergistic knockdown and cell death effect. The siRNAs were synthesized in good crude yields ($\geq 62\%$) and purified using IP-RP-HPLC to obtained sequence purities ($\geq 97\%$) whose identities were confirmed by ESI-MS (**Table 2.1**).

The RNA templates were hybridized with their complementary sequences in Tris annealing buffer using stoichiometric ratios that promoted self-assembly. A native PAGE was used to confirm hybridization and self-assembly into higher-order structures, (**Figure 2.2**). CD and thermal denaturation studies showed retention of the A-type helical geometries (**Figure 2.3 A, B**), as well as high thermal stability (**Figure 2.4 A, B**) which are crucial for RNAi activity.

The lead siRNAs produced the most pronounced GRP78 knockdown and apoptosis of the AN3CA cancer cells. Furthermore, this study also revealed the influence of multiple GRPs (GRP-75, 78 and 94) on MDA-MB-231 (breast cancer), HeLa (cervical cancer), AN3CA (endometrial cancer) and MRC5 (non-tumorigenic lung cells) cells' survival. The Y-shaped siRNA targeting multi-chaperones (GRP-75, 78 and 94) revealed synergistic effects of silencing the GRP chaperone in cancer (**Figure 2.5 A, B**). More specifically, cancer cells were found to be more susceptible to siRNA silencing relative to the control, non-cancerous cells (**Figure 2.5 C**). Therefore, the self-assembled siRNA hybrids targeting multiple GRPs may provide specific and more potent anticancer activities. These findings are not only important for enhancing the gene therapy effects of siRNAs but also for screening the influence of oncogene targets on the progression of cancer.

4.1.2 Fluorescently Labeled siRNAs and their Theranostic Applications in Cancer Gene Therapy

Gene therapy has re-emerged as a promising precision nano-medicine strategy in the targeted detection and therapy of cancer. The integration of therapy and diagnostics “theranostics” have gained significant traction in the development of new and improved gene therapeutics that effectively diagnose and treat cancers at the onset of the disease. Building on the work described in Chapter 2, Chapter 3 of this thesis reports a theranostic application in which a fluorophore, fluorescein isothiocyanate (FITC), was covalently attached to the siRNAs to produce a library of higher-order FITC-labeled siRNAs. These newly synthesized FITC-siRNAs provide the unique opportunity to track mechanism of action by monitoring cell uptake, co-localization and biological activity of a wide range of GRP-silencing siRNAs, including those adopting linear, V-shape and Y-branch nanostructures. The linear and V- shaped FITC-siRNAs were synthesized in moderate yields (~20%) and purified using IP-RP-HPLC to obtained sequence purities ($\geq 95\%$) with

identities were confirmed by ESI-MS, (**Table 3.1**). The Y- shaped FITC-siRNA was not successfully synthesized using our solid-phase bioconjugation approach. In order to overcome this limitation, the Y-shape RNA template was hybridized with complementary sense RNA strands which contained the FITC label. This self-assembly procedure was also adopted with the V-shape RNA template, and provided the opportunity for the incorporation of multiple FITC probes within single molecular, RNA nanostructures.

A native PAGE was used to confirm hybridization of the FITC-siRNA sequences, (**Figure 3.5 and 3.6**). Moreover, CD and thermal denaturation studies revealed A-type helical geometries (**Figure 3.7A**) as well as similar hybrid stability (**Figure 3.8B**), of the FITC-siRNA constructs when compared to their non-labeled counterparts (**Figure 3.8A**). Fluorescence spectroscopy showed that upon conjugation with the linear and V- shaped siRNAs the fluorescence intensities was quenched, (**Figure 3.10A**) In an effort to overcome the quenching effects, the non-labeled linear, V- and Y- shaped templates were hybridized with their complementary FITC-linear stands to afford siRNAs containing multiple FITCs within a single construct. Incorporation of the multiple FITCs did not overcome the quenching effect, (**Figure 3.10B**); however, increases in the fluorescence emission intensities were observed for these multi-FITC labeled siRNAs.

Silencing efficiency of the FITC-labeled siRNAs within a prostate cancer cell line (PC-3, ATCC® CRL-1435™) was determined via RT-PCR and western blot. In all cases, FITC-siRNA hybrids (50nM) exhibited less mRNA knockdown (~10-30%) when compared to their non-labeled counterparts (~40-80%), (**Figure 3.11A**). Incorporation of the FITC probe onto the sense strand of the siRNAs regains mRNA knockdown (~50-<90%), (**Figure 3.11B**) which also translates to more potent cell death over a 72 h period (~20-95%), (**Figure 3.15 A, B**). Uptake efficiency of the multi FITC-siRNAs, monitored via flow cytometry, revealed the most cellular uptake within 2-4

h, (**Figure 3.12 A, B**). However, the multi FITC-labeled siRNA maintains strong fluorescence, (**Figure 3.13**) even up to 72 hours post-transfection as discerned by flow cytometry, (**Figure 3.12 B**). The lead Y-shaped siRNA, was selected to validate the effects of GRP knockdown on cell viability. Western blot revealed slight knockdown of GRP75 and 78 at the protein levels (**Figure 3.14 A**), whereas RT-PCR showed mRNA knockdown of GRP78 and 94 (**Figure 3.14 B**). Taken together, the data presented within this thesis outlines the unique potential for these novel multifunctional siRNA nanostructures to behave as potent theranostics for cancer gene therapy.

4.2 Future Work

While the data presented within this thesis is self-sufficient, further work can be accomplished by improving the theranostic capability of these FL-siRNAs. This thesis describes the incorporation of a single fluorophore, FITC; other fluorophores (e.g. Cy3/5) can be used to extend the dynamic range of detection into the red or near-IR regions of the electromagnetic spectrum. Incorporation of additional fluorophores would enable multiple wavelengths of detection, which would allow for in depth mechanistic studies related to uptake, co-localization and RNAi activity of the novel V- and Y-shape siRNAs. The incorporation of FRET probes (e.g. Cy3/5) within these FL-siRNAs could also allow for enhanced mechanism of action studies, including new insights on structure dynamics related to siRNA processing during the RNAi mechanism. For example, in the hybrid form, the siRNA labeled with the FRET pair would quench the fluorescent signal, however, upon incorporation into RISC, the FL-siRNAs would denature and separate the FRET pair enabling fluorescence emission. This would allow for accurate determination of the kinetics involved in siRNA incorporation within RISC for processing activity. Additionally, our solid phase RNA synthesis strategy allows for the incorporation of modified

nucleic acids (e.g. 2'OMe and 2'F RNA) which would enhance siRNA stability and improve silencing activity.

Moreover, siRNA delivery is another important aspect of our proposed future work. A transfection agent applicable for *in-vitro* assays is not easily translated *in vivo* or within clinical applications. Therefore, we envisage combining the FL-siRNAs with a cancer targeting or cell penetrating peptides to improve internalization specificity and efficacy of the FL-siRNA nanostructures in cell lines and within *in vivo* xenograft tumor models. The latter can be used to develop a cancer-targeting gene therapy approach to selectively silence oncogene activity within tumors while leaving healthy ones unscathed. We anticipate the development of novel precision medicine approaches to address many of the shortcomings associated with non-selective forms of cancer therapy. In this manner, our biological probes may be effectively translated from pre-clinical to clinical utility.

4.3 Publications, Invention Disclosures and Conference Presentations

4.3.1 Accepted Manuscripts for Publication

- Patel, MR; Kozuch, SD; Cultrara, CN; Yadav, R; Huang, S; Samuni, U; Koren, J; Chiosis, G; Sabatino, D. *Nano Letters* **2016** 16 (10), 6099-6108
- Patel, PL; Rana, NK; Patel, MR, Kozuch, SD; Sabatino, D. *ChemMedChem* **2016**, 11, 252.
- Twomey, EC; Cordasco, DF; Kozuch, SD; Wei, Y; PLoS ONE **2013** 8 (12): e83421

4.3.2 Manuscripts in Preparation/Review

- Kozuch, SD; Cultrara, C.N.; Zilberberg, J.; Sabatino, D. **Fluorescently Labeled siRNAs for Theranostic Activity in Prostate Cancer**. *Manuscript in preparation*.

4.3.3 Poster Presentations

- Kozuch, SD; Sabatino, D. **Fluorescently Labeled siRNAs for Theranostic Applications in Cancer Gene Therapy**. *TIDES Meeting*, Boston, MA. May 2018. (**Poster Presentation**)
- Kozuch, SD; Cultrara, CN; Shah, S; Beck, AE; Heller, CJ; Zilberberg, J; Sabatino, D. **Cancer Gene Therapy using siRNA Nanotechnology and Bioconjugation**. *New York Academy of Sciences Meeting*, New York, NY. May 2018. (**Poster Presentation**)

- Kozuch, SD; Cultrara, CN; Shah, S; Beck, AE; Heller, CJ; Zilberberg, J; Sabatino, D. **Cancer Gene Therapy using siRNA Nanotechnology and Bioconjugation.** *Petersheim Academic Exposition*, Seton Hall University, April 2018. **(Poster Presentation)**
- Kozuch, SD; Cultrara, CN; Shah, S; Zilberberg, J; Sabatino, D. **Cancer Gene Therapy using siRNA Nanotechnology and Bioconjugation.** *New York Academy of Sciences Meeting*, New York, NY. May 2017. **(Poster Presentation)**
- Kozuch, SD; Cultrara, CN; Shah, S; Zilberberg, J; Sabatino, D. **Cancer Gene Therapy using siRNA Nanotechnology and Bioconjugation.** *Petersheim Academic Exposition*, Seton Hall University, April 2017. **(Poster Presentation)**
- Patel, MR.; Kozuch, SD.; Sabatino, D. **Self-Assembled siRNA Nanostructures: Modern approach for targeting multiple site of GRP78 oncogene for gene cancer therapy**, 27th Annual Dr. George Perez Research Colloquium, Seton Hall University, April 2016. **(Poster Presentation)**
- Carrión NE.; Kozuch, SD.; Patel, M.; Patel, H.; Patel, P.; Borland, E.; Sabatino D. and Gorun SM. **Cancer-Targeting Fluoroalkyl Methal Phthalocyanine Bioconjugated for Photodynamic Therapy.** *New York Academy of Sciences Meeting*, New York, NY. May 2016. **(Poster Presentation)**
- Carrión NE.; Kozuch, SD.; Patel, M.; Patel, H.; Patel, P.; Borland, E.; Sabatino D. and Gorun SM. **Cancer-Targeting Fluoroalkyl Methal Phthalocyanine Bioconjugated for Photodynamic Therapy.** *Petersheim Academic Exposition*, Seton Hall University, April 2016. **(Poster Presentation)**
- Carrión NE.; Kozuch, SD.; Patel, M.; Patel, H.; Patel, P.; Borland, E.; Sabatino D. and Gorun SM. **Cancer-Targeting Fluoroalkyl Methal Phthalocyanine Bioconjugated for Photodynamic Therapy.** *New Jersey Academy of Sciences Meeting*, Kean University, April 2016. **(Poster Presentation)**
- Carrión NE.; Kozuch, SD.; Patel, M.; Patel, H.; Patel, P.; Borland, E.; Sabatino D. and Gorun SM. **Cancer-Targeting Fluoroalkyl Methal Phthalocyanine Bioconjugated for Photodynamic Therapy.** *American Chemical Society Meeting*, Boston, MA. August 2015. **(Poster Presentation)**
- Carrión NE.; Kozuch, SD.; Patel, M.; Patel, H.; Patel, P.; Borland, E.; Sabatino D. and Gorun SM. **Cancer-Targeting Fluoroalkyl Methal Phthalocyanine Bioconjugated for Photodynamic Therapy.** *New York Academy of Sciences Meeting*, New York, NY. May 2015. **(Poster Presentation)**

- Carrión NE.; Kozuch, SD.; Patel, M.; Patel, H.; Patel, P.; Borland, E.; Sabatino D. and Gorun SM. **Cancer-Targeting Fluoroalkyl Methal Phthalocyanine Bioconjugated for Photodynamic Therapy.** *Petersheim Academic Exposition*, Seton Hall University, April 2015. (Poster Presentation)

APPENDIX

TABLE OF CONTENTS

A. SUPPLEMENTAL IP-RP-HPLC AND ESI-MS CHROMATOGRAMS

Figure A1	¹ H NMR OF 5'-OLV 2'-OMMT RIBOURIDINE BRANCHPOINT AMIDITE	A2
Figure A2	RP IP HPLC ANALYSIS OF LINEAR GRP78A1 (Table 3.2, 1)	A3
Figure A3	RP IP HPLC ANALYSIS OF LINEAR GRP78S1 (Table 3.2, 2)	A4
Figure A4	RP IP HPLC ANALYSIS OF LINEAR GRP94S1 (Table 3.2, 3)	A5
Figure A5	RP IP HPLC ANALYSIS OF V-GRP78A194A1 (Table 3.2, 5)	A6
Figure A6	RP IP HPLC ANALYSIS OF V-GRP78A178A2 (Table 3.2, 6)	A7
Figure A7	RP IP HPLC ANALYSIS OF Y-GRP78A194A175A1 (Table 3.2, 7)	A8
Figure A8	RP IP HPLC ANALYSIS OF FL-GRP78A1 (260nm) (Table 3.2, 8)	A9
Figure A9	RP IP HPLC ANALYSIS OF FL-GRP78A1 (488nm) (Table 3.2, 8)	A10
Figure A10	ESI-MS ANALYSIS OF FL-GRP78A1	A11
Figure A11	RP IP HPLC ANALYSIS OF FL-GRP78S1 (260nm) (Table 3.2, 9)	A12
Figure A12	RP IP HPLC ANALYSIS OF FL-GRP78S1 (488nm) (Table 3.2, 9)	A13
Figure A13	ESI-MS ANALYSIS OF FL-GRP78S1	A14
Figure A14	RP IP HPLC ANALYSIS OF FL-GRP94S1 (260nm) (Table 3.2, 10)	A15
Figure A15	RP IP HPLC ANALYSIS OF FL-GRP94S1 (488nm) (Table 3.2, 10)	A16
Figure A16	ESI-MS ANALYSIS OF FL-GRP94S1	A17
Figure A17	RP IP HPLC ANALYSIS OF FL-V-GRP78A194A1 (260nm) (Table 3.2, 12)	A18
Figure A18	RP IP HPLC ANALYSIS OF FL-V-GRP78A194A1 (488nm) (Table 3.2, 12)	A19
Figure A19	ESI-MS ANALYSIS OF FL-V-GRP78A194A1	A20
Figure A20	RP IP HPLC ANALYSIS OF FL-V-GRP78A178A2 (260nm) (Table 3.2, 13)	A21
Figure A21	RP IP HPLC ANALYSIS OF FL-V-GRP78A178A2 (488nm) (Table 3.2, 13)	A22
Figure A22	ESI-MS ANALYSIS OF FL-V-GRP78A194A1	A23

Figure A1 ^1H NMR OF 5'-OLV 2'-OMMT RIBOURIDINE BRANCHPOINT AMIDITE

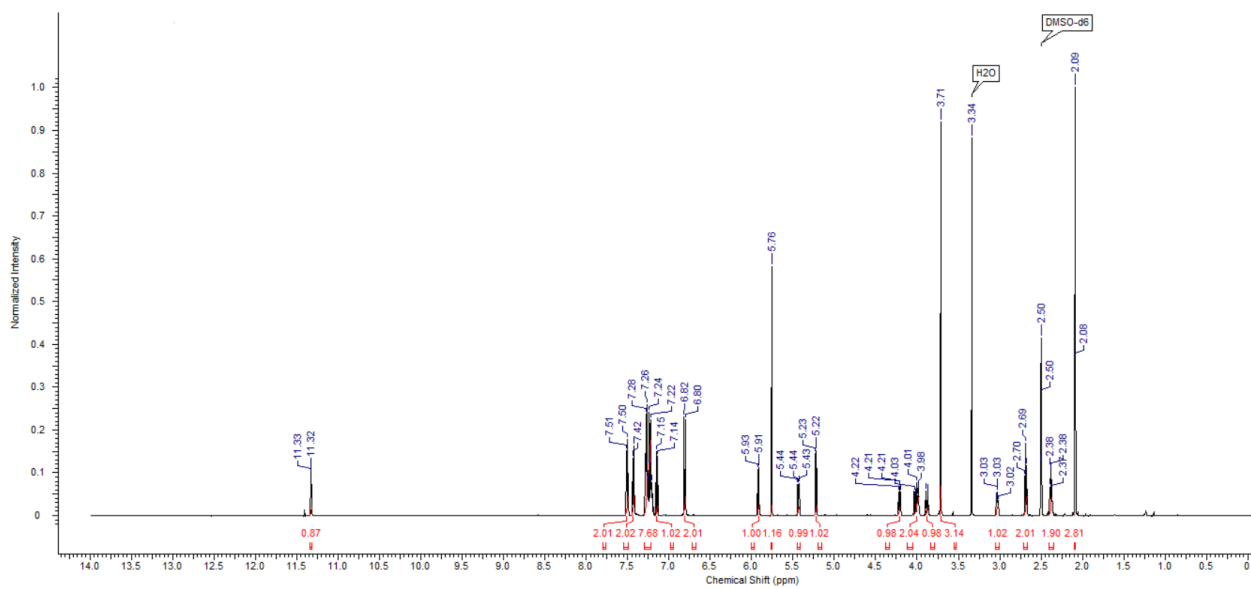
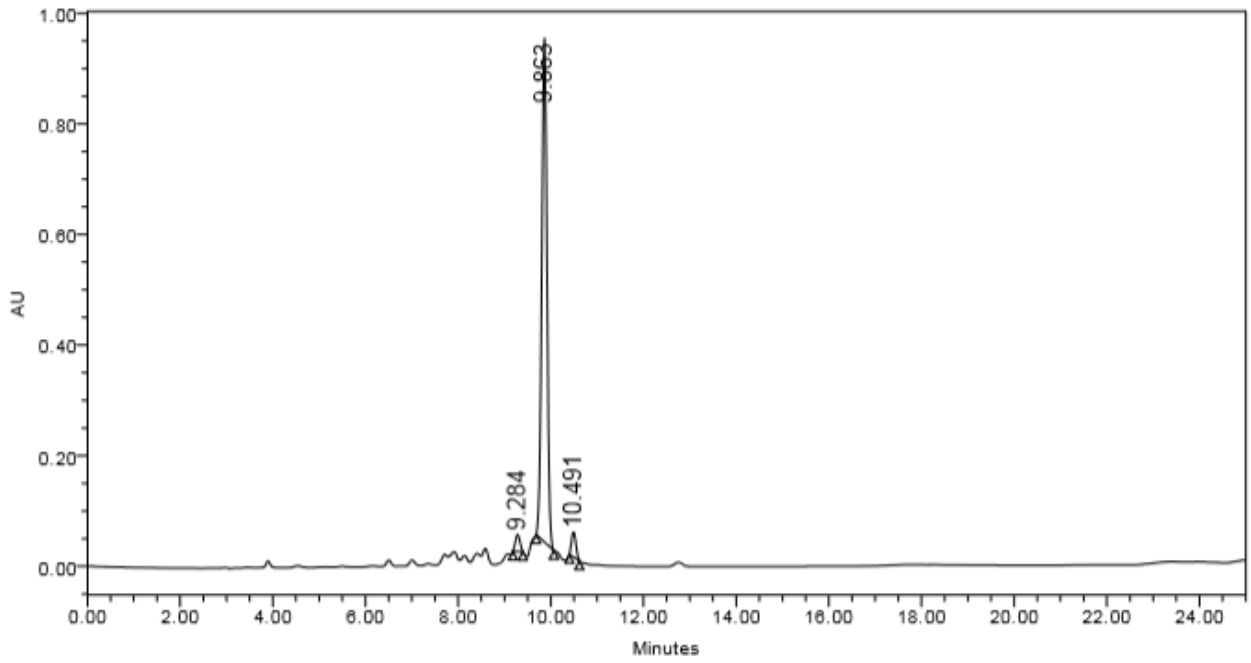
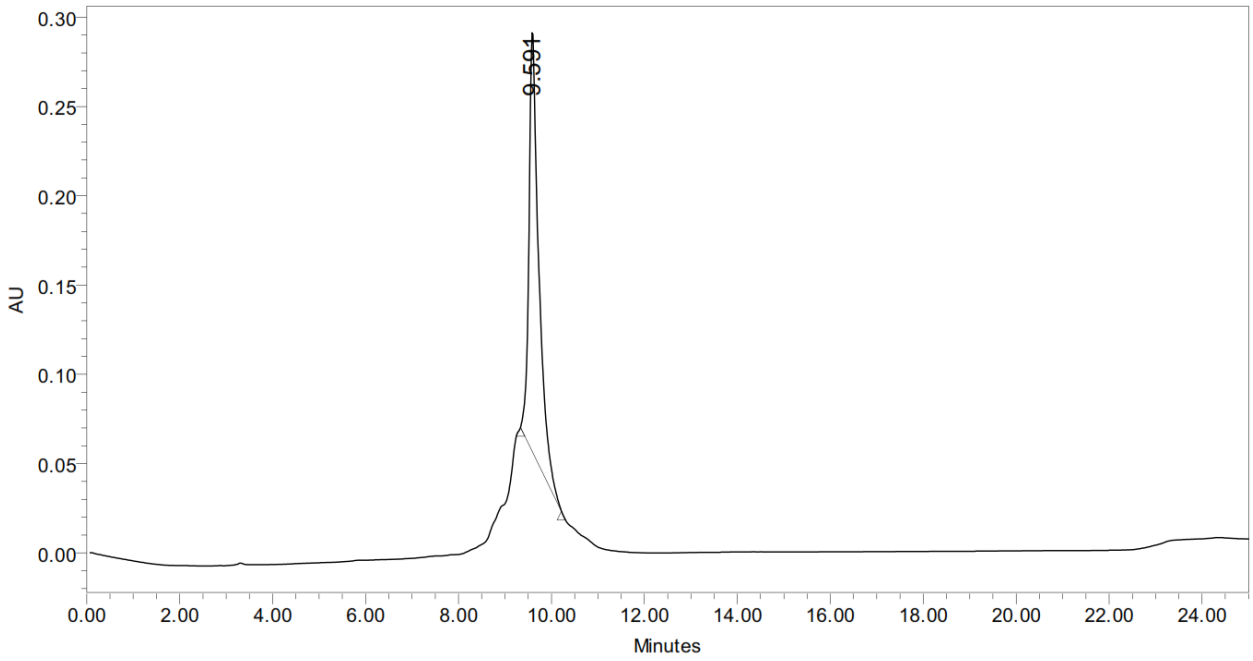


Figure A2 RP IP HPLC ANALYSIS OF LINEAR GRP78A1



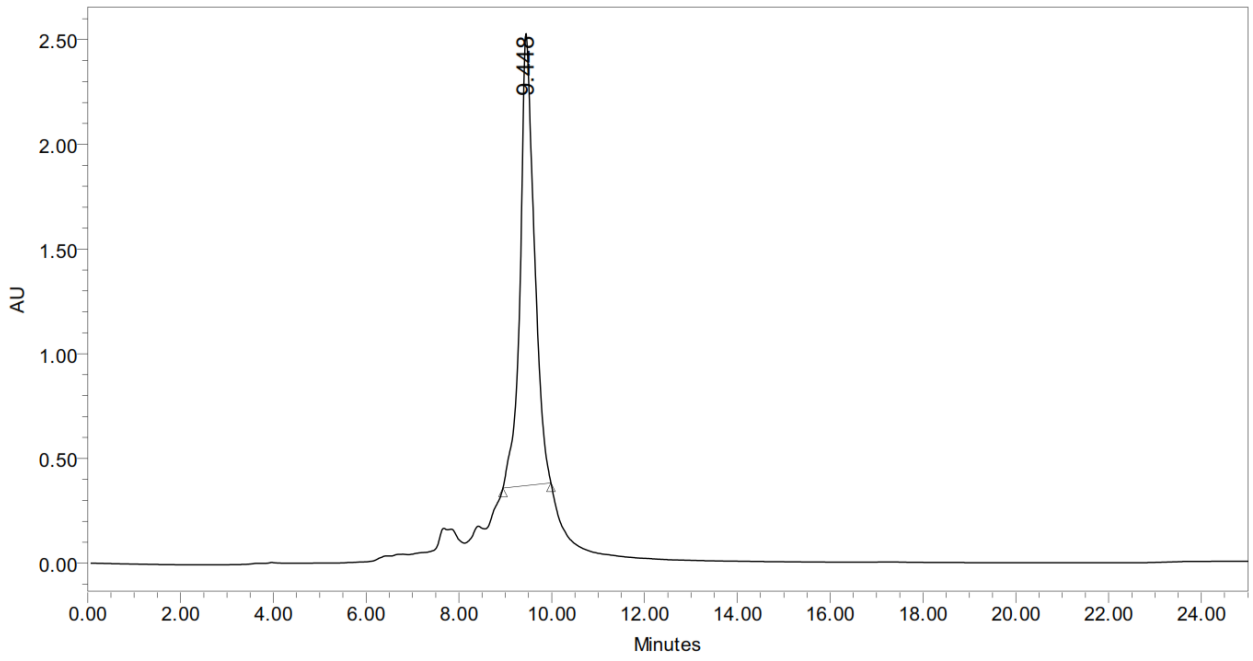
	RT	% Area	Area ($\mu\text{V}\cdot\text{sec}$)
1	9.28	2.78	211473
2	9.86	93.29	7107854
3	10.49	3.93	299732

Figure A3 RP IP HPLC ANALYSIS OF LINEAR GRP78S1



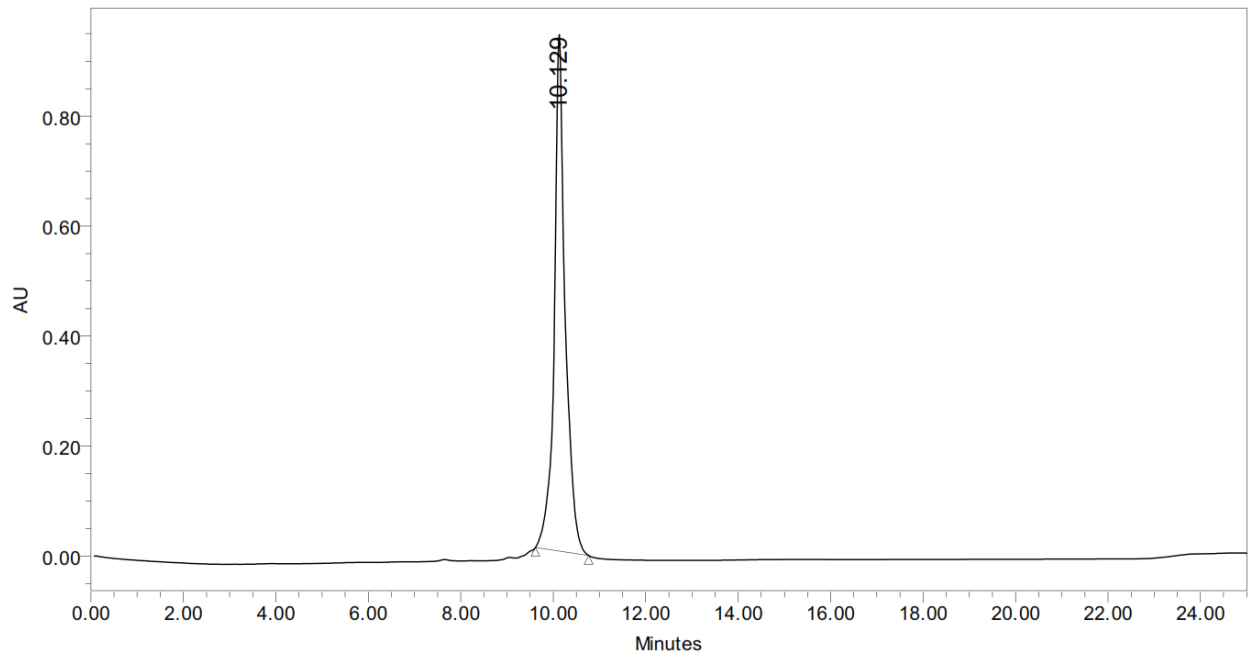
	RT	% Area	Area ($\mu\text{V}\cdot\text{sec}$)
1	9.59	100.00	3449874

Figure A4 RP IP HPLC ANALYSIS OF LINEAR GRP94S1



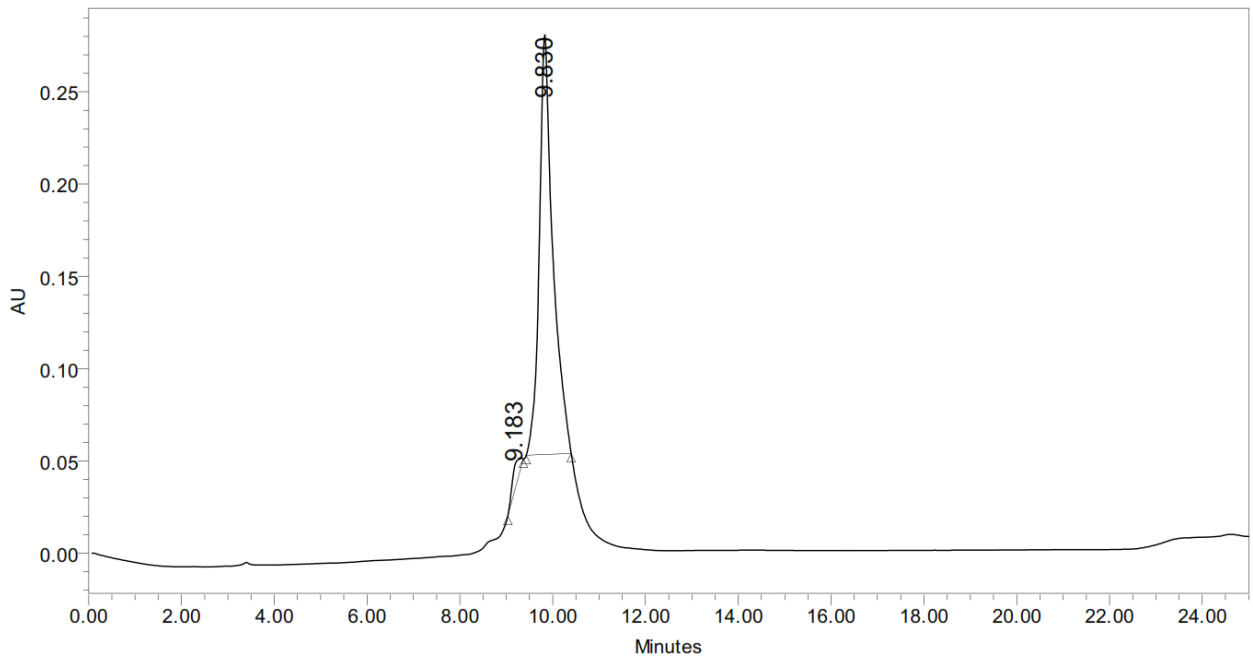
	RT	% Area	Area ($\mu\text{V}\cdot\text{sec}$)
1	9.45	100.00	45867536

Figure A5 RP IP HPLC ANALYSIS OF V-GRP78A194A1



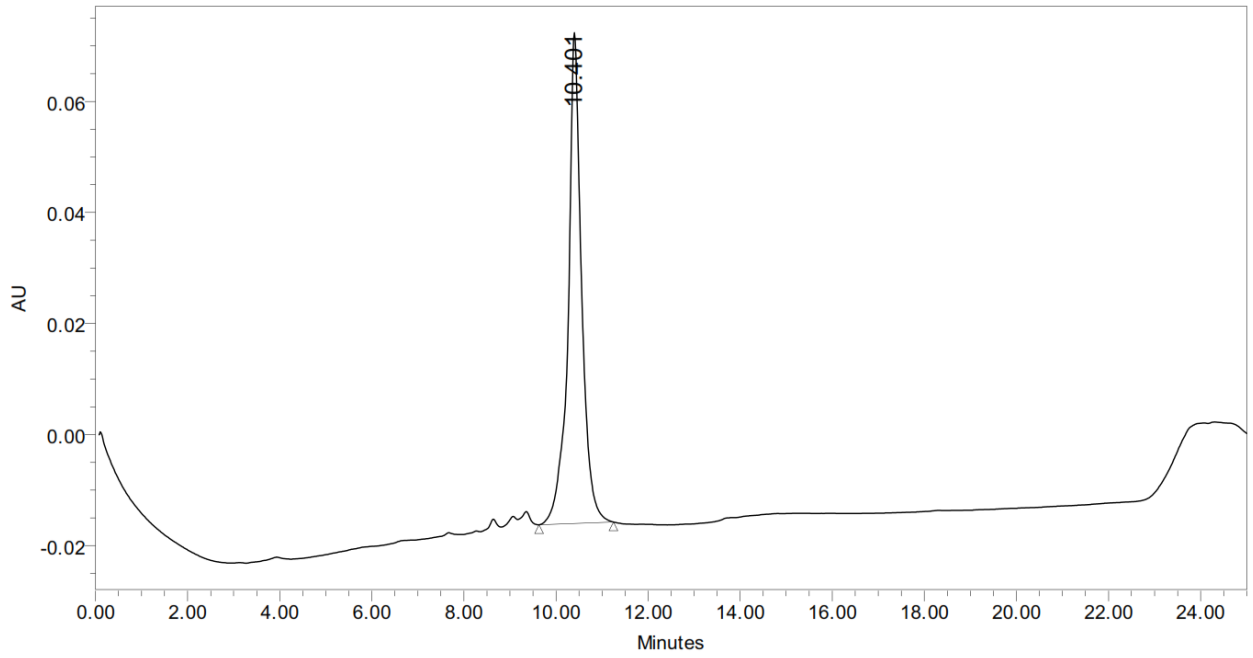
	RT	% Area	Area ($\mu\text{V}\cdot\text{sec}$)
1	10.13	100.00	15461777

Figure A6 RP IP HPLC ANALYSIS OF V-GRP78A178A2



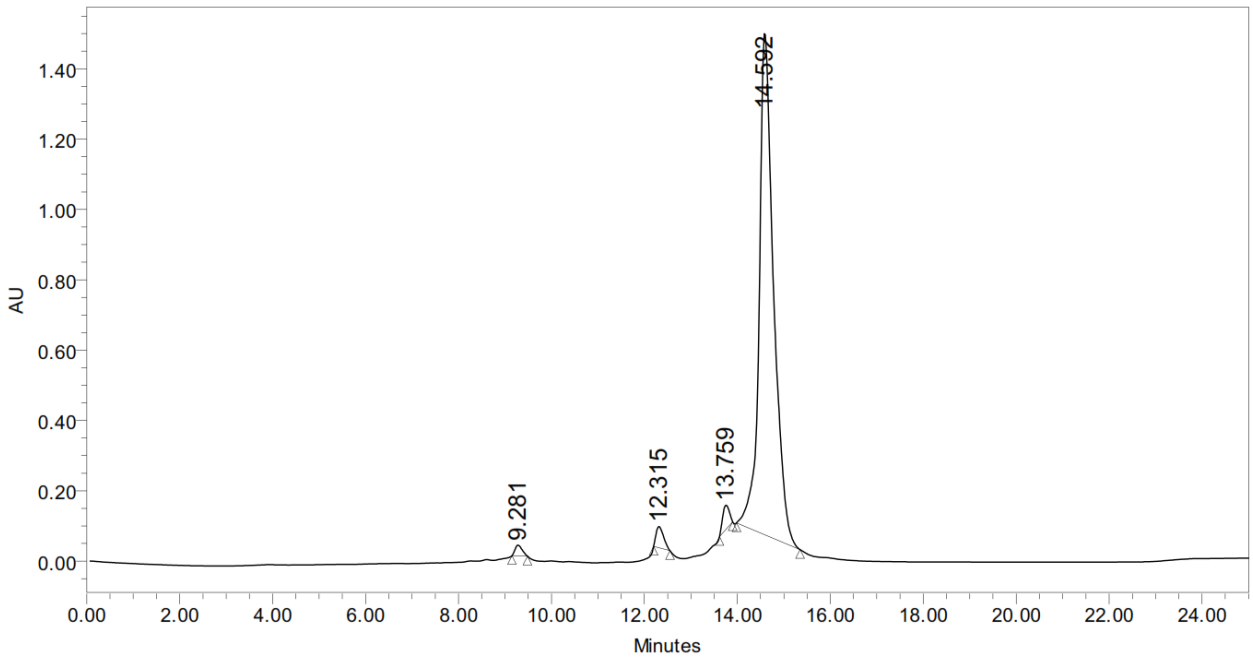
	RT	% Area	Area ($\mu\text{V}\cdot\text{sec}$)
1	9.18	3.07	146735
2	9.83	96.93	4626292

Figure A7 RP IP HPLC ANALYSIS OF Y-GRP78A194A175A1



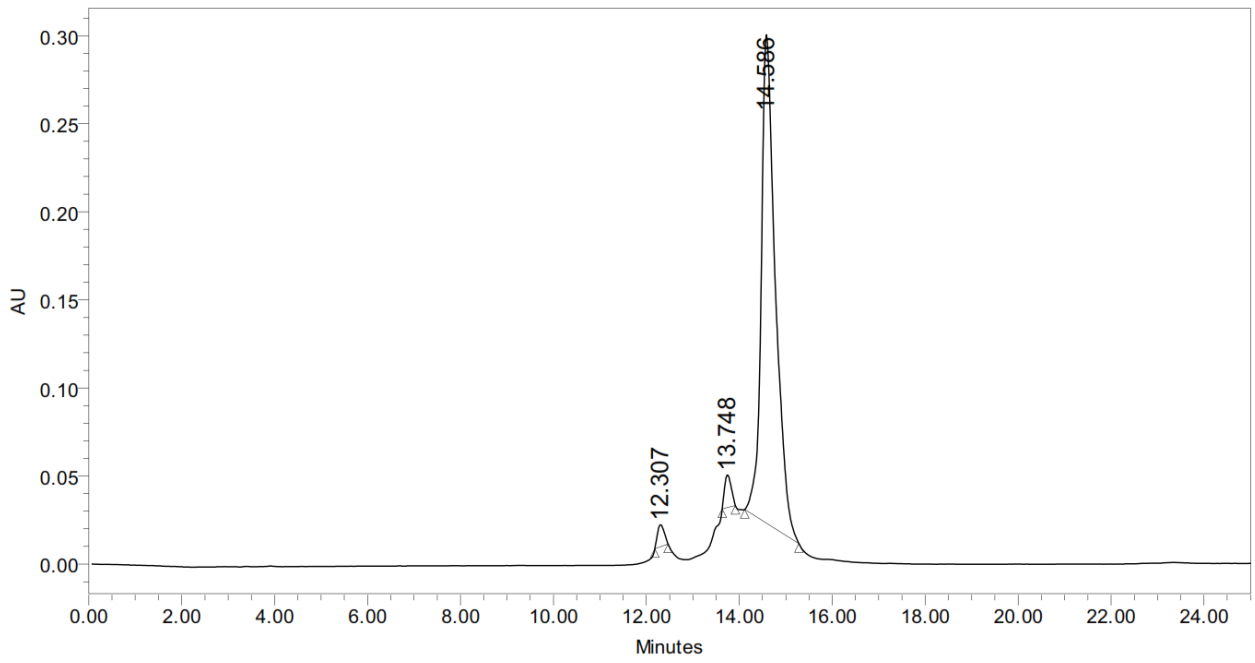
	RT	% Area	Area ($\mu\text{V}\cdot\text{sec}$)
1	10.40	100.00	1797312

Figure A8 RP IP HPLC ANALYSIS OF FL-GRP78A1 (260nm)



	RT	% Area	Area ($\mu\text{V}\cdot\text{sec}$)
1	9.28	1.00	324879
2	12.32	2.10	678728
3	13.76	2.10	680619
4	14.59	94.80	30706756

Figure A9 RP IP HPLC ANALYSIS OF FL-GRP78A1 (488nm)



	RT	% Area	Area ($\mu\text{V}\cdot\text{sec}$)
1	12.31	2.00	123746
2	13.75	2.95	181980
3	14.59	95.05	5866825

Figure A10 ESI-MS ANALYSIS OF FL-GRP78A1

Deconvoluted Mass Spectrum of FITC-GRP78A1 (P1), RT = 0.141 min:

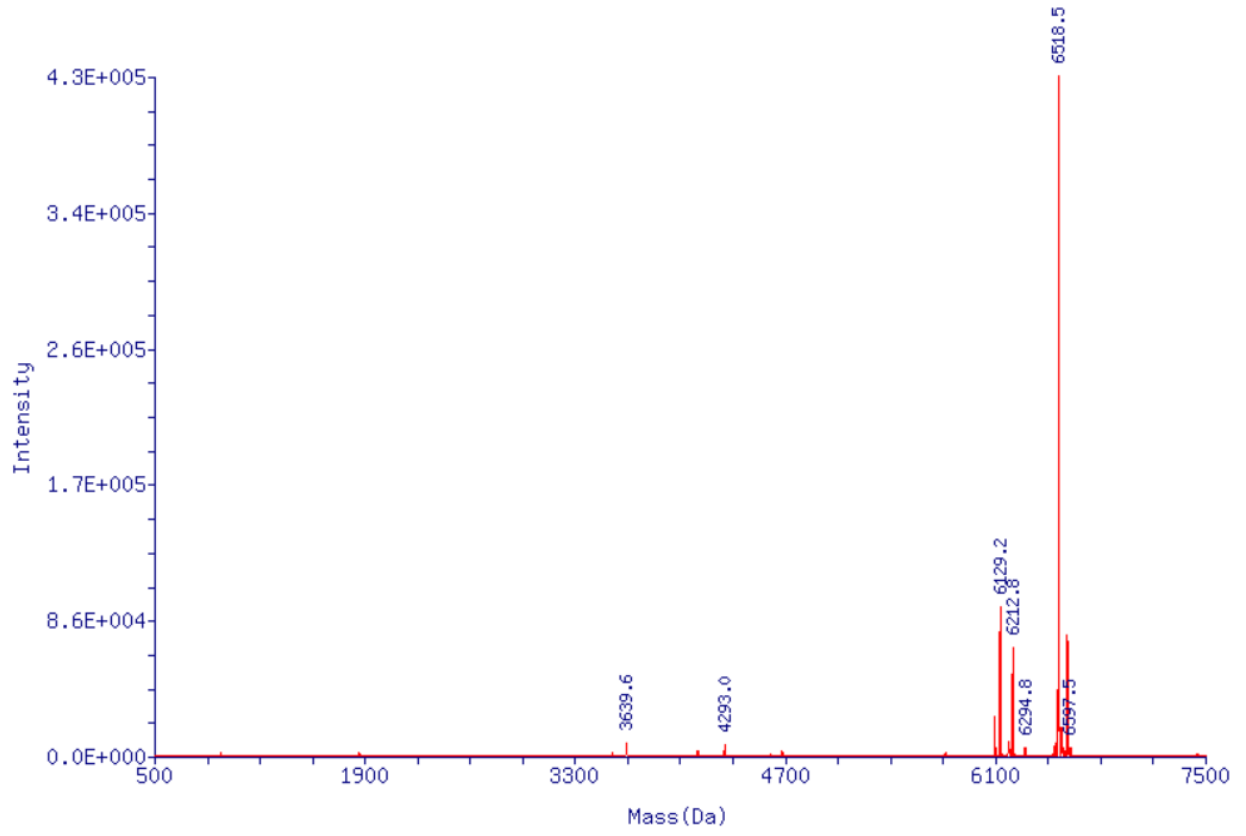
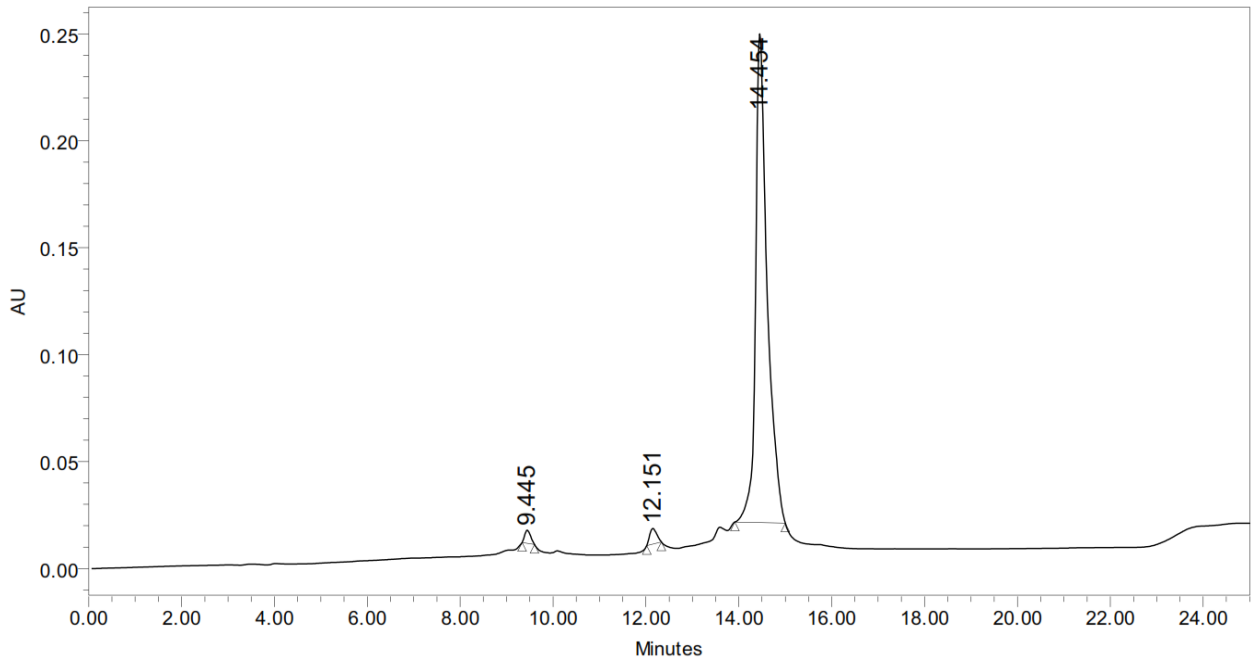
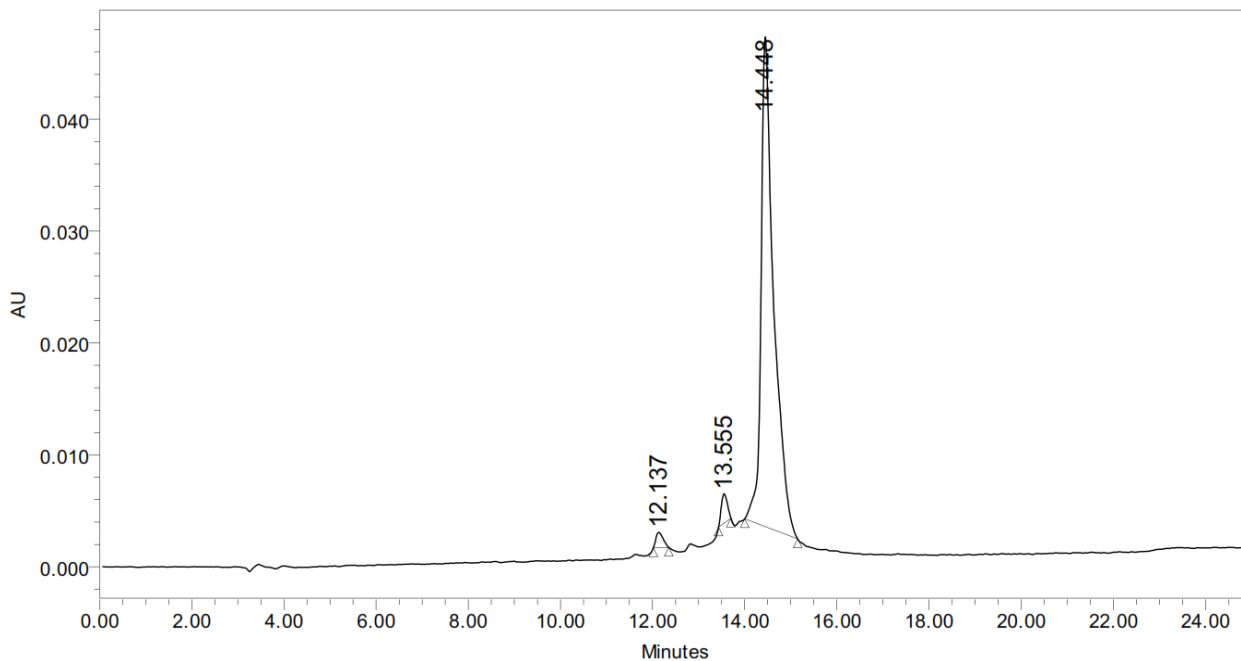


Figure A11 RP IP HPLC ANALYSIS OF FL-GRP78S1 (260nm)



	RT	% Area	Area ($\mu\text{V}\cdot\text{sec}$)
1	9.45	1.29	53177
2	12.15	1.86	76557
3	14.45	96.84	3981950

Figure A12 RP IP HPLC ANALYSIS OF FL-GRP78S1 (488nm)



	RT	% Area	Area ($\mu\text{V}\cdot\text{sec}$)
1	12.14	1.69	14785
2	13.56	2.70	23639
3	14.45	95.61	836278

Figure A13 ESI-MS ANALYSIS OF FL-GRP78S1

Deconvoluted Mass Spectrum of FITC78s1, RT = 0.344 min:

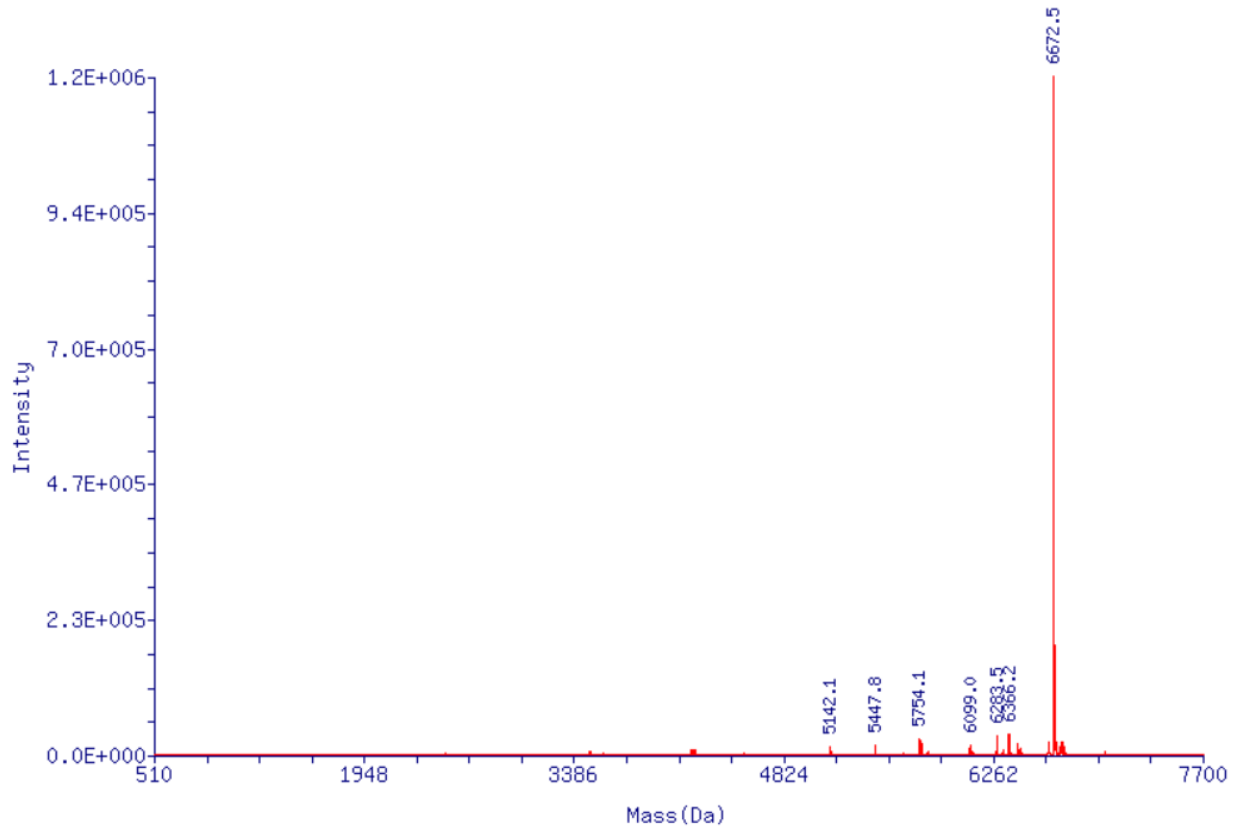
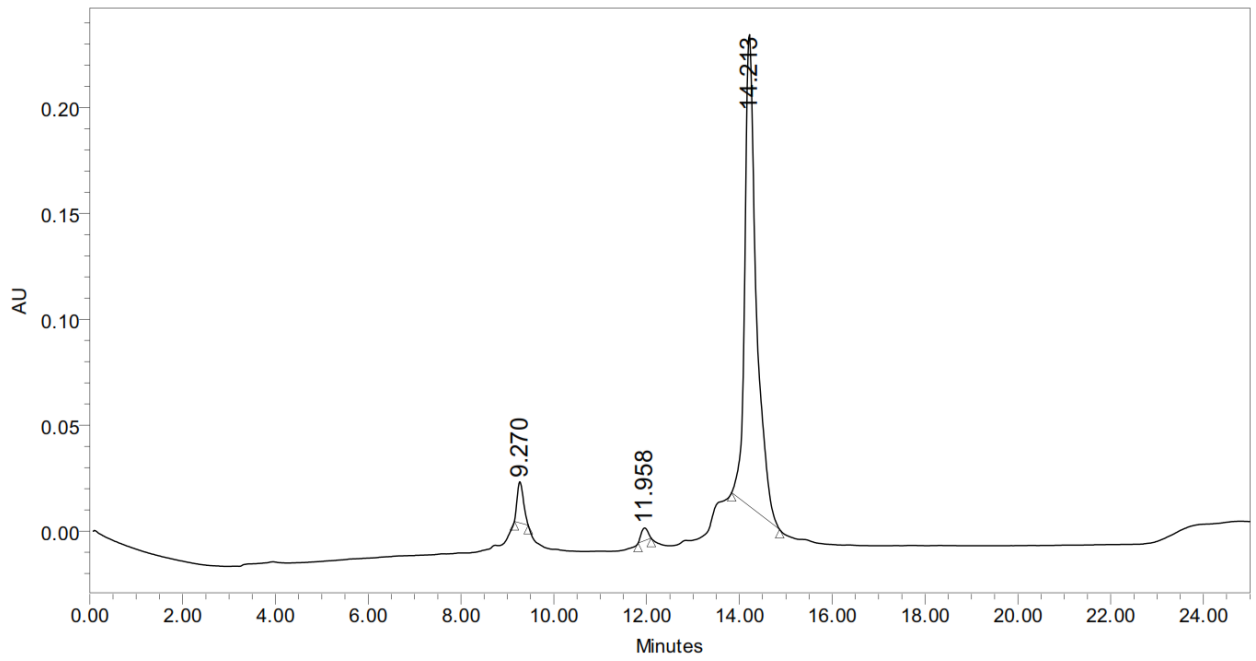
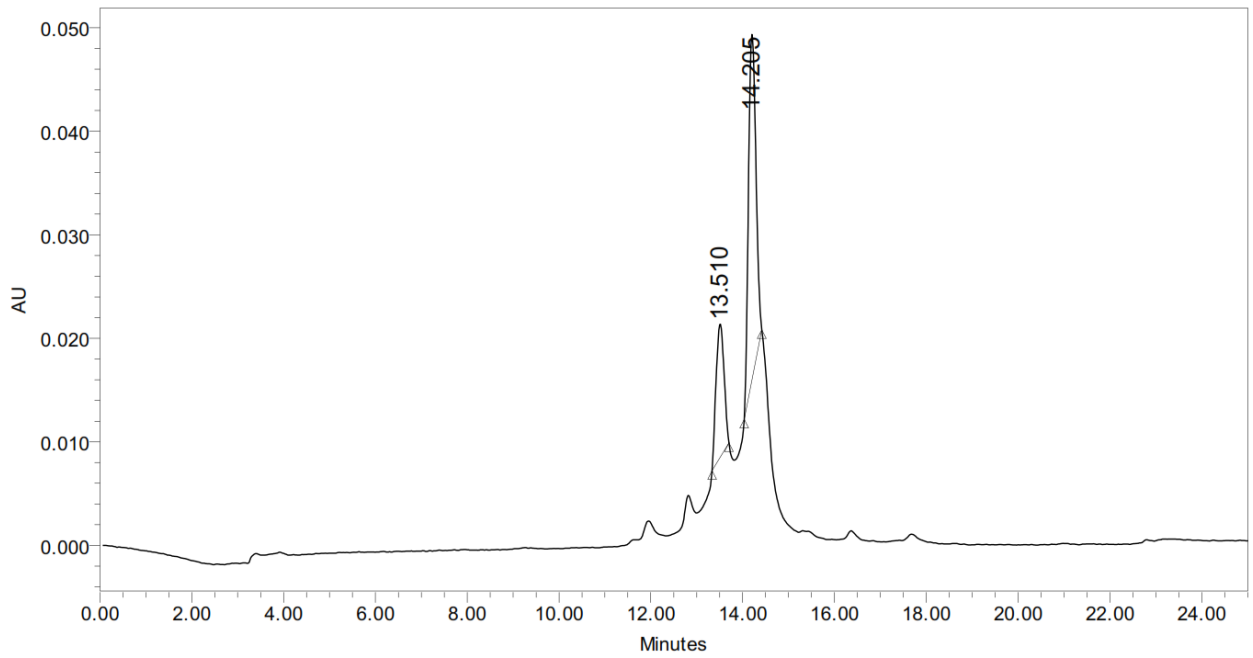


Figure A14 RP IP HPLC ANALYSIS OF FL-GRP94S1 (260nm)



	RT	% Area	Area ($\mu\text{V}\cdot\text{sec}$)
1	9.27	4.44	180347
2	11.96	1.47	59631
3	14.21	94.09	3818389

Figure A15 RP IP HPLC ANALYSIS OF FL-GRP94S1 (488nm)



	RT	% Area	Area ($\mu\text{V}\cdot\text{sec}$)
1	13.51	29.34	155543
2	14.20	70.66	374581

Figure A16 ESI-MS ANALYSIS OF FL-GRP94S1

Deconvoluted Mass Spectrum of FITC94s1, RT = 0.344 min:

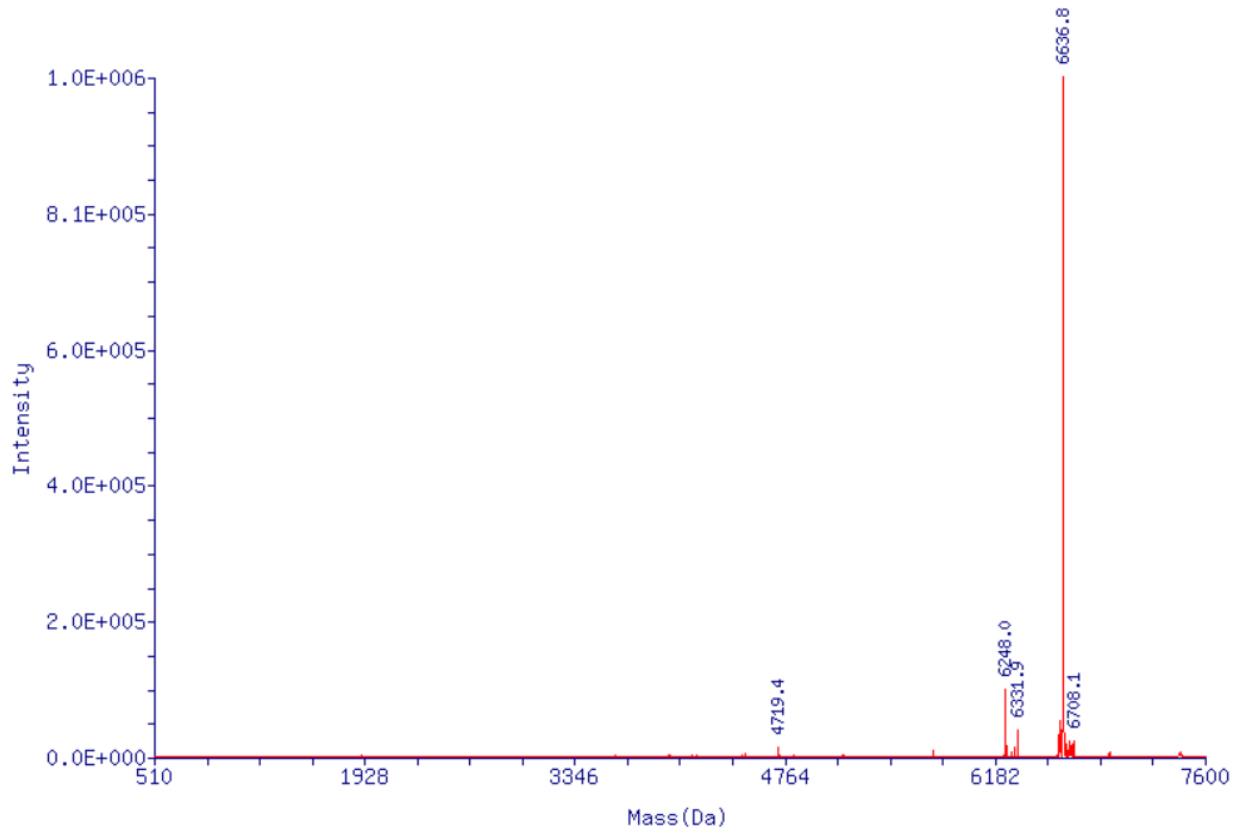
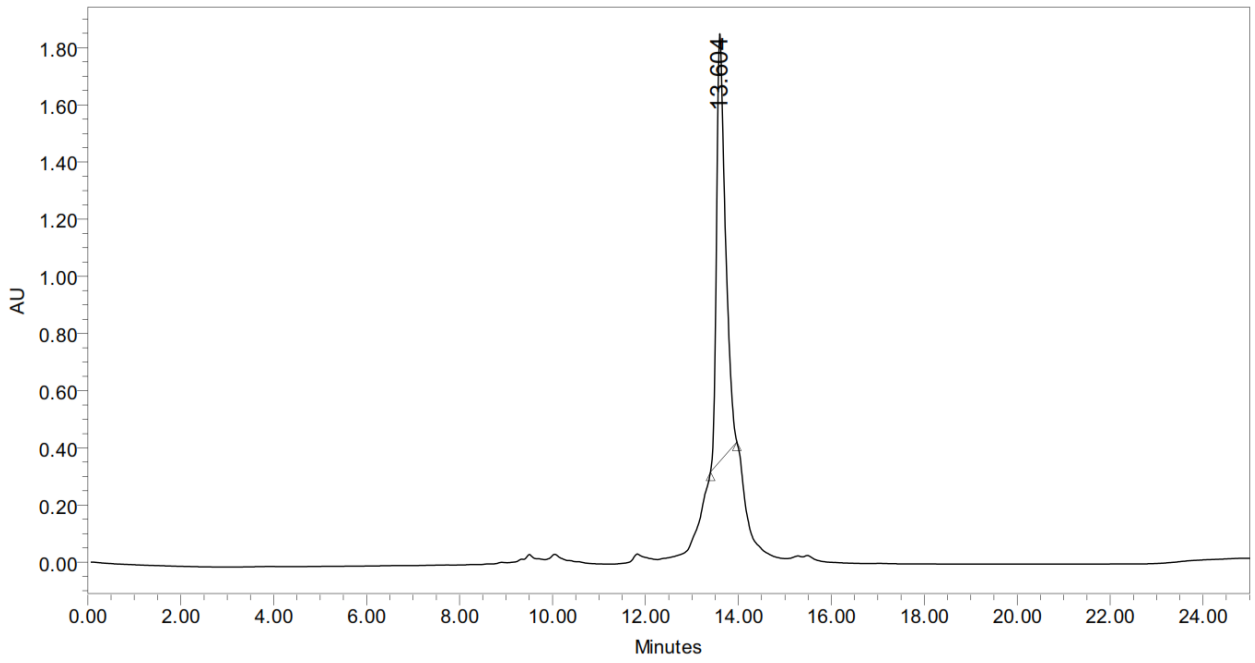
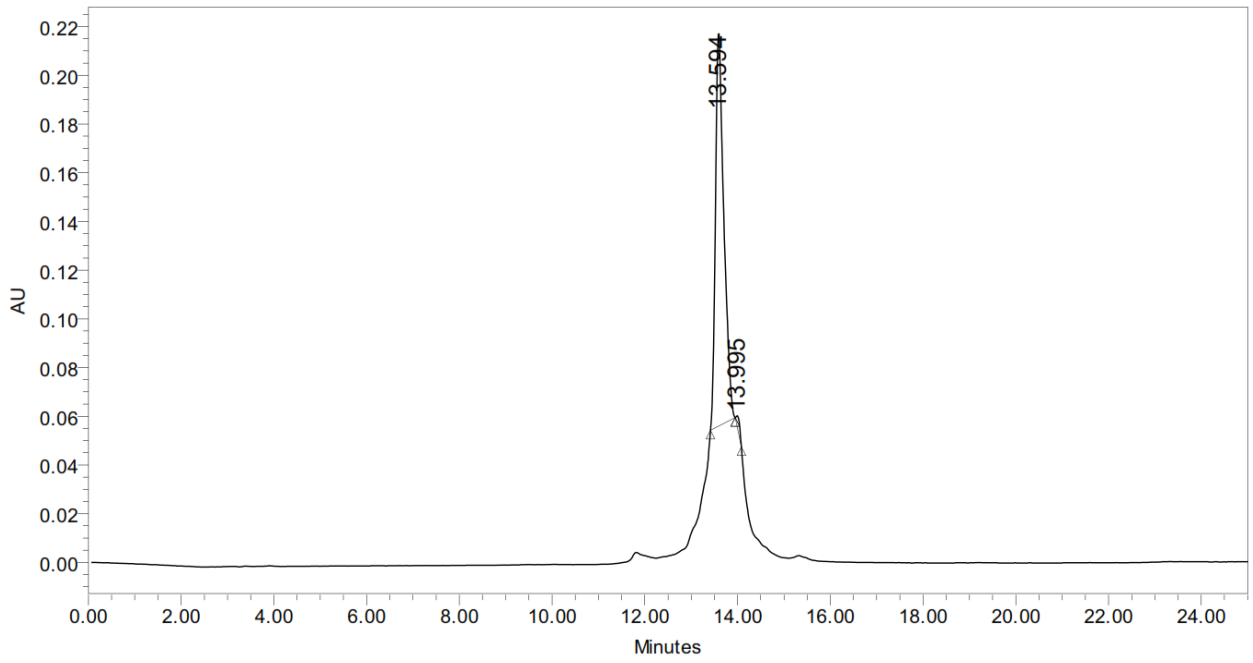


Figure A17 RP IP HPLC ANALYSIS OF FL-V-GRP78A194A1 (260nm)



	RT	% Area	Area ($\mu\text{V}\cdot\text{sec}$)
1	13.60	100.00	19780457

Figure A18 RP IP HPLC ANALYSIS OF FL-V-GRP78A194A1 (488nm)



	RT	% Area	Area ($\mu\text{V}\cdot\text{sec}$)
1	13.59	98.58	2031207
2	14.00	1.42	29335

Figure A19 ESI-MS ANALYSIS OF FL-V-GRP78A194A1

Deconvoluted Mass Spectrum of 7894_amino_FITC, RT = 0.135 min:

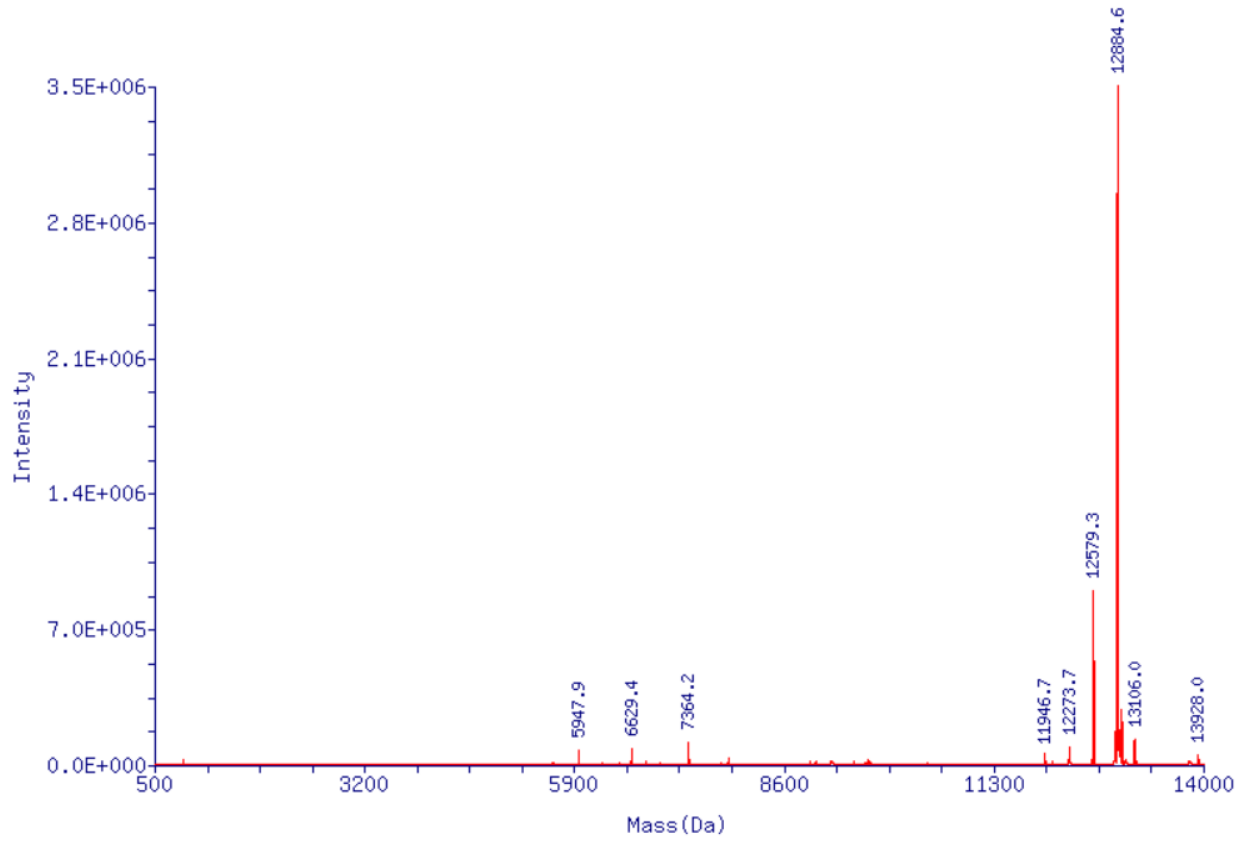
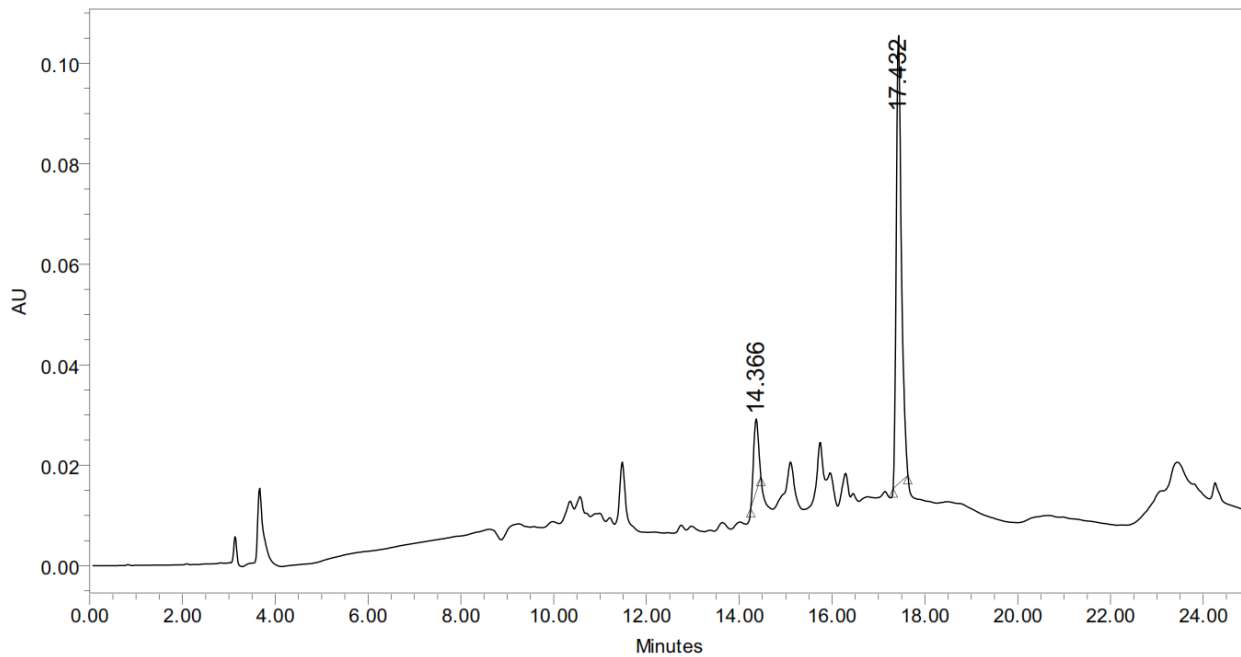
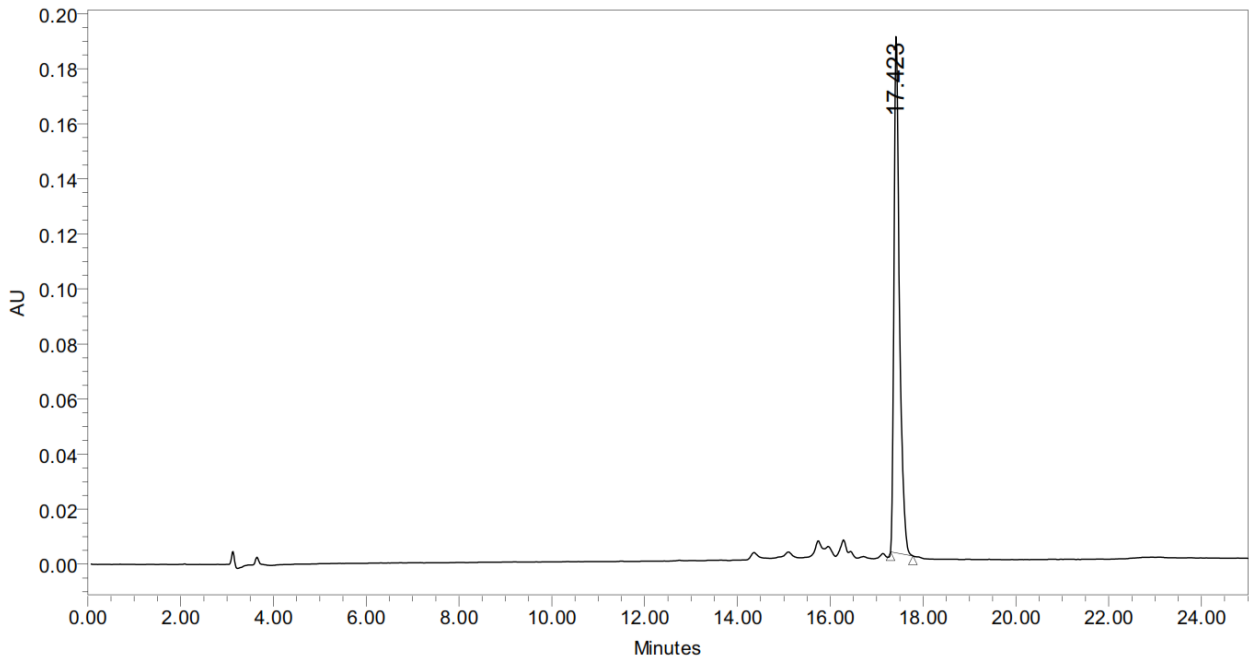


Figure A20 RP IP HPLC ANALYSIS OF FL-V-GRP78A178A2 (260nm)



	RT	% Area	Area ($\mu\text{V}\cdot\text{sec}$)
1	14.37	13.26	104709
2	17.43	86.74	684834

Figure A21 RP IP HPLC ANALYSIS OF FL-V-GRP78A178A2 (488nm)



	RT	% Area	Area ($\mu\text{V}\cdot\text{sec}$)
1	17.42	100.00	1533861

Figure A22 ESI-MS ANALYSIS OF FL-V-GRP78A178A2

Deconvoluted Mass Spectrum of 78a1a2_amino_FITC, RT = 0.125 min:

